ACCELERATOR R&D AND CONSTRUCTION

COHERENT OSCILLATIONS PRODUCED BY THE RAPID SKIRTING OF AN INTEGRAL RESONANCE

M. M. Gordon and Felix Marti

It is well known that accelerating a cyclotron beam through an integral resonance generates a coherent radial (or vertical) oscillation of the beam, but it is less widely known that such oscillations can also be produced just by rapidly skirting the same resonance. The latter will occur whenever the perturbing field or the radial (vertical) tune changes so rapidly in the vicinity of the resonance that the accelerating beam cannot smoothly follow the resultant nonadiabatic shift on the equilibrium orbit.

An interesting example of this phenomenon has been found in superconducting cyclotrons when there is a large difference in current between two adjacent trim coils. The resultant change in field gradient can produce a fairly sharp dip in the ν_r vs. E curve which temporarily brings the value down close to ν_r=1.

This type of behavior occurs, for example, in the ν_r curve shown in Fig. 1 for the case of C^{4+} ions having a final energy of 30 MeV/A. Here the value of ν_r drops from 1.065 at 20 MeV/A down to 1.027 at 22 MeV/A, and then rises to 1.082 at 24 MeV/A. Although this is the region of interest here, we should also note that ν_r then drops through ν_r=1 near 27.5 MeV/A which corresponds to the start of the extraction process.

The phenomenon under discussion here can be readily demonstrated by examining the results from computed orbits. Fig. 2 shows, for example, a plot of p_x vs. x for one such orbit between 19

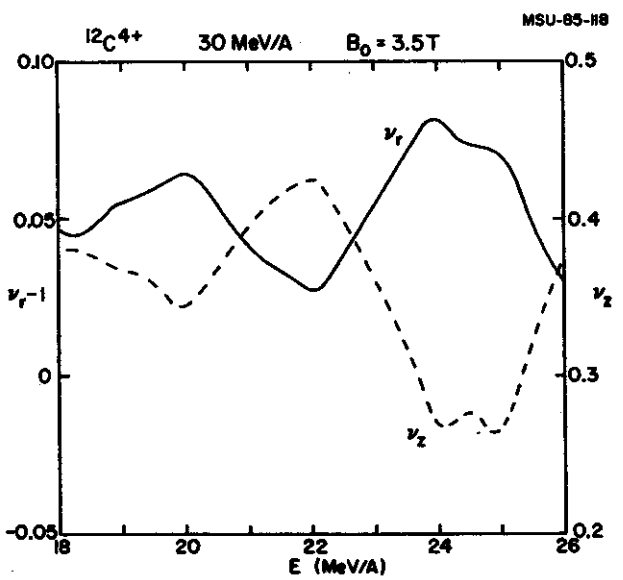

Fig. 1 Plot of ν_r (left scale) and ν_z (right scale) vs. E for a magnetic field designed to accelerate C^{4+} ions up to 30 MeV/A. Between 20 and 24 MeV/A, the value of ν_r drops rapidly down to 1.027 and then rises sharply to its normal value. Note the corresponding peak in the ν_z curve. This effect results from a large difference in currents between trim coils #12 and # 13.

MSU-85-169

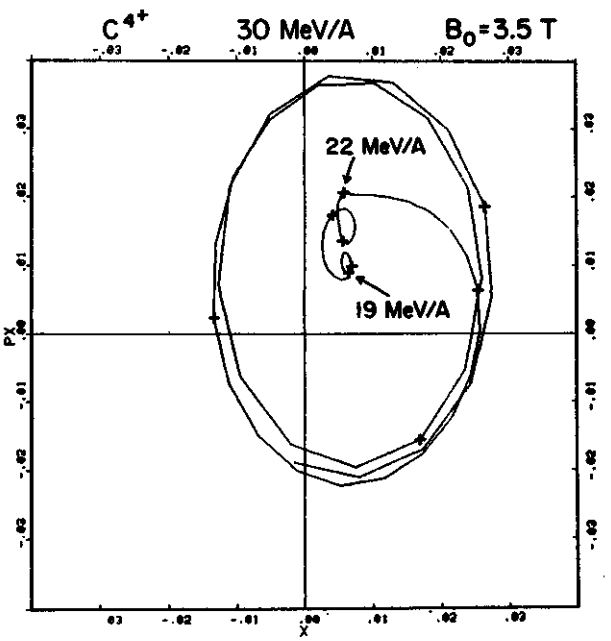

Fig. 2 The solid curve represents (x,p_x) points plotted once per turn for an orbit accelerated from 19 to 25 MeV/A with an energy-gain per turn of 70 keV/A. The (x,p_x) value at every tenth turn is marked by a cross. Note that p_x here is actually $p_x/(m\omega)$. The orbit starts out very well-centered and then develops an oscillation amplitude ΔA = 30 mils as a result of skirting the ν_r=1 resonance.

and 25 MeV/A where the energy gain per turn is 70 keV/A. The phase space coordinates (x,p_x) give the deviation of (r,p_r) from the equilibrium orbit values at each energy, and we should note that all orbits here are calculated in a realistic magnetic field which includes, in particular, a first harmonic (n=1) component having an amplitude of 4.3 gauss in this region. It is this component, of course, that drives the $\nu_r=1$ resonance and which also produces the effects being discussed here.

The solid curve in Fig. 2 represents (x,p_x) points plotted once per turn with every tenth turn marked by a cross. For the first 14 turns between 19 and 20 MeV/A, the points execute a very small loop of radius 2 mils, which indicates that the orbit is very well centered on the appropriate "accelerated equilibrium orbit." For the next 27 turns, the points trace out a second loop and arrive at 22 MeV/A where the ν_r curve in Fig. 1 has a sharp minimum. At this point, the curve in Fig. 2 exhibits a cusp which indicates an abrupt change in its development. From here on, the curve swings rapidly outward and ends on a much larger loop having a radius of about 30 mils. Thus, if this orbit represented the central ray of the cyclotron beam, one would find that the beam developed a coherent oscillation with an amplitude of about 30 mils between 20 and 24 MeV/A as a result of this phenomenon.

The coherent oscillation is caused by the rapid skirting of the $\nu_r=1$ resonance described above. A relatively simple theory has been developed which not only accounts for this effect, but which also shows under what conditions such nonadiabatic effects can be expected to occur. A paper on this theory will be presented at the forthcoming Particle Accelerator Conference scheduled to meet in Vancouver this coming May, and it will suffice here to describe the pertinent results.

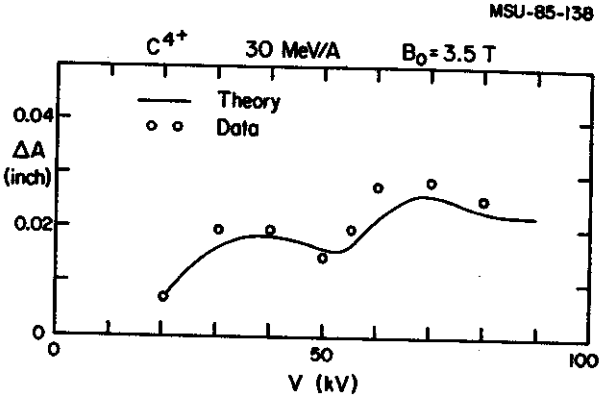

Fig. 3 Comparison of theory (solid curve) and orbit data (circled points) for the amplitude growth ΔA generated by the process illustrated in Fig. 2, as a function of the dee voltage V (which happens to coincide here with the energy-gain per turn in keV/A). As V increases, the process of skirting the resonance becomes faster and therefore less adiabatic.

Fig. 3 shows a plot of ΔA, the increase in amplitude resulting from this effect, as a function of the dee voltage V, which for this ion happens to be numerically equivalent to the energy-gain per turn in keV/A. The solid curve was calculated from the theory while the plotted points were extracted from computer data like that shown in Fig. 2. The agreement between the theory and the data is as good as one could expect, all things considered.

We should note in conclusion that this phenomenon will influence the first harmonic field bump used in the extraction process to guide the beam into the aperture of the electrostatic deflector. That is, the ΔA found here must be added vectorially to the amplitude growth produced when the beam traverses the $\nu_r=1$ resonance in order to generate the total coherent oscillation amplitude necessary for the extraction process. It is this total amplitude, in combination with the radius-gain per turn, which enables the beam to clear the septum of the electrostatic deflector when it finally reaches the extraction energy.

IMPROVED FOCUSING-BAR FIELDS FOR EXTRACTION CALCULATIONS

M.M. Gordon, D.A. Johnson and V. Taivassalo

The orbit codes used to carry out design calculations for the extraction systems of superconducting cyclotrons have been modified during the past year to incorporate more accurate formulas for the fields produced by focusing bars. Many sets of such bars are used in conjunction with electrostatic deflectors to bend and focus the beam along its path out of the cyclotron field. These focusing bars are particularly effective since they provide significant bending action together with strong gradients.

The new formulas for the focusing-bar fields are based on the H field produced by a uniformly charged rectangular surface parallel to the median plane, mainly because this H can be calculated exactly at any point from simple analytical formulas. By using two such surfaces at $z=+z_0$ and $z=-z_0$ with equal and opposite charges, one can represent a rectangular iron bar which is uniformly magnetized in the z-direction.

The iron bars used in the extraction system consist of sets of focusing bars, such as those shown in Fig. 1, and sets of compensating bars which are added to the system in order to cancel the first harmonic field component at the $\nu_r=1$ resonance. The extraction code calculates the resultant field of all these bars at each point along the orbit by superimposing the fields produced by individual bars.

In the standard extraction program, which is used for all basic design computations, the median plane field is calculated exactly while the field off the median plane is calculated correctly to first order in z. The revised version of this program now allows for the simultaneous calculation of the central ray orbit, plus two sets of orbits representing the linear displacements in the radial and vertical directions. Both transfer matrices are

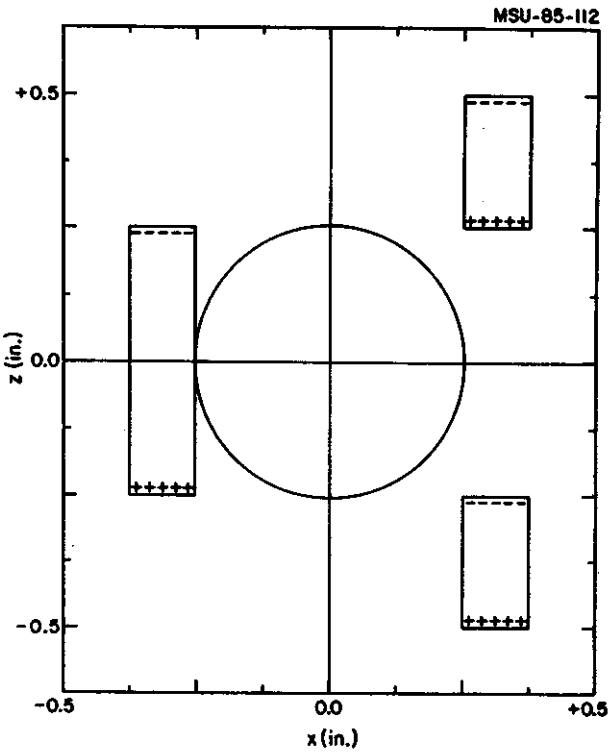

Fig. 1 Cross section of a standard set of focusing bars used in the K500 superconducting cyclotron. The main field is vertically downward and is assumed to uniformly magnetize the bars with a field of 21.4 kG. The +x axis is radially outward, and the +y axis gives the beam direction. Each bar has a width $\Delta x = 0.125$ in., and a length $\Delta y = 3.2$ in. The circle of radius $\rho_0 = 0.25$ in. shown here specifies the region of validity for the multipole expansion.

therefore obtained in this single integration process which speeds up the design work considerably.

A new orbit code has also been developed which now makes it possible to carry out a systematic study of nonlinear effects arising in the extraction process. Such effects should be important first of all because of the rapid fall-off of the main magnetic field in this region, and second because the effectiveness of the focusing bars requires that their own magnet gap be very small. The resultant nonlinear effects will, of course, manifest themselves

through increases in the emittance of the extracted beam.

The new orbit code is an extension of the "z^4 Spiral Gap Code" which was developed in 1978 to examine the effects of nonlinear coupling resonances. In this code, the median plane field data are processed to allow for the calculation of the main field components correct to order z^4. The new extraction code now adds to this main field the "exact" fields produced by all of the focusing bars and compensating bars. This combined field is computed as needed along the orbit through the extraction system.

In order to establish a basis for understanding the results of the orbit computations, it was decided to first carry out a multipole analysis of the field produced by a standard set of focusing bars in the region occupied by the beam. To do this, we represent the field by a scalar potential ψ defined by $\vec{H} = -\nabla\psi$, and then expand ψ in a multipole series as follows:

$$\psi = \sum_m \left(\frac{\rho_0}{m}\right) H_m \left(\frac{\rho}{\rho_0}\right)^m \sin(m\phi),$$

where $x = \rho\cos\phi$ and $z = \rho\sin\phi$ define the polar coordinates (ρ,ϕ), and where ρ_0 is a parameter which specifies the expansion region: $\rho \leq \rho_0$. For the standard configuration shown in Fig. 1, we take $\rho_0 = 0.25$ inch.

The form of the above expansion was specifically chosen so as to simplify the resultant expressions for the field components. Thus we find:

$$H_\phi = -\sum_m H_m \left(\frac{\rho}{\rho_0}\right)^{m-1} \cos(m\phi),$$

which is valid at all points within the circle $\rho = \rho_0$ shown in Fig. 1. In particular, the median plane field becomes:

$$H_z = -\sum_m H_m \left(\frac{x}{\rho_0}\right)^{m-1},$$

so that H_1 gives the dipole field component directly, while the quadrupole coefficient $H_2 = -\rho_0(dH_z/dx)$ gives the linear focusing gradient. Although the above multipole coefficients H_m differ somewhat from those frequently used in beam transport programs, these coefficients are much better suited to our specific application.

In particular, we note that if the focusing bars were infinitely long in the y direction, then the values of H_m would all be constants. It turns out that the average length ($\Delta y = 3.2$ in.) is sufficiently large compared to the aperture ($\Delta z = 0.5$ in.) that the values of H_m are practically independent of ρ within the circle of interest shown in Fig. 1.

The dependence of H_m on the distance y is shown in Fig. 2, and as can be seen, the values are almost constant near the center ($y = 0$), and then fall off in magnitude quite significantly as the ends ($y = 1.6$ in.) are approached. At $y = 0$, the dipole coefficient $H_1 = -1.15$ kG indicates the bending capability of this element, while the value of $H_2/\rho_0 = 8.8$ kG/inch shows the radial focusing gradient it produces.

The remaining terms ($m \geq 3$) are responsible for the nonlinear effects, and their importance generally decreases rapidly as m increases. As shown in Fig. 2, the sextupole term H_3 is quite small while the octupole term H_4 is relatively large. Moreover, the higher order terms with even m values always predominate over the preceding odd term, which is just what one would expect for this type of geometry.

The radial positions of the different sets of focusing bars are adjusted empirically (along with other elements) in order to optimize the beam current extracted from the cyclotron. The radial location of the beam's central ray is therefore somewhat uncertain and could deviate from the symmetry axis of the focusing bars by as much as ±0.1 in., perhaps.

In order to evaluate the effects of such deviations, we recalculated the values of H_m at $y = 0$ as a function of Δx_0, the displacement of the beam axis from the symmetry axis. These

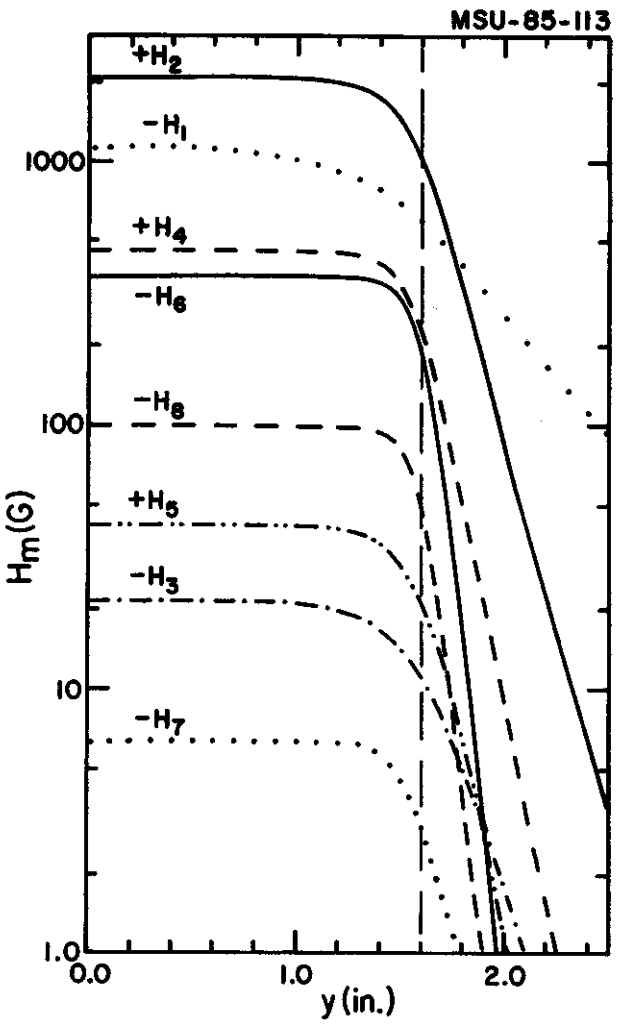

Fig.2 The dependence of the multipole coefficients H_m on the longitudinal distance y. The center of the bars is at y=0 and the end is at y=1.6 in. These H_m have been scaled so that their values are in Gauss. Note that the sextupole coeffecient H_3 is quite small, while the octupole coefficient H_4 is relatively large.

values are shown in Fig. 3, and as can be seen, the nonlinear terms change very rapidly. In particular, in going from Δx_0 = -0.1 to +0.1 in., the value of H_3 changes from -290 to +320 Gauss. These results emphasize the importance of centering the beam within the focusing bars.

Extensive orbit computations using the new code are now in progress, and a report on the results will be presented at the Particle Accelerator Conference meeting in Vancouver this coming May.

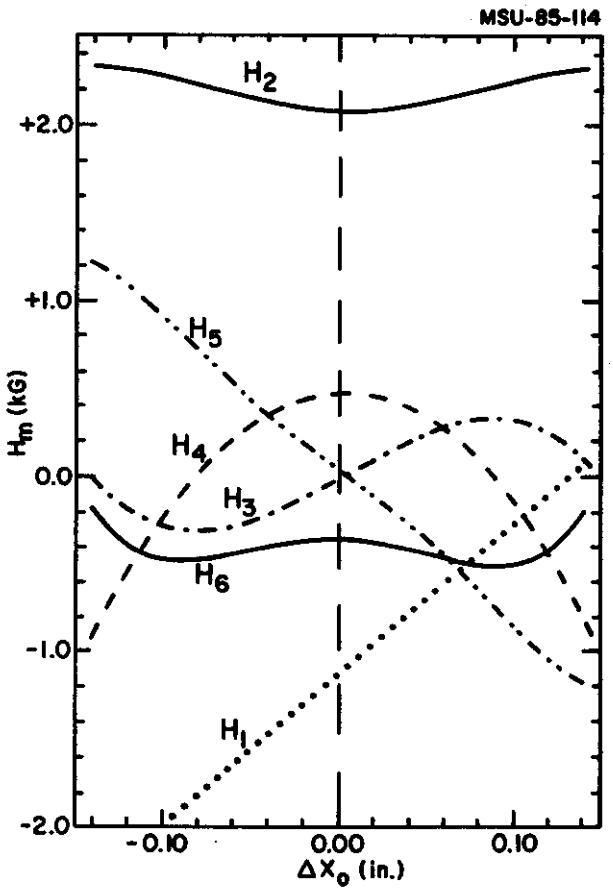

Fig. 3 Values of H_m at y=0 as a function of Δx_0, the displacement of the beam axis from the symmetry axis shown in Fig. 1. The sextupole coeffieient H_3, along with higher order coefficients, change rapidly with Δx_0, which indicates the importance of centering the beam within the aperture.

A COMPREHENSIVE, USER-FRIENDLY, HIGH-SPEED CODE FOR PARTICLE DYNAMICS IN THE NSCL CYCLOTRONS

L.H.Harwood

Design of the extraction system for K800 cyclotron has proved a formidable task and has placed itself squarely in the critical path for the project. Ideas for the system were not lacking, but an efficient translation of these ideas into calculations seemed to be a lacking. It was decided to continue with the existing procedures and, in parallel, write new software that would address the problem at hand in a more comprehensive and consistent fashion.

The basic steps in doing an extraction calculation are:

1. Determine the coil and trim-coil currents needed to get an acceptable phase curve,
2. Determine ν_r and ν_z . Extraction is at $\nu_r \approx 0.8$.
3. Determine electric and magnetic deflector positions and strengths necessary to get the beam out.
4. Check focusing of extracted beams.
5. Go back to 1) and make sure everything is consistent.

The dominant feature in all steps of the procedure is calculation of the field; thus speed in calculating the field is essential. As usual, one can trade speed for accuracy, but this is a case where both are needed. The major difference in the K800 extraction system from the K500 system is the close proximity of dipole bars to the internal orbits, the more tightly packed turns near extraction, and the disturbingly large phase slip at large radii. The beam passes so close to the bars that interpolation in a calculated/measured grid (the usual procedure) is unacceptable at times. Analytic equations exist for the field of a uniformly magnetized rectangular piece of iron; these were coded and a test showed that calculating the field of each bar for every integration step took about 30 sec. of VAX 11/780 time for one turn.

Two solutions are being used to beat this accuracy/speed conflict: first, the analytic equations will be used to build a grid for interpolation unless the field point is too close to the bar where the equations themselves will be used and, second, an FPS-164 was purchased, this is an attached processor with approximately 5-10 the computing power of the 780.

The program being written will do the following functions and will supercede the noted codes:

accelerated orbits	-	SPIRALGAP
equilibrium orbits	-	GENSPEO
accel. equil. orbits	-	unnamed
fit coil currents for good phase curve	-	TCFIT

Field plots and fourier analysis of the field will be available along with the usual plots of interest ($r-P_r$, $Z-P_z$). User friendly interaction is emphasized.

The code is being written and tested on the VAX and the calculational part will be moved to the FPS when a useable fraction of the package is completed. At that point, the philosophy of the code is to have the VAX section of the code act as a "perfect" and omniscient cyclotron console and the FPS serve as a numerical cyclotron with as much of the decision making as automatic as possible. In the end, we will have a single code to take the beam from the center of the cyclotron, through extraction, and out of the cyclotron and the operation will take less than an hour while now it can take 1-2 days with the existing procedures. Such a code should enable us to concentrate more on the extraction problem and less with the calculating question.

A SYSTEM FOR MAGNETIC MAPPING OF THE NSCL K800 CYCLOTRON MAGNET

L.H. Harwood, J.A. Nolen, Jr., M. Fowler, R. Fox, H. Hanawa, and A. Zeller

The NSCL K500 superconducting cyclotron was mapped in 2° angular intervals and 12.5 mm radial intervals by using 55 flip coils mounted on a radial bar. Each coil had its own precision voltage integrator, all of which were multiplexed into a single digital voltmeter. This system produced high quality data for the K500. The 60% larger radius of the K800 cyclotron magnet increases the scale of the mapping hardware and calibration and mapping times by the same factor. Hence the present scheme is being developed to make the absolute calibration less time consuming and more accurate as well as to decrease the time required for mapping.

The new method involves two types of magnetic magnetic measurements: 1) a D_2O NMR probe to read the absolute field at the center of the cyclotron where the peak field is about 5 T and the field is sufficiently uniform is enough for the NMR resonance to be visible, and 2) a search coil to measure the difference in the field between the center and any other point (and thus only needs a dynamic range of ± 0.8 T). The output of the search coil is input to a precision bipolar voltage-to-frequency (v/f) convertor; the field change is directly proportional to the difference in the total "positive" pulses and the total "negative" pulses. The v/f scaler is read "on-the-fly" when strobed by signals from a radial position sensor. The coil starts on one side of the axis of the cyclotron, moves through the axis and on the end of its travel (the range of the cart the coil rides on is -0.1m to 1.1m), steps to the next angle, returns to the starting location, and steps to the next angle. Measurements are made in both radial directions. Some details of the hardware are described below; for more information see ref. 1. The NMR system was commercially obtained and was used with no modifications. Finding the resonance proved to be much easier than anticipated; in most cases the signal was large enough for the internal electronics to lock-on to the the resonance once the setting was made close enough manually. The v/f convertor was obtained from LBL and was used without change. The unit has an inherent 1 part in 10^4 accuracy, so a 1 G error could be expected for the 0.8 T range that the coil would see; this error is due to a differential non-linearity.

The coil is mounted in a G-10 cart which rides on a graphite composite bar; this bar serves as the support for the whole mapper hardware in the median plane of the magnet. The cart is driven radially by a Kevlar string which is, in turn, driven by a motor two meters below the cyclotron. The radial position of the cart is known in two independent ways: 1) the drive motor is a stepping motor, so a counter in the control software shows the location of the cart and 2) the cart carries a glass bar with 2.5 mm wide silvered stipes on it every 5.0 mm, the photosensor attached to the bar can tell when any edge goes by and issues a logic signal that is used as the trigger to read the scalers. As a calibration of each scan the first data point for which both photosensors fire is used as a reference point (two sensors were necessary to cover the full range of motion of the cart (45 in.) and not have to find a precision glass scale of the same length). The angular motion is done with a gear-chain drive from a stepping motor to a shaft on the cyclotron axis. Angular position is determined using an incremental angular encoder which ouputs 1000 pulses per degree of motion.

Calibration was an inportant step. The radial position calibration was done using a laser interferometer. The laser was mounted over the outer end of the bar. A corner-cube

was mounted on the coil cart. The interferometer electronics produced a pulse as each fringe was crossed; the pulse was fed to the counting electronics in place of the v/f output. The result was to give us a direct measurement of the radii at which v/f scaler values were read; the stripes on the glass proved accurate to better than .025 mm absolute. The "gauss/pulse" factor that had to be applied to the data was initially determined in a separate magnet and was confirmed by measuring the field on the median plane in the center of a rf dee stem penetration and comparing the difference between that value and the NMR value at the center of the machine with the search coil value; the agreement was better than expected, ie. we didn't have to change the calibration constant.

Data are taken with a FALCON(cpu)-CAMAC based system. The v/f pulses and the output of a fixed rate pulser are fed into CAMAC scaler modules. When strobed by the photosensors, the FALCON reads the scalers and reads registers containing the current angle, radial drive motor position, and photosensor states. After enough data are obtained to fill a buffer, the data is transfered to a VAX 11/750 where it is checked for errors and written to tape. The software for the asynchronous data transfers was taken from existing software for collecting nuclear physics data. Several schemes for checking the data were investigated. The best on-line check involved checking the constancy of the fixed rate pulser values; if the pulser values fluctuate, then there had to be some error in the location of the cart when the scalers were read.

The system can map the magnet rapidly. It takes about 40 minutes to do a 360° map in 1° steps with 440 data per radial scan. At the end of the map the data has been checked for errors, the operators have been notified if any angles require remeasuring, the data has been written to tape, and the data has been preprocessed to make display and fourier analysis of the field possible. The first mapping of the magnet has been completed and analysis of the data shows both the mapper and the magnet are working quite well. The analysis of the data continues.

References

1. Harwood,L.H. and J.A.Nolen,Jr.; Proc. 10th Int. Conf. of Cyc. and their App. ; April 30-May 3, 1984; East Lansing, Mi. USA; pg. 101.

STUDY OF MAGNETIC FORCES IN THE K800

B. F. Milton and L. H. Harwood

INTRODUCTION

This study was performed at the beginning of 1984, after the magnet design was finalized but before the magnet was completed. The purpose was to determine the safe operating limits of the magnet and to determine a set of currents at which the field should be mapped.

POISSON CALCULATION

To calculate the fields present at all points in the magnet we used the bidimensional magnetostatic code "POISSON", which computes the vector potential over a relaxation grid (lattice)[1]. Both the current grid and the lattice (fig. 1) used were similar to those in the "TRIM" runs for field fitting. Following the procedure used then, different B-H tables are used to describe iron rings of different magnetization in the areas not having cylindrical symmetry. These are generated by assuming the magnetization, M, is reduced according to B=uH+FM, where F (the stacking factor) is the ratio of the volume of iron to the volume of the ring used to simulate it[2]. In order to improve the quality of the yoke fields more points where used in this area in the "POISSON" runs, and the median plane penetrations were treated using stacking factors instead of a single hole as had beeen done in the "TRIM" runs. Figure 1 shows the layout of the various regions used in the lattice along with the percentage iron used in each region.

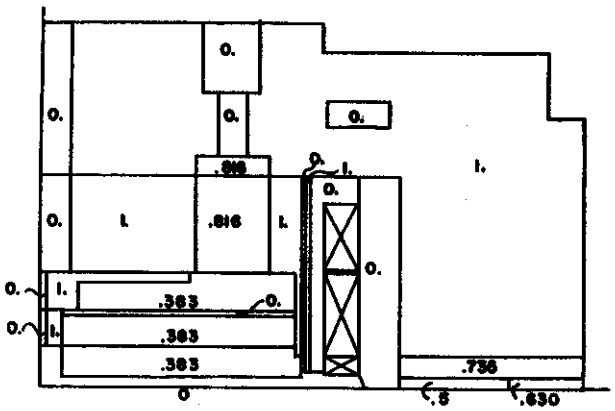

Fig. 1. The simple lattice used for the initial "poisson" calculations. The numbers are the iron fraction associated with each region.

One unplanned use for the field data was in the area of fringe fields. It turned out that the data from the poisson calculations using the enlarged grid (described later) provided quite

NUM	Ialpha A/cm2	Ibeta A/cm2	B(0) kG	Fz large Tons	Fr large Tons	Fz small Tons	Fr small Tons	1 Tons	2 Tons	3 Tons
1	1,500	3,000	36.8	331	1,015	-903	1,165	-850	116	39
2	1,500	0	26.5	-218	602	3		-432	-10	-2
3	3,750	-1,000	39.6	-230	2,953	744	-266	-1,101	-218	-52
4	3,750	3,000	51.5	-492	4,034	-2,331	1,600	-1,363	-91	0
5	1,500	4,000	39.9	504	1,132	-1,273	1,843	-737	182	54
6	1,500	2,000	33.5	153	886	-589	618	-587	72	25
7	1,500	1,000	30.0	-29	761	-273	226	-493	30	11
8	1,500	-1,000	21.9	-473	399	321	-63	-341	-64	-18
9	2,250	-1,000	28.8	-801	1,046	440	-135	-627	-104	-27
10	2,250	0	32.3	-595	1,279	6	0	-682	-88	-14
11	2,250	1,000	35.6	-389	1,484	-437	298	-739	-31	-1
12	2,250	2,000	38.8	-36	1,376	-898	753	-814	8	12
13	2,250	3,000	38.8	228	1,529	-1,393	1,350	-894	49	26
14	2,250	4,000	41.9	484	2,013	-1,925	2,068	-978	92	41
15	2,750	4,000	48.1	372	2,694	-2,341	2,196	-1,136	45	32
16	2,750	3,000	45.2	63	2,515	-1,715	1,464	-1,054	3	17
17	2,750	2,000	42.2	-237	2,310	-1,114	837	-975	-36	3
18	2,750	1,000	39.1	-587	2,089	-544	343	-901	-73	-10
19	2,750	0	35.9	-932	1,852	9	0	-838	-107	-22
20	2,750	-1,000	32.6	-1,299	1,590	542	-182	-792	-141	-35
21	3,250	-1,000	36.1	-1,705	2,226	642	-228	-950	-178	-43
22	3,250	0	39.3	-1,342	2,517	12		-996	-150	-32
23	3,250	1,000	42.5	-940	2,786	-651	385	-1,062	-116	-18
24	3,250	2,000	45.5	-552	3,030	-1,325	915	-1,134	-81	-5
25	3,250	3,000	48.4	-177	3,244	-2,024	1,565	-1,210	-43	8
26	3,250	4,000	51.2	183	3,439	-2,745	2,315	-1,291	-3	23
27	3,750	4,000	54.2	-77	4,254	-3,142	2,429	-1,444	-52	13
28	3,750	2,000	48.6	-918	3,807	-1,530	986	-1,289	-127	-15
29	3,750	1,000	45.7	-1,363	3,556	-755	426	-1,219	-161	-28
30	3,750	0	42.7	-1,823	3,271	16	0	-1,155	-182	-41
31	1,500	-2,000	11.3	-1,019	397	1,007	-64	-1,798	-94	-54
32	2,250	-2,000	23.9	-1,376	687	1,061	-147	-531	-154	-42
33	2,750	2,000	28.8	-1,746	1,255	1,163	-225	-710	-176	-47
34	3,250	-2,000	32.7	-2,236	1,691	1,319	-309	-898	-207	-55
35	3,750	-2,000	36.3	-2,819	2,597	1,504	-393	-1,068	-244	-64

Table 1, The current settings and computed forces for the 35 small "Poisson" cases.

REGION	SMALL GRID FORCE IN TONS	LARGE GRID FORCE IN TONS
1	-1440 (-1058)	-1075 (-982)
2	-52 (-244)	71 (-125)
3	13 (-64)	37 (-32)
D		-1528 (-648)
E		-185 (-62)
F		-548 (-162)
G		-520 (-211)

Table 2. Forces are shown for the +,+ limit of 3750,4000 and in parenthesis the +,- limit of 3750,-1500. See fig. 2 for an explanation of regions.

R inches	Z inches	Measured field kG	Calculated field kG
0.0	69.5	7.500	7.200
30.0	69.5	5.400	5.700
81.5	64.5	-.530	-.680
0.0	98.5	2.750	2.830
0.0	144.5	.760	.765

Table 3, Comparision of the measured and computed fringe fields.

adequate estimates of the fringe field below (or above) the magnet as demonstrated in table 3. With the feeling that this comparision confirms the validity of this method, table 4 lists the fringe field on a grid of points below the magnet.

FORCE CALCULATION

The code "FORCE", which is part of the poisson package, calculates the net force acting on a given region by integrating the Maxwell stress tensor around the boundry of the specified region.

$$F_\alpha = \int_S \sum_\beta T_{\alpha\beta} n_\beta da \qquad \text{(pg 239 Jackson)}$$

where S is the surface bounding the region. Since poisson is two dimensional $\vec{n}\cdot da = (dy,-dx,0)$

$$\vec{B} = (B_x, B_y, 0)$$

$$T_{\alpha\beta} = \frac{1}{4\pi}\left[B_\alpha * B_\beta - \frac{1}{2} B*B*\delta_{\alpha\beta}\right]$$

$$F_x = \frac{1}{8\pi}\oint \{(B_x^2 - B_y^2)dy - 2B_x * B_y dx\}$$

$$F_y = \frac{1}{8\pi}\oint \{2B_y B_x dy + (B_x^2 - B_y^2)dx\}$$

where the contour is the curve bounding the surface of the region.

The value of B_x and B_y are computed from the vector potenial stored by Poisson.

The four sections of iron and the two coils, identified as the areas of interest, correspond to the regions shown in figure 2. The results for these regions are given in table 2.

In the case of region 1 the force studied was that on the bolts which anchor this region to the cap (region D). The plan is to preload these bolts to 120% of the maximum operating force, by heating the bolts while they are being tightened. The effective area of each bolt is given by:

$$A_t = \pi\left(\frac{R}{2} - \frac{0.16238}{N}\right)^2 \qquad A_{hole} = 11.0471 \text{ inch}^2$$

$$N=6 \quad R=3.8788 \qquad A_{hole} = \pi\left(\frac{3}{2.4}\right)^2 = .4418$$

Z\R	B(0)	B(12)	B(24)	B(36)	B(48)	B(60)	B(72)	B(84)	B(96)
60.	0.00	1.08	4.42	5.47	8.18	4.75	1.92	0.954	1.09
72.	0.00	1.34	2.69	3.56	4.94	3.29	2.26	1.09	1.40
84.	0.00	0.90	1.72	2.32	6.26	3.10	1.82	1.28	1.11
96.	0.00	0.59	1.11	1.47	1.63	3.40	1.71	1.10	0.83
108.	0.00	0.39	0.74	0.98	1.09	1.07	1.01	0.93	0.71
120.	0.00	0.27	0.50	0.67	0.77	0.78	0.74	0.78	0.59
132.	0.00	0.18	0.35	0.48	0.55	0.58	0.56	0.52	0.50
144.	0.00	0.13	0.25	0.35	0.41	0.44	0.50	0.43	0.40
60.	7.72	1.08	9.23	6.71	5.22	-0.06	-1.37	-.12	-.16
72.	6.79	6.96	6.03	4.54	1.98	0.70	-.07	-.16	-.44
84.	4.71	4.56	4.00	3.18	1.10	0.96	0.25	0.05	-.15
96.	3.21	3.10	2.73	2.18	1.54	1.16	0.57	0.20	0.62
108.	2.21	2.14	1.91	1.56	1.15	0.75	0.45	0.33	0.14
120.	1.55	1.50	1.35	1.14	0.88	0.63	0.40	0.30	0.17
132.	1.09	1.06	0.97	0.83	0.66	0.49	0.34	0.21	0.14
144.	0.78	0.75	0.69	0.60	0.92	0.38	0.28	0.19	0.12

Table 4, Computed fringe fields at maximum excitation.

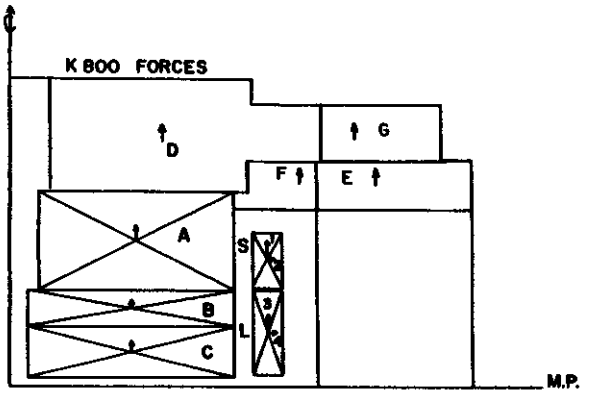

Fig 2. The regions refered to in tables 1 and 2 are identified. Region 1 is the sum of A,B & C, 2 is the sum of B & C, while 3 is just region C.

If the yield strength of the bolt material is 'S' and allowing for a 10% error margin,

$\frac{S*A}{1.1}$ = Maximum force permitted on one bolt

Thus if F_m is the maximum magnetic force and F_g is the weight of region 1 (18 tons):

$$1.2*(F_m + F_g) = 3*S*A/1.1$$

$$F_m = \frac{3}{1.2} * \frac{S*A}{1.1} - F_g$$

So if S=900,000 lbs/in (new 4140 steel) F_m=1,112 tons, or if S=105,000 lbs/in² (4140 hardened to 250 brinel) F_m=1,300 tons. The limitations these two possible yield strengths would place on the operating currents are illustrated in figure 3.

The force on region 'D' ,the cap, was only calculated for the 3750,4000 case, the result being -1340 tons. It should be noted that this cap force is very similar in magnitude to the force on the pole root, so it is expected that the two should deflect similarly and thus not form a gap between the root and the cap. This deflection was calculated to be not more than 4 mils at the center of the magnet so it should not significantly alter the magnet gap or stretch the trim coil leads.

A couple of simple estimates of the force acting on a piece of iron in a magnetic field can be made if the iron is assumed to be saturated. As a first case place a piece of iron

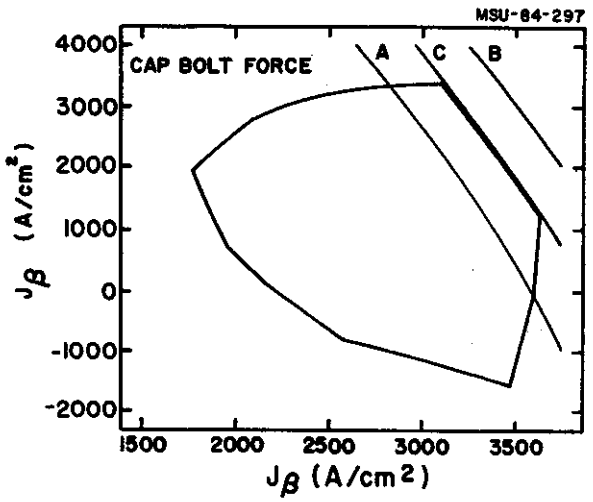

Fig. 3. The maximum allowable current settings assuming 3 different hardness of the steel for the bolts used to hold the pole root to the cap. "A" corresponds to a hardness of .9 Mlbs/in and "C" to 1.05 Mlbs/in.

in a solenoid with a B_0=5 T. If this iron rod is then moved a distance dx, as shown in figure 4, then the energy is changed by an amount:

$$\Delta U = -\vec{M}\cdot\vec{B}_0 * A * dx$$

where A is the cross sectional area of the bar and M is the saturation magnetization of the iron

$$\vec{P} = \frac{\vec{F}}{A} = \vec{M}\cdot\vec{B}_0 \qquad \vec{F} = -\vec{\nabla}\cdot U$$

$$B_0 = 5.0E4\ G \qquad M = 21.4E3/4\pi$$

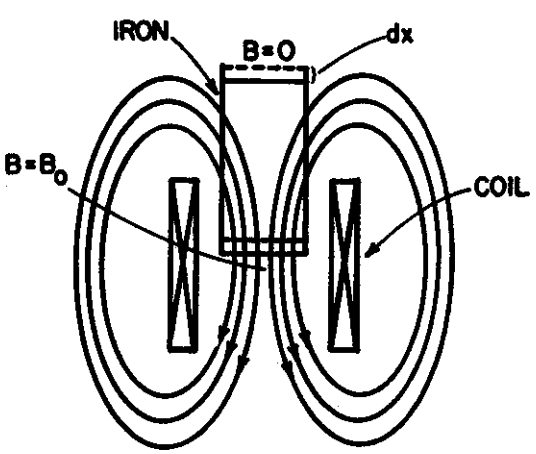

Fig. 4. A simple estimate of the force can be obtained by computing the energy change when a bar of iron is moved a distance dx into a field. One end of the bar is at zero field while the other end is at B_0.

$$P = 5*10^{4}*\frac{21.4}{4\pi}*10^{3} \text{ dynes/cm}^2$$

$$= 8.51*10^{7}*1.45*10^{-5} \frac{\text{lbs}}{\text{in}^2} = 1200 \text{ PSI}$$

In the second case we make use of more accurate values for the field above and below the part in question;

$$F = M\int\int(B_{top} - B_{bot})\, r\cdot d\theta\cdot dr$$

$$= 2\pi M\int(B_{top} - B_{bot})r\cdot dr$$

$$= 2\pi M\Delta r\{\sum_{i=1}^{n} \Delta B\cdot r_i\}$$

The term in { } can be computed from the appropriate poisson output. If B is in kG and r is in inches,

$$F = 2\pi*\frac{21.4}{4\pi}*.5\{\Sigma\}*(2.54)^2*10^6 \text{ dynes}$$

$$= \frac{21.4}{4}\{\Sigma\}(2.54)^2*10*\frac{2.2}{9.8}*\frac{1}{2E3} \text{ Tons}$$

$$= 3.9*10^{-2}\{-25840\} = 10^3 \text{ Tons}$$

This compares favourably with the first estimate since the pole radius is 42 inches and thus the pressure averages about 360 PSI, which acording to the first estimate corresponds to a delta B of 1.5 Tesla, the value given by "Poisson". At similar field levels the code "Force" computes 10^3 Tons.

MAPPING GRID

In reference 3 the Milan group reported that at low excitations the net axial force on the coils was away from the median plane. To check the magnitude of this force in our case during turn-on, field calculations were done along two possible turn-on lines. In one case the currents in the both coils were equal and in the other the current in the large coil was four times that in the small coil. The results of these computations are shown in fig 5. As can be seen the total force away from the median plane is never greater than 100 Tons, which it was

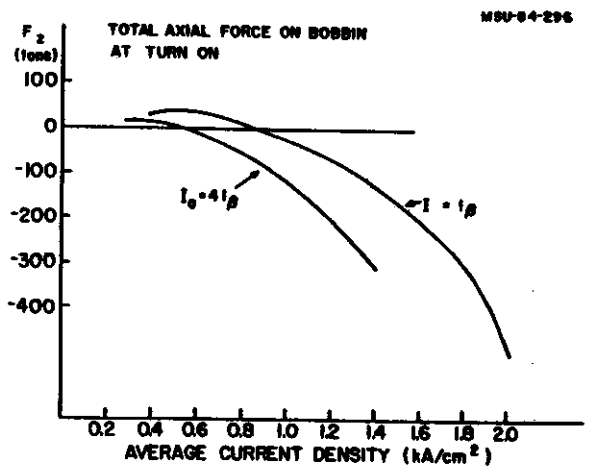

Fig. 5. At sufficiently low current settings the coils on either side of the median plane repel one another, but this force was deemed to be sufficiently small to be ignored.

felt could be easily handled by the existing bobbin structure. Since force considerations were deemed unimportant the turn-on line could be chosen to be orthoganal to lines of constant flux in the yoke which are characterised by $I_\beta - 4I_\alpha$ = constant. Thus a ramping procedure which would minimize hysterisis would be to travel up the line $I_\alpha = 4I_\beta$ until the appropriate flux level is reached and then travel along the constant flux curve to the desired current setting.

The mapping points were selected to lie on a regular rectangular grid and to make the transition from one point to another by the afore mentioned presciption easy. Thus one axis of the grid is a constant flux line and the other is prependicular to it. The grid shown in figure 6 is the result of these considerations, and trying to keep all the mapping points within the safe operating limits. A couple of points do not lie on the regular grid since those points lie outside the "safe region". The intention is that these points will be used to extrapolate the regular points which will then only be used to interpolate for points in J_α, J_β space inside the mapped points.

ENLARGED GRID

As can be seen in figure 1 the relaxation

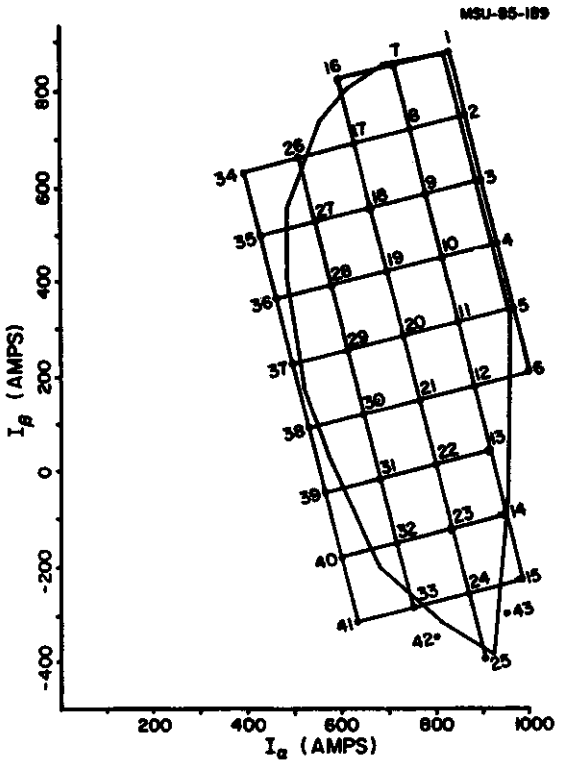

Fig. 6. Shown are the current settings at which full field maps will be made.

num	I alpha in Amps	I beta in Amps
1	833.	884.
2	887.	749.
3	901.	613.
4	935.	478.
5	969.	342.
6	1,003.	207.
7	716.	855.
8	750.	719.
9	783.	584.
10	817.	448.
11	851.	313.
12	885.	177.
13	919.	42.
14	953.	-94.
15	987.	-229.
16	598.	826.
17	632.	690.
18	666.	554.
19	700.	419.
20	734.	283.
21	767.	148.
22	801.	12.
23	835.	-123.
24	869.	-259.
25	903.	-394.
26	514.	861.
27	548.	525.
28	582.	389.
29	616.	254.
30	650.	118.
31	684.	-17.
32	718.	-153.
33	751.	-288.
34	397.	631.
35	430.	496.
36	464.	360.
37	498.	225.
38	532.	89.
39	566.	-46.
40	600.	-182.
41	634.	-318.
42	800.	-350.
43	950.	-300.

Table 5, The current settings corresponding to the points shown in fig. 6.

grid used in the bulk of these calculations contains some rather crude approximations to the real physical magnet structure. To check the validity of the force calculations the computations were repeated at two current settings using an enlarged grid (fig 7). This larger grid contains 17,500 relaxation points as compared to the 3,441 points in the smaller grid, and requires about ten times the cputime

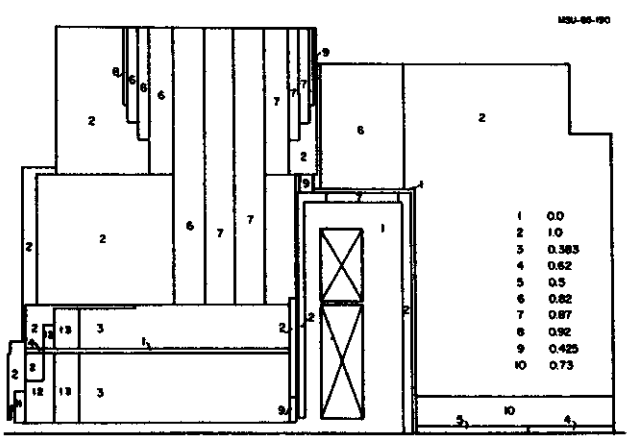

Fig. 7. The lattice used for the enlarged "Poisson" cases. Compare with figure 1.

(12 hrs). In order to accomodate this large number of grid points and region numbers a new version of "Poisson", capable of 124 regions and 40,000 points, was created. In this enlarged grid large holes, such as the dee stems, have have been broken into regions with different stack factors to compensate for the variation in the ratio of the air to iron in a given ring. Special attention was paid in getting the iron geometry near the upper inner corner of the coil tank correct since most of the force on the pole base is generated in this region. As can be seen in figure 8 the flux lines are very similar except in the dee stem region and at the corner of the cryostat, exactly the areas poorly represented in the small grid. The effective straightening of the flux lines probably accounts for the observed difference in the forces on the four inch bolts. The subtle difference in these two grids suggests that all force calculations should be used with large margins for error.

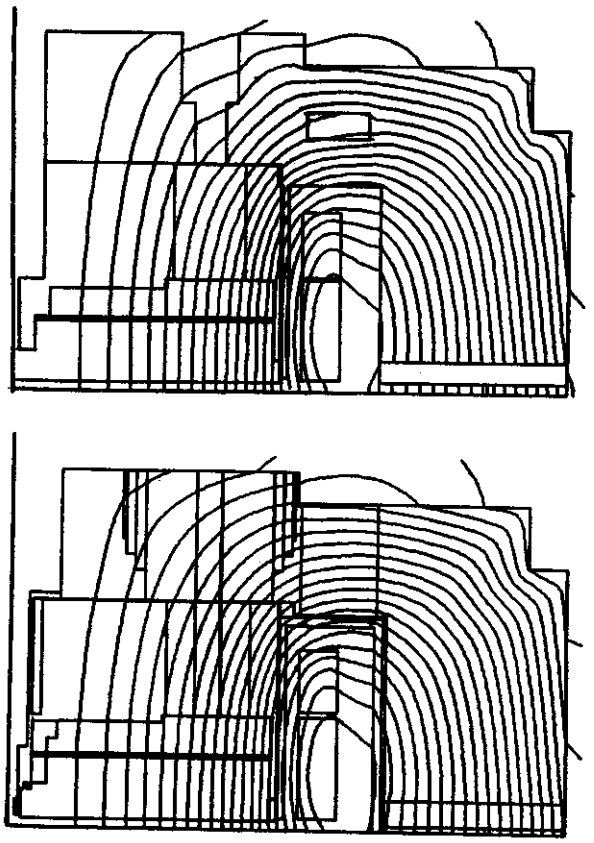

Fig. 8. A comparision of the computed flux lines between the small and large lattices. Qualitativly they are very similar, but the lower one (the large grid) is better behaved in the upper right corner of force region "C".

STANSOL

To determine the point at which there is a danger of the wire in the coil not being under sufficient compression to prevent axial motion of the wire the code "STANSOL" was used. This program computes the effects of cooling, preload, and axial field on a collection of materials representing a slice through the coil at a fixed z. The values of the field in the coil as calculated by "Poisson" was used as input data for Stansol. This allowed a full Stansol calculation to be preformed at 14 different z positions in the coil for each of the possible coil excitations. The stress results for the 3750,4000 point at several z values are shown in figure 9. From this it is already apparent that the coil cannot be run at 3750,4000.

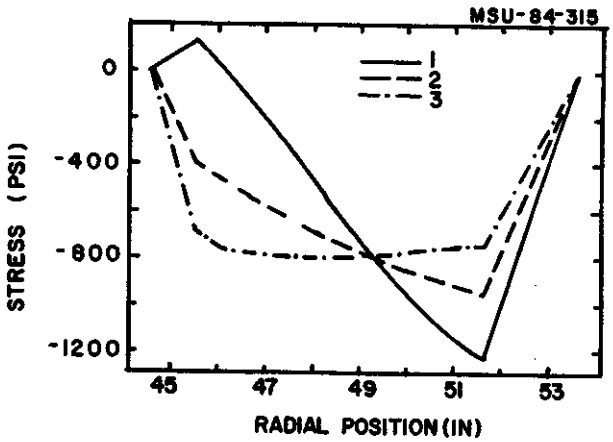

Fig. 9. The radial stress on the wire as a function of radial position in the coil, for 3 different axial positions.

The code "DSTORE" was then used to sort all this data and store it in a single file. This program also computes the net axial force at each data point and stores the result along with the rest of the data. The net axial force is defined as:

$$F_n = F_{fric} - |F_z|$$

where if, $F_r < 0 \quad F_{fric} = \mu * |F_r|$

$$F_r \geq 0 \quad F_{fric} = 0 \ ,$$

F_r = radial force

μ = coefficient of friction between conductor and G-10 pickets

and, $F_z = I * B_r * 5.71 * 10^{-7}$

It should be noted that this formulation does not result in F_n being the unbalanced force. The value for F_{fric} given above is actually the maximum possible value the friction can assume. If this value is greater than the axial force then the real unbalanced force is zero whereas this definition of F_{fric} gives a positive result. The advantage of this method is that the positive value can be used to find the critical point by interpolation. If the value of F_n is less than zero then the critical point has been

passed, but in either case the sign of F_n says nothing about the direction of the axial force.

To plot this data the program "FPLOT" was written, which will plot contour lines in various subsets of the data. For example it will find the maximum or minimum of any of the 4 variables at each excitation level, and then plot 10% contours in this data as seen in J_α, J_β space. This aids in locating the extreme cases as a function of current settings. This type of output is shown in figure 10. The program will also plot contour levels in any of the 4 parameters for a given current level as a function of position in the coil to help localize where the extreme values are coming from, as shown in figure 11 from which it is obvious that the corners of the coil are the difficult regions. Figure 12 shows the contour in J_α, J_β space along which the maximum frictional force on the wire, for three different values of the coefficient of friction (which is uncertain), is equal to the magnetic axial force on the wire, at some point in the coil.

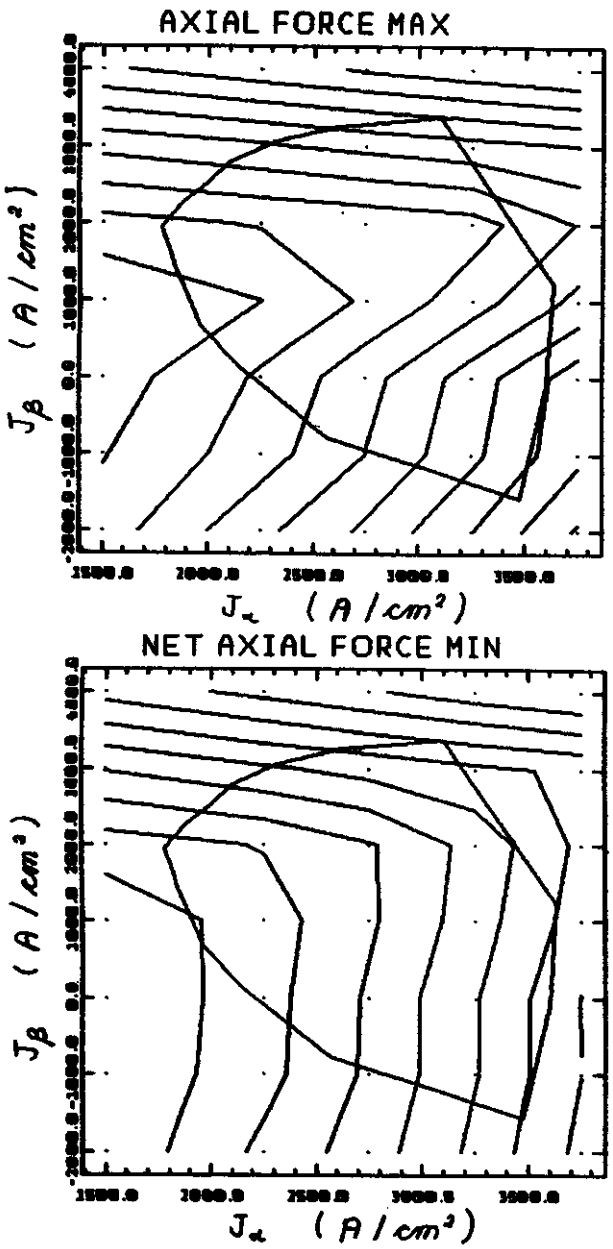

Fig. 10. Examples of the contours in J_α, J_β space produced by the code "Fplot". Shown here are minimum net axial force for all r,z combinations at a current setting, and the maximum axial force. Note the relationship between the two as the currents get high.

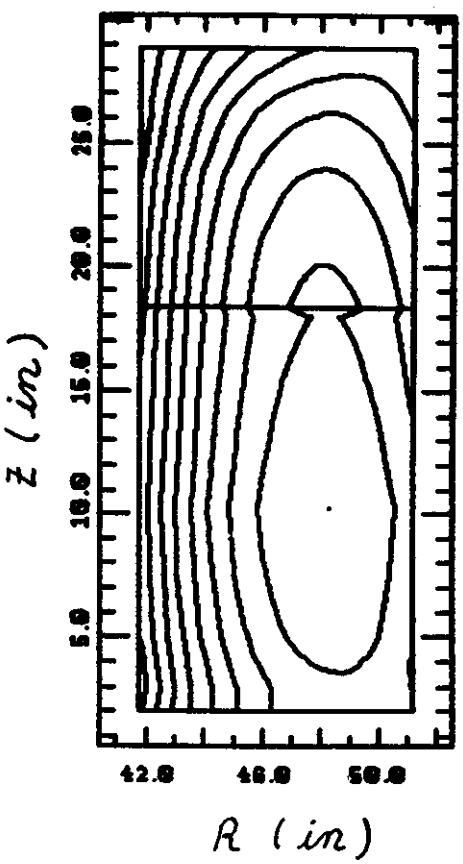

Fig. 11. Contours in an r,z slice through the coil, of the net axial force. The current settings are 3750,4000 and the coefficient of friction is (.22). Note the upper inner and lower inner corners are the least stable points in the coil.

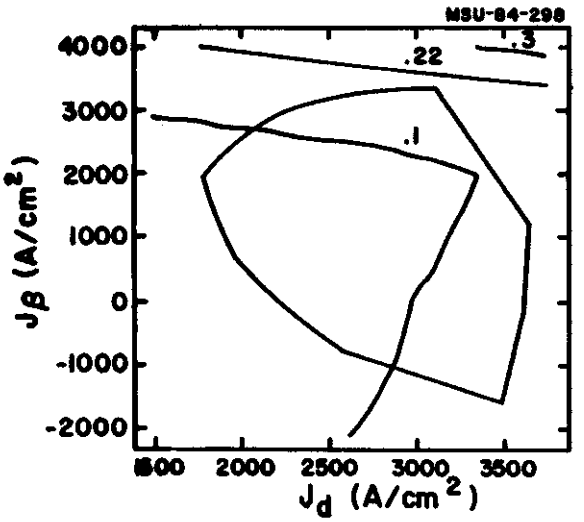

Fig. 12. Contours showing the current settings at which the net axial force (see text for def.) on the wire is zero at some point in the coil, for 3 different values of the coefficient of friction. The best available number for the coeffient of friction of solder coated copper on G10 is (.22).

Conclusions:

As expected the forces are most extreme for the high excitation cases. Initially values for the pole forces were larger than expected but crude estimates suggest that they are reasonable. As shown in plots 9 and 12 the preloading of the coil becomes insufficient as the currents approach the 3750,4000 amp/cm^2 point thus preventing the magnet from running at this high excitation. The forces on the cap bolts,shown in figure 3 , become quite large at the upper end of the operating region so care should be taken when approaching this region.

---

1. A.M. Winslow, Journal of Computational Physics 2,149-172(1967).
2. L.H. Harwood and D. Johnson, Procedings of the Tenth International Cyclotron Conference, F. Marti, ed., (1984) pg 99.
3. E. Fabrici, Istituto Nazionale Di Fisica Nucleare report TC-82/10.

CALCULATIONS OF THE HARMONIC COMPENSATION OF THE K800 FIELD DUE TO YOKE MEDIAN PLANE PENETRATIONS

L.H.Harwood

In the extraction region of the cyclotron it is important that the magnetic field have little or no first or second harmonic. This is nearly true for the K500 but could possibly be improved. The requirement is stricter for the K800 and thus a better understanding of the coupling between iron distribution and field distribution may lead to the desired result.

Iron on the median plane of the cyclotron can be magnetically modelled by bars of magnetization. The field at any point in space due to these bars is simply a linear superposition of the fields from each bar. If all bars are magnetized uniformly, then the spatial distribution of the field depends only on the spatial distribution of the bars. One can easily show that a sufficient condition for no amplitude of the "n-th" fourier component in the field is that there is no amplitude of the same fourier component in the iron distribution (with both analyses using the same origin). One can also show that it is possible to make an amplitude small at a particular radius with finite values for that term in the iron distribution if the iron values at different radii serve to cancel each other at that field radius; the latter was the procedure used for the K500 magnet.

To apply the former procedure to the K800 magnet, the median plane penetrations were divided into two groups, 3" holes and 10" holes (total height). The 3" holes were treated together with the central 3" of the 10" holes. The upper(lower) 3.5" sections of the 10" holes were treated separately. The idea was to remove the 1st and 2nd harmonics in the iron distribution (fourier analysis centered on the axis of the magnet) at all radii and thereby ensure that the iron would contribute no 1st or 2nd harmonics to the field. One can do the compensation in several ways. One can treat all the holes together (weighting by height), use two holes for compensating the first and second harmonics together, or correct the two

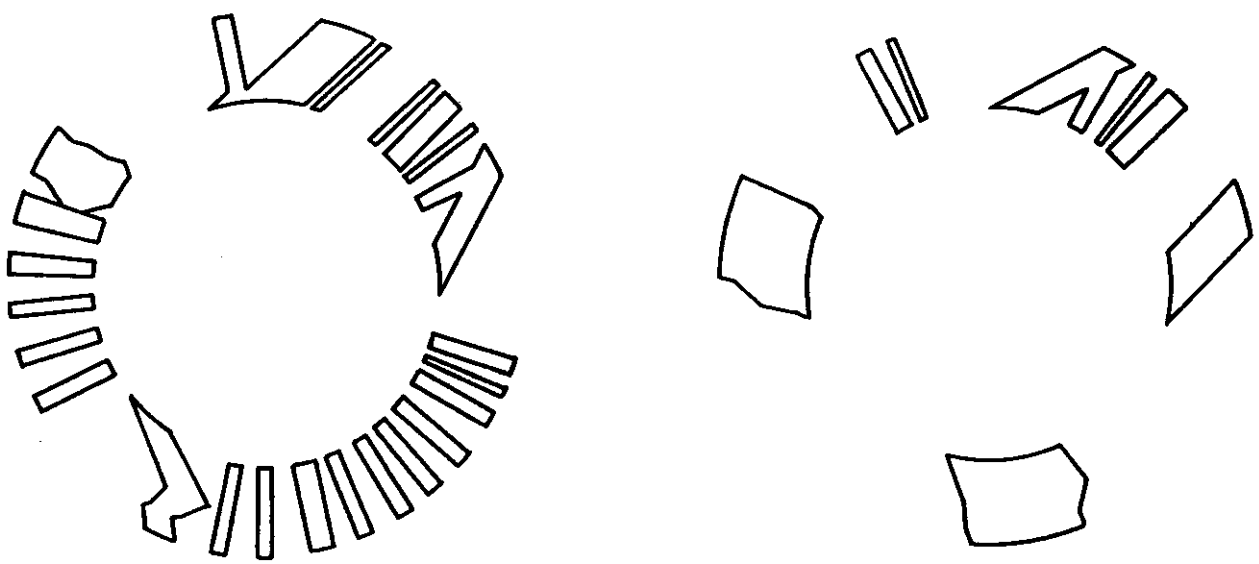

Fig. 1 Plan view of penetrations in K800 magnet median plane. Penetrations have no 1st or 2nd harmonic components. On the left are shown penetrations extending from Z=0" to Z=±1.5" and on the right are those from Z=±1.5" to Z=±5".

separately with three holes. The best compensation is achieved by treating the different "layers" separately and the least iron is removed with three holes. With these choices, it is straight-forward to do the compensation, but tedious; thus, an interactive program was written to ease this process.

The resulting set of penetrations for the K800 median plane are shown in fig 1). The majority of the holes have straight sides. Only two in each layer were permitted to have non-straight sides. The level of compensation in the field was rather sensitive to the accuracy of the curves used to approximate the holes in the field calculations. Thus, the final shape of the compensation holes will be reached with a balancing of the desire for small harmonics and the desire to machine the parts. This process will be repeated after the final injection/extraction designs are finished and the final set of penetrations are known.

CURRENT STATUS OF THE K800 RF

J. Vincent, J. Ottarson, J. Brandon, D. Scott

1. Introduction

The K800 rf system has progressed from the original sketches, concepts, and geometries to the highly optimized designs currently being detailed, fabricated, or finalized. Early in this period, we were forced to re-design and re-build the final resonator of the K800 amplifier. Fortunately, we were able to directly implement the major components from the old design into the new design. Another problem encountered this period, involved the 1.2 MW final anode D.C. power supply we purchased. The main transformer and enclosure were poorly designed. Two attempts to repair it failed, and we were forced to retain an adequate amount of the purchase price to address the problem ourselves. During the last period we also optimized the dee resonator design, and successfully achieved a 35% reduction in I**2*R losses over the original design. The design and construction of the rf control electronics has also progressed nicely. This paper will briefly describe the current designs and status of these projects.

2. Basic System Definition

The K800 rf system consists of three linear 250 KW rf amplifiers strings along with the necessary control/regulation electronics, interlock systems, and power supplies. These amplifiers feed a cluster of three half wave resonant cavities on the K800 cyclotron. The operating frequency band of this system is from 9 to 27 MHZ. The basic electrical model of each of the cyclotron resonant cavities consists of 2 capacitively loaded quarter wave coaxial resonators connected together at the high voltage node (dee shells). This effectively produces a halfwave resonator with the maximum voltage occurring at, and symetric about, the center or median plane as desired. Each of these quarter wave resonators contain a uniform coaxial section 135 inches long with a sliding short. The resonant frequency of the half wave structure is then adjusted by symetric positioning of the upper and lower sliding shorts. The structure is further fine tuned and the input coupling held matched by hydraulically positioned planes electrically connected to the central region rf liner. These planes face the upper and lower shells of the dee and allow a variable capacitive reactance. Energy is coupled to each half wave structure capacitively with a probe inserted into a cup in the lower dee shell. The probe is hydraulically positioned within the cup to acheive exactly the correct capacitance to yield an input impedance to the half wave structure which is 50 Ohms and real. The cup and probe are designed to yield the correct range of capacitance (as a function at probe location within the cup) to couple over the required frequency band while maintaining the surface electric fields at a minimum.

When the system is tuned and matched, the phase between the transmission line side of the input coupling capacitor and an r_f signal obtained from a small loop on either of the two sliding shorts is approximately 0 degrees. This phase relationship is nearly perfect due to the high Q of this cavity, and is exploited to regulate the input coupling. The signals, mentioned above, are phase detected against one another, and the resulting error signal, which is generated, is used to closed loop actuate the previously described dee fine tuning capacitors.

Each of the half wave cavities is capacitively coupled to its two nearest neighbors in the center of the median plane where the adjacent dee tips can see one another. To allow independant voltage and phase adjustments on each system, and to remove the cross talk between regulation loops from system to system; the capacitance from system to system

must be nuetralized out. The nuetralization is accomplished by calculating the equivalent dee to dee capacitance transformed up and out of the resonator vacuum region where it is mechanically and electrically feasible to address it. Loops are then inserted in this location and they are connected to adjacent stem loops with a short section of coaxial transmission line. The loops are rotated to couple just enough into the rf magnetic field to circulate exactly the same amount of energy that the dee to dee capacitance transformed to this point on the stem would. When these loops are adjusted properly each system is almost perfectly isolated from one another. Although perfect neutralization can only be achieved (in a system such as this) if the system were lossless , we have a high enough Q to allow us to neutralize much better then is actually necessary.

The rf system will be completely tuned from either of two locations. All controlled axes will be tunable from the rf console. These axes may be adjusted at each individual control module or from a local control computer console. Some of the rf controls will also be controlled from the main control room to efficiently tune and extract the various beams from the cyclotron. The signals that will also be controlled from the main control room console are: 1)Individual Dee Volts, 2)The Dee to Dee phase, and 3)The referance position for the Dee fine Tuners. All of the rf status signals, such as spark indicators, over currents, etc., will also be available to the cyclotron operators in real time displays at the main control console.

This last section has basically described the rf system currently being put in place. We expect the entire system from controls and status displays thru each amplifier power string to be in place by December 1985. The Dee resonators will be ready shortly there after. Refer to Fig 1. for more information about this system.

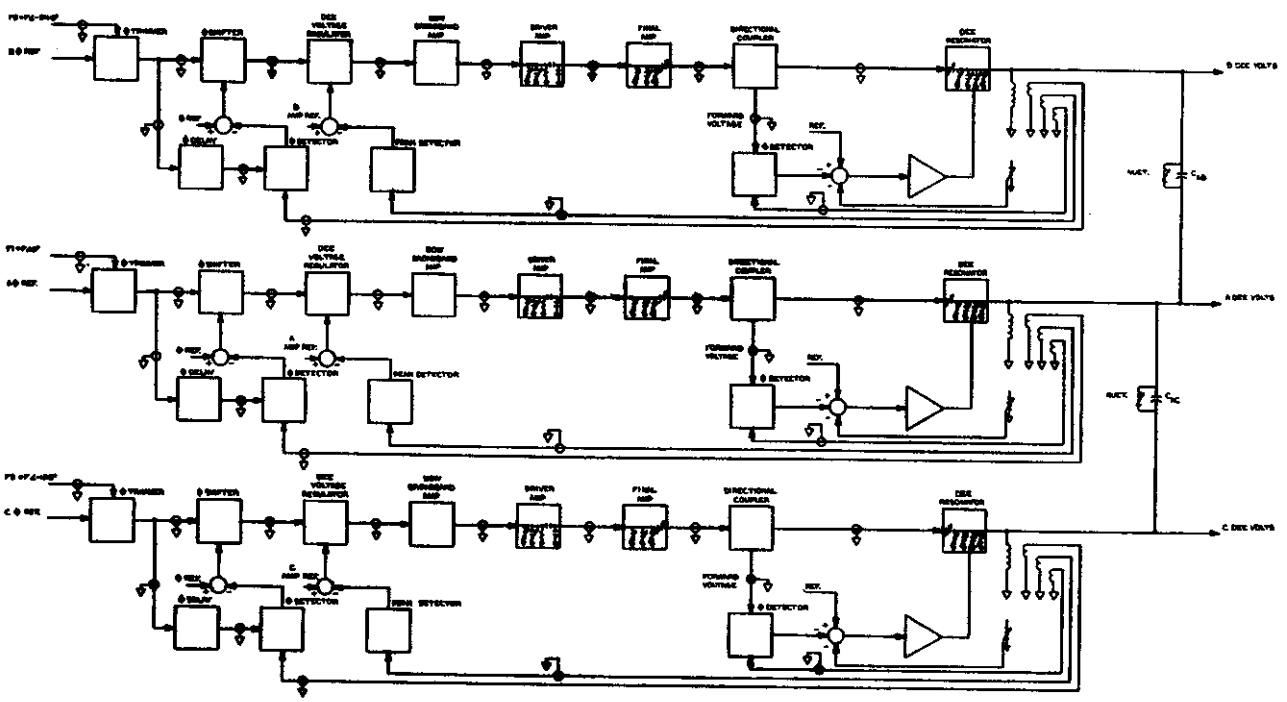

Fig. 1 Simplified systems diagram of the K800 rf showing amplitude, phase, and matched input coupling regulation loops.

3. RF Amplifiers

The K800 final amplifier string is in the final stages of developement. This amplifier consists of three stages: 1)a purchased broadband 50 watt amplifier, 2)a driver stage, and 3)a final power stage.

The driver stage is a class AB amplifier which uses 2 Eimac 4CW2000 water cooled tetrodes, operating in tandum, as the driving elements. The anodes of these tubes are coupled to a tank circuit which includes the grid to cathode capacitance of the final tube as one of the reactive elements. The Q of this driver is held basically constant by a water cooled 1200 Ohm resistor inserted in shunt.

The final stage uses a RCA 4648 tube as the driving element operated in class C. The grid of the 4648 tube is swamped to 50 Ohms by a small water cooled load. Stability is further enhanced with degenerative feedback from the anode tank circuit via a small capacitive pickup plate. The signal from this plate is fed back to the grid of the 4648 by a short length of transmission line coupled to a DC blocking capacitor at the grid. The final anode tank circuit consists of a quarter wave, non-uniform, coaxial resonator. Tuning of this tank circuit is accomplished with a sliding short. Coupling from this tank to the 50 Ohm transmission line is done by a single variable capacitor. We refer to this method of coupling as "loose coupling".

Although loose coupling to the transmission line is mechanically simple, it has the drawback that in the limit as the frequency approaches infinity the coupling approaches unity. This is undesirable because the small harmonic content inherently present in a cavity resonator, when class C driven, becomes more pronounced on the transmission line. Although the higher harmonic standing wave ratio thus generated is normally of little consequence, it is desirable to hold it to a minimum. One can reduce this ratio by inserting another larger capacitor to ground immediately following the coupling capacitor. This new arrangement approaches the ratio of coupling capacity to capacity to ground in the limit as the frequency approaches infinity.

Irregardless of what form of coupling to the transmission line we choose, the K800 amplifier is basically complete. The prototype has delivered 250 KW at 27 MHZ and over 130 KW at 9 MHZ. The calculated queiscent need for each dee resonator is 190 KW at 27 MHZ and 30 KW at 9 MHZ. We therefore have more than adequate amounts of power available to closed loop regulate the Dee voltages at any required levels. The mechanical departments will have both of the other amplifiers fabricated and assembled by late 1985. Refer to figures 2 through 5 for more information pertaining to the K800 rf amplifier.

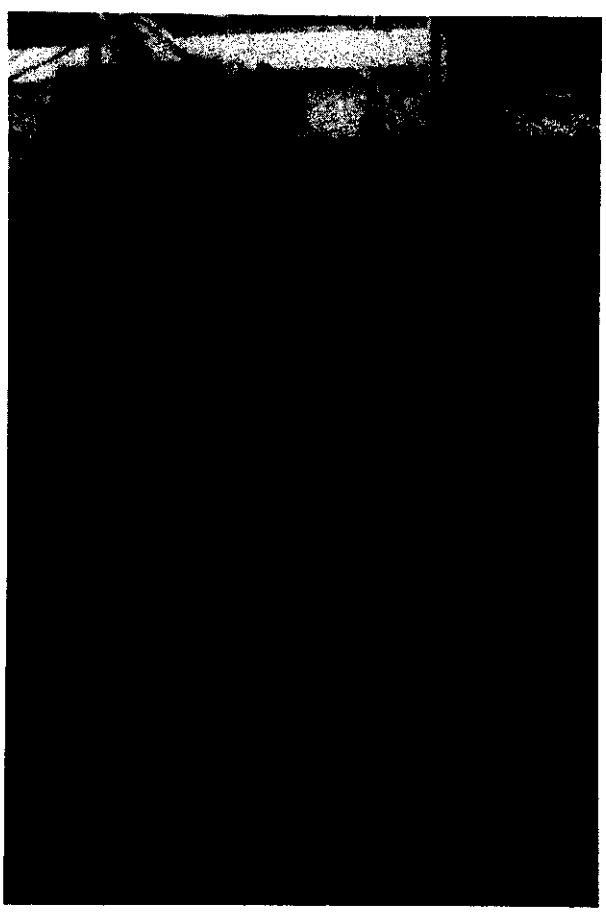

Fig. 2 Picture of the exterior of the prototype K800 rf amplifier.

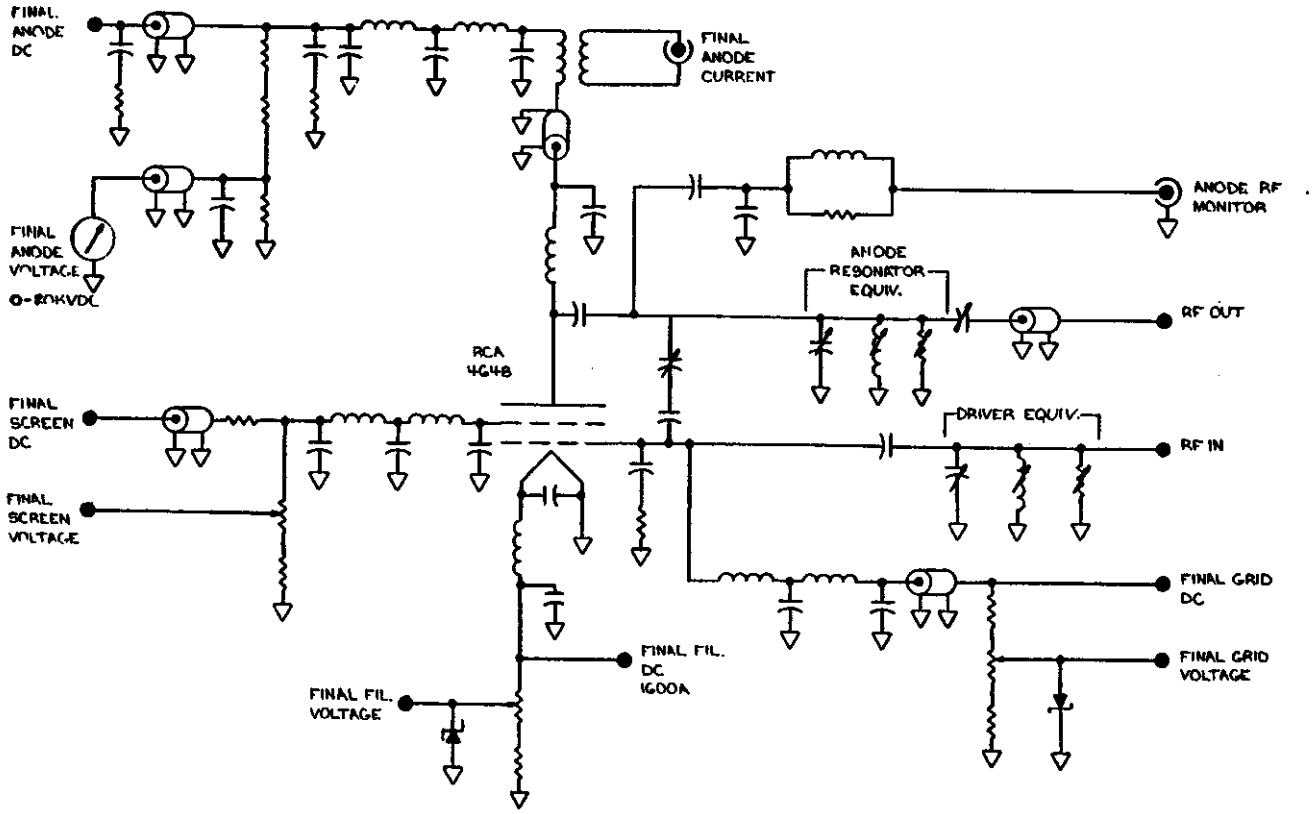

Fig. 3 Electrical schematic of the prototype K800 final amplifier.

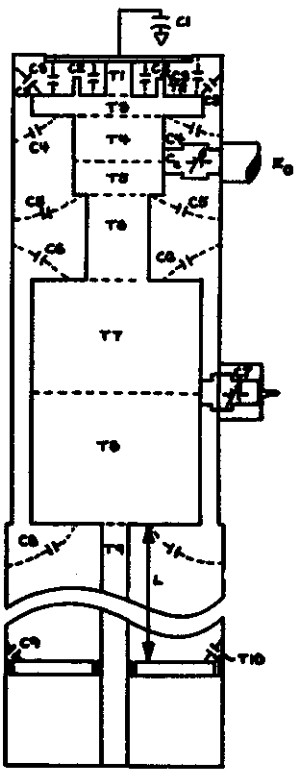

Fig. 4 Basic mechanical detail of the prototype K800 final amplifier tank circuit showing transmission line sections and discontiniuty capacitances.

4. 1.2 MW D.C. Power Supply

This power supply is designed to supply 20 KVDC @ 20 ADC to each of the three rf final amplifiers. We have had various problems with this supply since we accepted delivery. The problems involved: 1)The step start time constant was incorrect, 2)The crowbar circuitry did not function correctly, and 3)the outdoor rectifier and transformer tank was poorly designed and failed our power tests twice. The manufacturer spent some time here correcting items 1 and 2. But, after two attempts at repairing the transformer, mentioned in item 3, we felt the manufacturer was unable to deliver this portion of the supply in a reasonable time frame and condition. We have since accepted a Bid from an alternate manufacturer to build a suitable transformer and enclosure, and another manufacturer has bid on building yet another enclosure to house the rectifier, inductor, and snubber networks. Since we retained an adequate

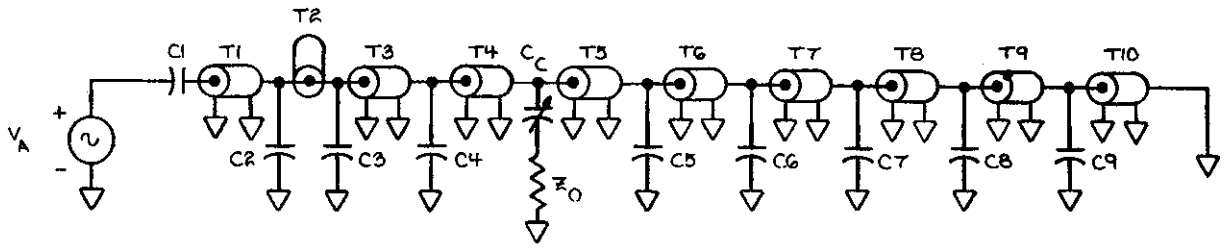

KEY				
NUM.	DESCRIPTION	SIZE		
		A	B	C
T1	ANODE EQUIV. OF 4648 TUBE			
T2	ANODE DC BLOCKING CAPACITOR			
T3	FIRST LOW Z SECTION	26	30	3
T4	TRANS. LINE	14	30	8
T5	TRANS. LINE	14	30	4
T6	HIGH Z SECTION	9	30	13
T7	LOW Z SECTION	26	30	18.25
T8	LOW Z SECTION	26	30	18.25
T9	SLIDING SHORT	4.125	32.5	L
T10	FINGER CONTACT SECTION			
C1	OUTPUT CAPACITY OF 4648 TUBE			
C2	ANODE COUPLING PLATE TO GND CAP.			
C3 C4 C5 C6 C7 C8 C9	JUNCTION CAPACITANCES			
CT	FINE TUNING AND HARMONIC SUPPRESSOR CAP. (0-250PF)			
C_C	OUTPUT COUPLING CAP. (0-75PF)			
Z_O	TRANS. LINE TO DEES			

NOTES: SIZE IS IN INCHES

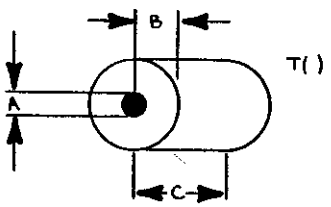

Fig. 5 Electrical equivalent of Fig. 4 used for design and analysis of the cavity modes.

and fair portion of the original purchase price, we are out nothing but a little time. We currently plan to have this supply up and running by mid July. If all goes well, the supply should be fully tested and ready for operation by mid August 1985.

5. Electronics

The electronics designed and built by us for the K800 rf system consist of the following types and quantities of circuits.

(1,133 MHZ Oscillator Mixer),(1,135 MHZ Oscillator Mixer),(1,4 Channel 50 MHZ Low Pass Filter),(1,4 Channel Rf Pre-Amp with AGC),(2,2 Channel Rf Amplifier),(1,4 Channel Signal Splitter),(1,4 Channel Quadrature Hybrid),(1,3 Channel Signal Splitter),(7,10 Channel Signal Buffer/Line Drivers),(1,Frequency Synthesizer),(1, 15 Volt @ 6A dc power supply),(1,-15 Volt @ 6A dc power supply),(1,24 Volt @ 4A dc power supply).

Two of the above group of electronics are built and tested. One of these will be used to upgrade the K500 rf system and the other is for the K800 rf system. This group of electronics is refered to as "The Frequency Generation and Distribution System".

(15, Mixer/Phase Detectors),(3, Phase

Trimmers),(3, Fast Phase Shifters),(3 Dee Voltage Regulators)

The prototype Fast Phase Shifter and Prototype Mixer/Phase Detector are currently being developed. The Dee Voltage Regulator and Phase Trimmer have not been started yet,but they are basically copies of what is used on the K500 and should therefore be simple and quick. This group of electronics allows the operators to adjust the individual dee voltage levels and dee to dee phases from the main or local control consoles. This group also accomplishes the closed loop regulation of these values. We expect all the electronics in this group to be fabricated by Dec. 1985.

(3, Mixer/Peak Detectors),(3, V+/V- Modules),(3, Voltage Limiters),(3, First Event Detectors),(3, Multichannel Spark Detectors),(1, Fast Trip Chasis)

The above group of electronics is responsible for the rapid turn off of the rf in the event of a multitude of possible problems. The Voltage Limiter also adjusts the ramp on time of the rf. The Mixer/Peak Detectors are due for assembly when parts arrive. The V+/V- modules and the Multichannel Spark Detectors are built. The Fast Trip Chasis and First Event Detectors will be initiated shortly and should be done by Dec. 1985.

(33, DC Motor Contollers),(6, Hydraulic Motor Contollers),(39, Local Motor Controllers)

The above group of electronics are responsible for all motion control. This includes transmitter tuning, Dee Fine Tuner actuation, Input Coupler actuation, etc. The prototype DC motor controller is currently being tested. The hydraulic motor controller prototype has been developed. We are currently waiting for PC artwork to be done and parts to arrive to assemble all of this. The DC motor controllers actuate P.W.M. amplifiers supplied by an outside vendor, while the Hydraulic Motor Controllers actuate Atchley Hydraulic Valves which in turn drive hydraulic pistons. Again we are looking at a Dec. 1985 due date for the majority of these electronics to be coming out of fabrication.

Aside from the above groups of electronics,a few "One of a Kind" type devices are also needed. These are already initiated and partially built or developed. Basically the electronics portion of this project has been and is on schedule. Whether they are all done by Dec. 1985 is not particularly important,as they will not be needed in total until probably mid 1986.

Also above and beyond all of the aforementioned electronics we have the major DC power supplies to contend with. These are:
(1, "DA2" 3 channel 3KVDC @ 6A total and 3 channel 1KVDC to 1.6KVDC @ 5A total),(1, "Ayden Power Supply" 2KVDC @ 60A total), (Various Screen and Grid DC power supplies).

The DA2 is built and running and only needs some regulator boards to come out of assembly and be installed to be completed. The Ayden Power Supply status has been described in another section of this report. The various Screen and Grid Supplies are purchased and in stock.

As can be seen,this portion of the rf project is heavily in progress.

6. DEE RESONATORS.

These resonators are basically described in sections 1 and 2 of this report. Just to recap some of the information contained there. They require (calculated values) 190KW @ 27 MHZ and 200 KVdeepeak and 30KW @ 9 MHZ and 100 KVdeepeak per each of three complete half wave resonators. We have spent alot of time and study optimizing the design of these resonators and are now proceeding with the mechanical detailing in preparation for fabrication and assembly. The panels used for the outer conductor of the 135 inch sliding short sections are fabricated and in stock. The Mechanical Engineering Department currently projects a completion date for assembly of mid 1986. Figure 6 basically displays the mechanical detail of one of the quarter wave sections. Remember two of these

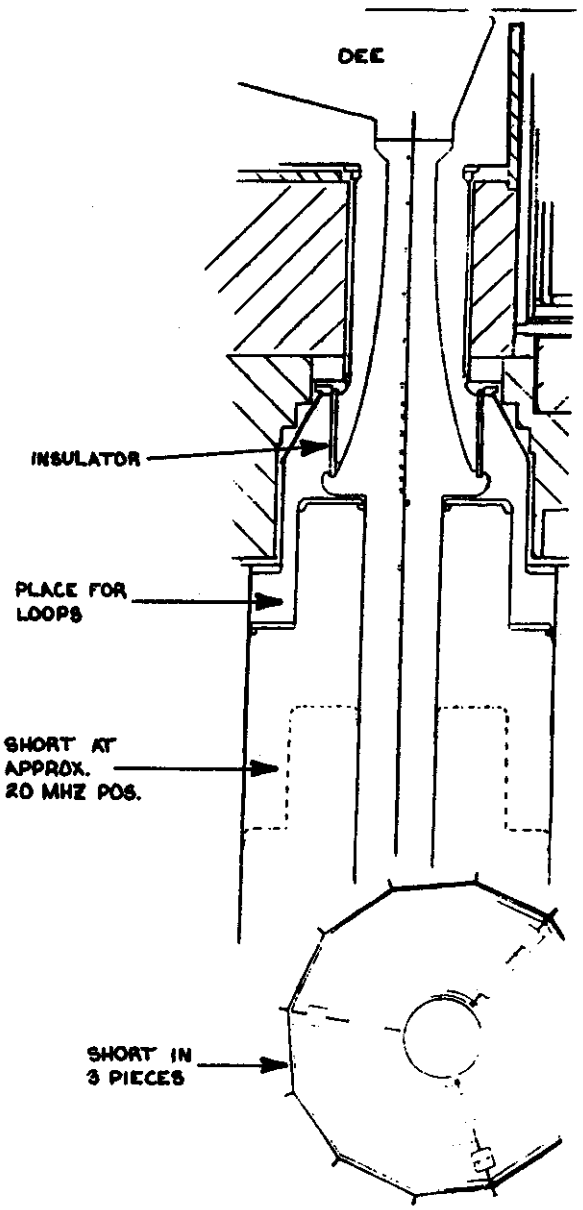

Fig. 6 Basic mechanical sketch of a lower quarter wave dee resonator.

quarter wave sections coupled together at the dee shells make one complete half wave resonator.

7. Conclusion.

This is a rather massive and complex project. A great deal of work has gone into this project to get us to where we are now, and alot more is yet to come. We believe if the design,construction,and development continues at the pace we are now experiencing, this project should basically be completed by late 1986 as projected.

NICKEL PLATING THE K800 CRYOSTAT

J.A. Schmid, J.S. Counseller and H. Hilbert

Vacuum specifications for the operation of the cyclotron require that materials with low outgassing rates be used for the vacuum chamber. Nickel plated steel offers both corrosion protection and outgassing rates that are considerably lower than clean non-oxidized steel. For this reason it was decided to nickel plate the inside surface area of the cryostat.

Investigation into the various methods for nickel plating was done in order to determine the most efficient and practical procedure. Nickel plating can be applied to steel by using electric current (electroplating) or autocatalytic depostion (electroless). the size, delicate nature and lack of industrial facility large enough to handle the cryostat ruled out the most widely used method of electroplating, where the part to be plated is completely immersed in a large tank containing the plating solution. Brush plating or selective electroplating was the method used for the previous cyclotron's (K500) cryostat and it proved to be inefficient with respect to the time it took to complete.

The electroless nickel plating process employs a chemical reducing agent (sodium hypophosphite) to reduce a nickel salt in a hot aqueous solution and to deposit nickel on a catalytic surface. The deposit obtained from the electroless nickel solution is an alloy containing from 2 to 15% phosphorus and is quite hard. Because the deposit is independent of the current distribution, it is uniform in thickness, regardless of the geometry or size of the surface to be plated.

Typical operating conditions for commercially available electroless baths are as follows: the temperature at which the chemical reduction can take place is in the range of 160° to 200° (F); the chemical composition depends on the particular bath used, although the concentration of reagents must be maintained by frequent additions during the plating process. The bath loading is the ratio of surface area to bath volume and is in the range of 0.1 to 1.0 (sq.ft./gal.). The rate of deposition under typical conditions is approximately 0.4 (mil./hr.).

The cryostat is made of two vertical concentric cylinders with a top and bottom plate which form a closed cavity between the cylinders while open through the center. Because the inner cylinder's inside surface is the only one that requires plating, the cryostat was used as its own plating tank by covering the open area at the bottom and filling the vessel with plating solution. It was apparent that completely filling the vessel would not yield the correct loading value. A third vertical cylinder was placed inside of the vessel and its radius was adjusted to produce the correct loading value when the solution is added between the inner cylinder of the cryostat and the third inserted cylinder. Due to the fact that a properly maintained bath may be reused a number of times, it was cost effective to plate one half of the cryostat at a time, thus halving the total volume of solution required. This was done by filling the system half full and plating the bottom half, and then inverting the entire cryostat system to plate the remaining half.

To generate the heat required for the system, the closed cavity formed by the two cylinders of the cryostat was filled with water, and heating elements were installed in the bottom plate to supply heat. Calculations were made of the total energy required to bring the system up to operating temperature and they showed that if the initial water temperature was close to the operating temperature, and the system was well insulated, that inexpensive home type water heater elements could be used to

supply all the heat needed. To ensure a good initial bond, the plating solution must be at operating temperature when it makes initial contact with the surface to be plated. A seperate system was used to heat the solution prior to initiating plating. This system was comprised of five 55 gal. drums with an individual heating element for each, all sharing a common outlet so that the solution could be pumped into the cryostat at the appropriate time. The initial heat up procedure was syncronized so that both the cryostat and solution systems would reach operating temperature at the same time.

When the operating temperature was reached, a three step cleaning cycle was used to prepare the surface. The pre-cleaning step using an alkaline solution applied by a pressurized sprayer was responsible for removing heavy contaminants such as oil, grease and soil. The activation step removes mill scale, oxides, rust and foreign inclusions providing a uniform

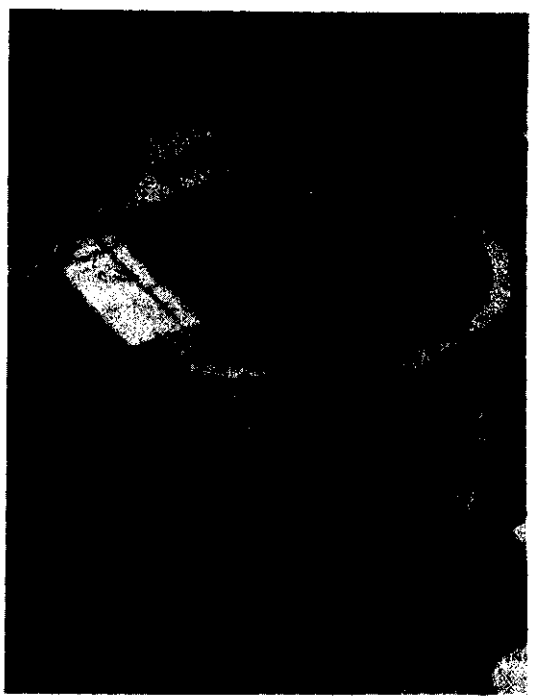

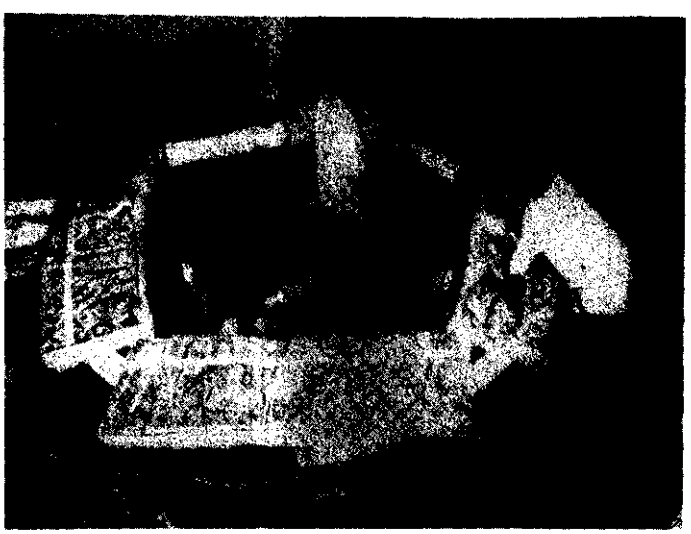

activated surface on which to initiate plating. This was accomplished by spraying an acid solution on the surface. However, acid activation does not initiate electroless plating as quickly as alkaline activation and it increases the potential for flash rusting. Thus, final activation with an alkaline solution was done to ensure good deposit adhesion and prevent rusting during plating solution transfer time. The surface was then rinsed with deionized water and the plating solution was pumped in.

During the plating process air agitation of the plating solution by means of a low pressure blower was used to remove hydrogen bubbles that form on the plating surface and inhibit plating. Continuous filtration of the plating solution was used to remove solid particles. This filtration both secures a smooth deposit and enhances bath stability by eliminating undesirable contaminates. Periodic measurements of the bath temperature and pH were made to monitor the bath stability. Replenishment of the reagents was done on a regular interval, based on experimental data taken from small scale tests. A small mild steel test piece prepared in a manner identical to that of the cryostat was suspended in the plating solution during the entire process so that the deposit thickness could be measured.

Each half of the cryostat was plated for five hours to achieve a desired deposit thickness of one mil or greater. After the completion of the first half, the cryostat was drained, the surface rinsed, and the deposit inspected. The quality of the nickel deposit was acceptable, although approximately 5% of the surface showed evidence of pitting, indicating that the cleaning solution was not able to remove the very heavy contaminants. It was evident that in order to ensure better results on the remaining half of the cryostat, the surface must initially be cleaned by hand. The nickel deposit on the second half was excellent, there was no pitting, and the surface was uniform and non-porus.

The data taken during the plating process indicates that the system is very stable and predictable. The estimated deposit thickness over the entire surface of the cryostat was 1.5 (mil.), thus a plating rate of 0.3 (mil./hr.) was achieved. The heating system maintained a constant temperature of 180 (F) to within about 5 (F). The reagent addition schedule maintained a constant pH value of 4.8 (pH) to within about 0.3 (pH). The percent activity of the plating solution, which is determined by a chemical titration process, was maintained over 100%. The results obtained in the cryostat plating process were very close to those obtained in the small scale tests. This verifies that the electroless nickel plating process can be used effectively to plate large, more complicated parts.

THE K-800 COIL CRYOSTAT DURING COOLDOWN AND STEADY STATE OPERATION.

H.Laumer, M.L.Mallory

The K-800 magnet with coil in place in its cryostat and temporary transfer lines for the needed cryogens, connected, was completed by April 26, 1984. To speed up the initial cooldown of the coil, cold nitrogen gas followed by liquid nitrogen was used to cool the coil to 77 K. The coil chamber was then pumped out to a vacuum of 28 inches of mercury. The chamber was then filled with helium gas and pumped out again. After three pump and purge cycles, accomplished in three hours, the coil cooldown was continued with helium gas supplied by the plant build by Cryogenic Consultants Incorporated. On May 1st at 6:30 p.m. the first liquid appeared in the coil. The coil has been cooled down from room temperature on a second occasion ,with helium gas from the start. In this mode of cooling down it took 7.7 days until the first liquid appeared on that occasion. To cool the coil a cold gas stream is set up in the space between the outside radius of the coil compression winding and the helium vessel wall. This is accomplished by two loops of pipe , with perforations, located at the bottom and at the midplane of the coil. Gas flows to the top of the coil to a return line to the helium refrigerator cold box. There are 11 platinum resistance thermometers installed at various points in the coil. Taking the average of these temperatures and plotting it vs. time results in the cooldown curve shown in Fig. 1. Table 1 is also based on this curve. It represents the rate at which heat is extracted at various stages of cooldown. The assumptions are that the coil temperature is given by the average temperature and that the mass being cooled is $1.07*10^7$g of copper plus $7.8*10^6$g of stainless steel.

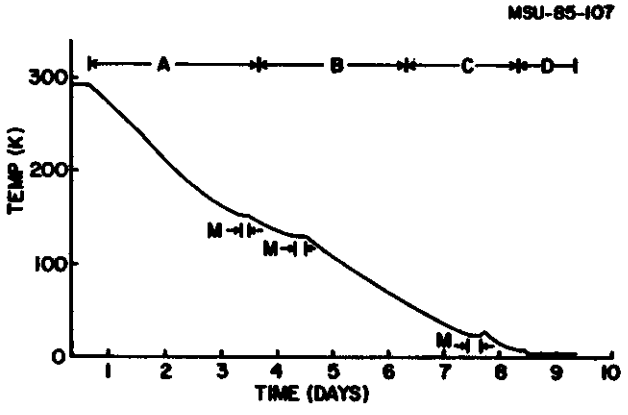

Fig. 1. K-800 coil cooldown. Time spans "A" through "D" indicate cooling mode.
A: cooling gas temperature ≈ 77K.
B: cooling gas temperature ≈ 25K.
C: cooling gas temperature 20K or less.
D: coil is being filled with liquid.
M: marks maintenance periods when coil was not being cooled.

Table 1.

A	B
Temperature(K)	Power(watt)
293	5100
180	3000
100	1800
50	755
30	275

A: the average temperature of the coil based on 11 platinum thermometers.

B: slope of cooldown curve yields rate at which energy is extracted from coil.

The insulation of the coil is multilayer, aluminized mylar and glass paper. There is a nitrogen cooled radiation shield and coil supports also have liquid nitrogen cooled heat intercepts. The steady state load of the cryostat on the refrigerator is inferred from so called boiloff curves. After steady operation with coil filled, the liquid feed is closed off and the helium level is monitored on a superconductor resistance level sensor. Fig. 2 is such a curve vs. time. The shape of the curve depends on liquid volume cross section and heat influx. The evaporation rate is highest initially and drops off until at the point where the last of the liquid is evaporated it is less

HELIUM LIQUEFIER EQUIPMENT OPERATION AND MODIFICATIONS.

H.Laumer, M. L. Mallory, A. Gavalya and R. Zarobinski

During the last year we have operated, often simultaneously, two helium reliquefiers. We continue to use the CTI-1400 to supply the needs of the K-500 cyclotron and its associated equipment. The refrigerator build by Cryogenics Consultants Inc.(called "Blue" hereafter) is principally used to supply liquid to the K-800 coil. However it at times supplies as well a test stand for beam line magnet coil development with liquid helium, and supplements the CTI-1400 when its efficiency falls short of the K-500 cyclotron requirements. At present it is possible to transfer liquid from the 2500 l dewar associated with the Blue refrigerator to the 500 l dewar associated with the CTI-1400 refrigerator. Cold gas from the K-500 cyclotron system can be returned directly to the Blue refrigerator. This facilitates maintenance procedures on the CTI-1400 ,though at present of limited duration(4 hrs.),without impeding K-500 cyclotron operation. At present the total line impedance from 2500l dewar to 500 l dewar to K-500 cyclotron devices is such that a 2500 l dewar operating pressure near the 14.7 psig safety device popoff limit is insufficient to sustain liquid transfer for unlimited operation. As the cryogen distribution system for the coupled cyclotrons is put in place the CTI-1400 will be phased out.

At the present time the capacity of the Blue refrigerator is essentially as was reported before . The plant was operated extensively to provide liquid helium to the K-800 as well as to the K-500 system. The need for supplying the K-500 system was occasioned by more frequent failures of our aging CTI-1400 compressors. The problems encountered included leaks in the oil to cooling water heatexchangers due to corrosion, motor windings burning out, and in one case a failing piston cracked open a crankcase. Our first step was simply to use the Sullair compressors to operate the 1400 coldbox, however, we immediately encountered difficulties. The CTI-1400 efficiency dropped due to contaminant buildup. Our usual method of clearing plugs is to flow warm gas through the CTI-1400 piping, trap contaminants in an external liquid nitrogen cooled adsorber and return the gas to the compressor. The external adsorber trap was found to plug up severely after a short time. Regeneration of the trap was extremely difficult. An oil filter element housing was installed upstream of the adsorber trap. It improved the performance of the regenerator system considerably. It was trapping an oil like substance. A one week operation would yield from 50 to 100 ml of oil. We inferred that the oil removal system for the Sullair compressors was inadequate. The gas was routed through the oil removal systems of the idle 1400 compressors. This did improve the operation of the CTI-1400 refrigerator but, within a week of operation its capacity again noticeably reduced and it had to be warmed up once every two weeks. The Blue refrigerator seems to be more tolerant, plugging up only once every month .

The cause of the failure of the oil removal system was investigated. The gas has at least 100 ppm of oil when it leaves the last water cooled heatexchanger from the compressor package. This gas traverses two units of Balston coalescers. The gas then flows through the charcoal bed and finally passes through a 0.3μ filter before flowing to refrigerator coldboxes. It was found that about 5 gallons of oil had accumulated in the charcoal bed. A test valve was installed and oil return orifices which where deemed to be possible culprits where removed and the charcoal was replaced. Upon resuming operation it soon became obvious that 0.2 to 0.5 liters of oil were again accumulating daily in the charcoal bed. The coalescers where removed and replaced by modular separate units

known to have worked properly in other applications. This system has now operated for a month and no oil is detected in the charcoal bed. Refrigerators appear to be performing better though one month operating time may be too short to make an authoritative statement. We are gratified by this performance, however, do not fully understand why the oil removal system did not operate properly in the original configuration.

The gas handling manifold of the 55 g/s Sullair compressors includes pressure regulators for compressor output pressure, compressor suction pressure, and a regulator to divert gas back to the storage tank. If a refrigerator is operated at optimum efficiency, and the refrigeration load increases to a point where more liquid is turned to gas then the plant can reliquify, then compressor suction pressure will increase. If no action is taken the pressure will rise to the safety valve limit and the excess boiloff is vented to atmosphere. A valve controlled by a signal from compressor suction pressure is used to return the excess gas to storage. The original equipment supplied to perform this function was inadequate. It has been modified by adding somewhat more sophisticated valves and controls and it now performs well. Popoff losses during unattended operation are no longer expected to occur under normal conditions. A two way valve has been added following the regulator controlling compressor output pressure to return this flow either to compressor suction or to gas storage. Considerable redundancy and flexibility of operation has resulted from these modifications.

During the initial cooldown and filling of the K-800 coil we experienced helium losses considerably higher than what was experienced during operation of the K-500 coil. The major losses where found to occur at leaking seals for piston rod and push rods of the expanders. The fact that the plate holding the seals operated near 0 C probably also contributed to this deficiency. A redesign and retrofitting of the seals , and introducing baffles in the dead space of the piston housing to impede helium convection has dramatically reduced helium losses from this source.

In the past year the demand for operating the refrigerator to satisfy liquid helium needs has increased considerably and not much time was available for experimenting with the refrigeration equipment. Some tests of the engines, suggested by the manufacturer have been carried out. This includes changing inlet cams, engine rotation direction and installing close tolerance pistons. The changes did not lead to dramatic improvements in performance; however, we are planning to continue engine tests to the extent that operation needs permit.

We have had a third expansion engine as a spare to replace either of the two operating at 70 K and 40 K. Originally it was planned to use this as a quick replacement for any of the two in operation. We soon realized that moving and realigning for fixed length transfer lines is not trivial. All maintenance operations encountered to date have been carried out with engines in place with very little impact on other operations. We are in the process of designing a cold box which will allow us to valve any of the three engines into either of the two points where they are presently coupled to the refrigerator heatexchangers. To change engines for maintenance purposes will then only involve valve operations.

The failing of the CTI-1400 compressors had no detrimental effect on the K-500 cyclotron operating program because redundant compressor capacity was available. To provide some redundancy for the near term operation as the CTI-1400 compressors are completely phased out we have ordered a 30 g/s helium compressor. We, of course, also anticipate carrying out performance tests on the Blue refrigerator using this extra capacity, and are eager to see if operating three engines in place of two will yield significant gains in capacity.

PHASE 2 CONTROL SYSTEM I: OVERVIEW

R. Au, R. Blue, L. Foth, R. Fox, H. Hanawa, J. Jenkins, E. Kashy, G. Siedelberg, A. Vandermolen

The control requirements of the combined K-500 and K-800 cyclotrons, their support equipment, the beam transport system, and the experimental apparatus are easily recognized as a major design challenge in the development of the NSCL facility. Fortunately the rapid advancements in microprocessor technology have made it feasible to adopt a system design in which processor power is distributed at multiple levels to a degree not commonly employed in similar systems of earlier design. The basic components of the control system are illustrated schematically in Fig. 1. Perhaps the principal

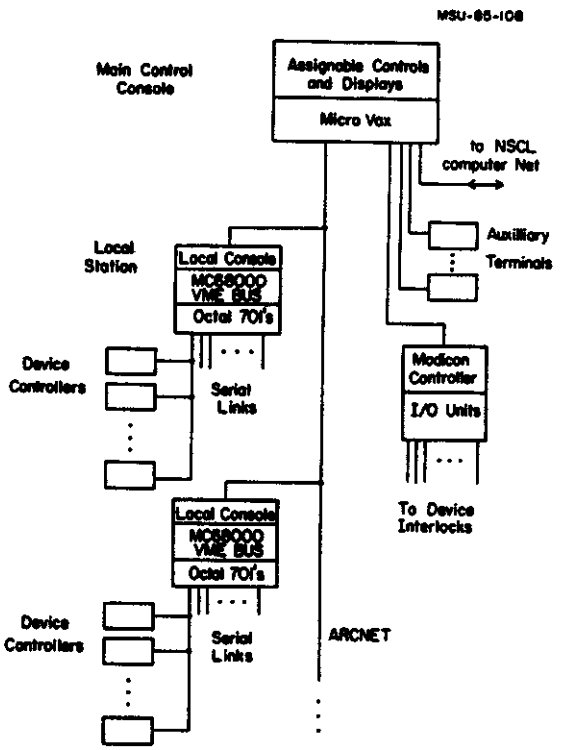

FIG. 1

benefits of this system design are its flexibility and expandability, however cost and manpower constraints also weighed heavily in favor of this approach.

Starting at the single device level all input/output functions for a device are integrated and controlled by a device controller. Each controller, is essentially a dedicated microcomputer interfaced to the device via ADC's, DAC's, and buffered logic signals. Illustrative of what is considered as a single device for which controllers have been developed are a servomotor, a DC power suply, or a multi-range beam current digitizer. Each device controller is designed as a self-contained unit in an enclosed chassis suited to service at virtually any location. The microprocessor selected for this lowest level is the MC68701, an 8-bit processor of the 6800 family. This processor has sufficient on-chip memory to handle the program requirements for a device controller. Most of the needs that are device specific can then be treated largely in software rather than as a hardware design problem.

In parts of the system variant forms of the controller may be used. Examples of this are found in the RF system where circuits are packaged in NIM modules. The MC68701 controller resides on a standardized subsection of the printed circuit cards used in these modules. Similarly each device operating on the present control system will be transformed to the new system design by the addition or substitution of a small PC card containing the MC68701 circuitry.

The connection to the next higher level in the control system is a high-speed asychronous serial communication link between the dedicated microcomputer and an identical processor which serves as a data concentrator as it handles input and output for as many as eight devices on a common daisy-chained data path employing a single twisted-pair of wires. The use of a serial link minimizes the complexity and cost of control cabling to each device and gives the desired flexibility with regard to the location of high-level system components relative to the devices being controlled.

At the second level the system design employs MC68000 microcomputers in VME bussed

crates. Here we have made extensive use of hardware and software designs from Fermilab (1). A given VME crate will typically handle all devices for a major component of the facility such as the K-800 RF system or the 40-20 power supply which powers the main coils of the K-800 cyclotron. With this level of integration 7 to 10 stations will handle the entire control requirements for the facility, but future additions to the system can easily be accommodated. Communication with the device controllers proceeds via dual-ported memory cards which serve as data buffers. Each buffer card contains eight MC68701 microprocessors serving as communications controllers for the serial links. Since each serial link handles 8 devices this "Octal 701 Board" accommodates a total of 64 devices. A given VME crate may house up to eight of these cards. The MC68000 accesses the buffer memory via the VME bus and provides all neccessary processing for inbound or outbound data. Special device interfaces such as those demanding data rates beyond the capability of the serial link may be connented to the system at the VME bus level.

The MC68000 is also interfaced to a "Locale Console" which consists of a CRT and a keyboard along with a small array of special function keys and an assignable control knob. All the local stations are linked together and to the main control console by a commercially available network system (ARCNET). Via this network each local console can be used to readout or control any device in the system with the exception of devices for which the system software restricts control access.

A microVAX computer has been selected to control the main console because its operating system provides a superior file handling capability. This feature is needed to deal efficiently with system data logging and automatic device initializations based on stored parameter sets. The main console user interface will consist essentially of software driven devices including color-graphics CRT's and user-definable knobs and meters. Modules which serve as extensions of the main console will be installed in each of the data-taking areas to give experimenters a convenient means to control the devices related directly to their experiment. It is also possible that standard terminals on RS-232 lines can serve as imput/output devices at specific locations where access to the control system is required.

Those control functions that fall generally into the category of interlocks are handled separately by a Modicon programmable controller, a device which operates on logical inputs and outputs via relay ladder logic. Intrinsic to the design of such devices are a high level of noise immunity and reliability as well as a predictable recovery mode following a power outage. Within the context of the control system design the Modicon provides a desirable redundancy which serves to minimize the possibility that a control system failure could be hazardous to personnel or equipment. Although its final form is yet to be selected, a communication link between the Modicon and the main control console will be added to provide operator access to the variables under Modicon control. The radiation safety interlocks will also be handled by a programmable controller, either the system Modicon or a separate unit. The latter choice may perhaps be prefered in the interest off assuring independent operation of these vital interlocks.

---

1. R.W. Goodwin and M.F. Shea, in "Tenth International Conference on Cyclotrons and Their Applications, (IEEE Service Center, Piscatway, NJ, 1984) edited by F. Marti, p.547.

PHASE II CONTROL SYSTEM CONSOLE LEVEL CONTROL

L. Foth, A. VanderMolen

The distributed architecture of the phase II computer control system is described. An overview of the hardware and software for the upper levels is presented, along with remarks on progress to date.

1. INTRODUCTION

The phase I control system (described in last year's report) is made up of two DEC PDP-11/34's and one PDP-11/45 which communicate through a shared multiport memory. Soon after this system was made operational, advances in microprocessor and local area network technology demanded that we re-think our control system design. As a result, the phase II control system is based around networked microprocessors.

The system requirements from before are still valid:

1. To control the K-500 and K-800 cyclotrons, the beam lines and experimental facilities;

2. To allow physicists to control their experimental equipment from the data taking and experimental areas, as well as from the control room;

3. To provide real-time response.

We considered several possible system architectures and finally decided on a "distributed" architecture in which both the database and the processing power are distributed across a dozen or more large microprocessors, several smaller microprocessors and three levels.

The first section below gives an overview of the phase II control system architecture. Next are discussions of the hardware, function and software of the middle level nodes. Section six describes the upper level hardware and software, and lastly we describe our progress to date.

2. OVERALL VIEW

Figure 1 shows the overall view of the phase II control system architecture. There are three levels of processors used in this system.

The upper level contains a microVax and supporting processors which make up the main console - the interface to the operators. The main console supports graphics and status displays, meters for analog data display, and knobs, touch screens and a keyboard for control input. In addition, it supports a disk for data logging and an interface to the Modicon programmable controller. The main console is networked (via Ethernet) to the other Vax's so that experimental apparatus can be monitored and controlled from a terminal connected to the Vax's. This level is described in section six.

The second level is made up of stand-alone Motorola MC68010 microprocessors (local stations). Each of these stations handles a

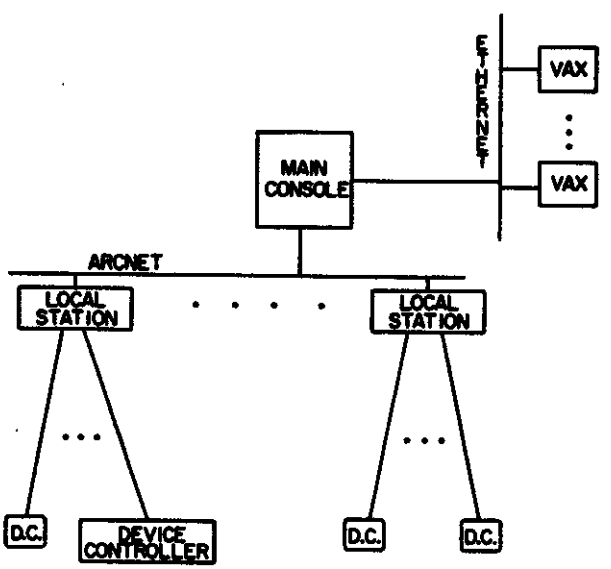

FIG. 1

subsystem (Rf, ECR, experimental vault, beam line) and is located close to the equipment it controls. The local stations communicate with each other and the main console via ARCnet, a local area network. This level is described in sections three, four and five.

The bottom level is made up of device controllers. These may be "smart" Motorola 68701 microprocessors (described in another paper) which use the serial, RS-422 protocol to talk to the local stations, or they may be "dumb" hardware controllers connected to the stations via Mil 1553B (a 1MHz serial bus), or GPIB (IEEE-488) or the Motorola I/O channel (a byte wide memory mapped bus). In any case, the local station CPU has a specific protocol to follow to talk to each type of device interface.

This three layer system allows for parallel processing, increasing the amount of work that can be done in a given amount of time. The lowest level can be taking readings and preparing them for transmission to the next level, while the local stations are monitoring previous readings for alarm reporting, and the microVax may be plotting data or reporting status to the operator.

Distributing the intelligence and data base across several local stations means that if one subsystem's controls malfunction or need to be disabled, the rest of the subsystems continue to function with the only noticeable effect being they can't receive data from the subsystem which is down. This makes expansion and repair easy since an individual subsystem can be put on line or taken off line at will. Also, the distributed database means each subsystem computer can do its work without having to access a central database - eliminating a potential bottleneck. Another potential bottleneck is eliminated because each of the local stations can talk over ARCnet to its peers directly, without having to go through a central computer.

3. LOCAL STATION HARDWARE

The local station hardware is shown in figure 2. The design of these stations (hardware and software) is derived from the system used to control the Fermilab 200Mev Linear Accelerator. Each station consists of a microcomputer chassis and bus, four printed circuit boards, a "local console" and whatever I/O interface boards are needed.

The microcomputer bus chosen is VMEbus (IEEE-P1014). It is a high performance, 16/32 bit bus which uses the Eurocard format with two-piece pin and socket connectors instead of edge connectors.

A Motorola MVME-110 CPU board houses the MC68010 microprocessor. It also provides eight 28-pin Jedec sockets - six of which house software in eprom and two of which contain local ram for system stack and variables - and a serial port. The serial port is used for uploading and downloading data and programs (during testing some programs can reside in ram) and for logging data to a printer or Vax disk.

The second VME board is a battery backed CMOS static ram card. This is also commercially available (Micro Memory Inc. MM6600CC). We

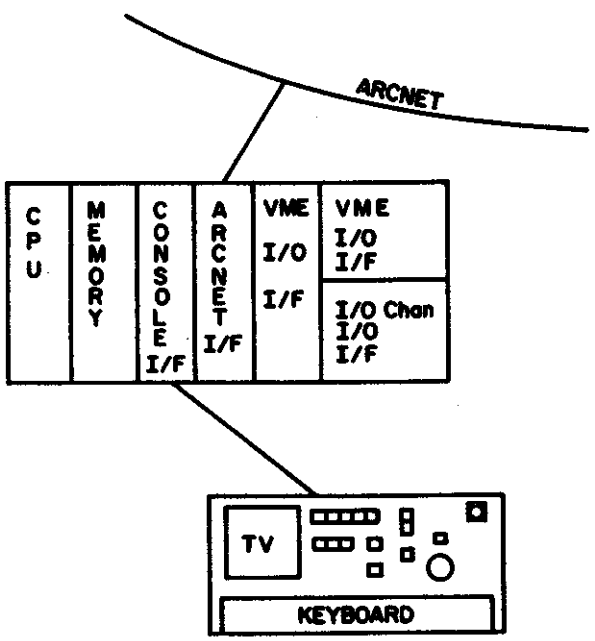

FIG. 2

purchase it one-half populated with 128K bytes of ram. This non-volatile memory houses the database for this station, dynamic memory for the CPU to use and special tables needed to control certain devices. The other 128KB can house either ram or eprom depending on the needs of each station. Because the memory is on-board battery backed, when we lose power we don't lose our database, and when power is restored, the system comes right back up operating again. Additionally, if a database were destroyed, we can re-download that database from the Vax to the memory board and then take that memory board out and install it in the system, which means we don't have to run Vax lines out to every local station for saving or restoring databases. (We maintain current copies of each station's database on the Vax for just such emergencies.)

The third VME board is the interface to the local console (both designed at Fermilab). It also provides option switches and status lights. We can monitor and control any device in the system (not just those connected to this station) from this local console. The console itself has a 5 inch TV monitor which displays 16 lines of 32 characters each, full keyboard, a shaft encoder knob, several push buttons and an enable key to prevent unauthorized updates. It is light enough to carry around anywhere so that is can be positioned wherever is suitable for checking out equipment. The knob and two "raise/lower" buttons give us relative control while the keyboard lets us make absolute settings. Data can be displayed in engineering units, volts or hex at the push of a button. In addition to readings and settings, any information in the database (or any other station's database) can be displayed.

The last board is the ARCnet interface and is also a Fermilab design. ARCnet is a 2.5MHz, peer protocol, token passing bus. One of the reasons this network was chosen is that large scale integration chips are available which handle all of the work associated with sending and receiving messages, passing the token and reconfiguring the network when a station is added or deleted.

4. LOCAL STATION FUNCTION

Each local station is responsible for data acquisition and monitoring of local hardware devices. One loop, or cycle, through the software is done each 1/15 second. On each cycle, all of the local analog and binary data is read into the local data pool and monitored for out-of-tolerance values. Any new alarm messages resulting from the alarm scan are reported to the main console. If any other stations have requested data from this node, ARCnet messages containing the requested readings are prepared and sent out. Any setting requests received are performed, as is any required closed loop control. Once all of these functions have been completed, an application program executes to service the local console and update the video display.

5. LOCAL STATION SOFTWARE

The local database and method of requesting data are central to the software design. Once they have been discussed, we will examine the software routines.

Each analog or binary "thing" is called a "channel". The local database contains channel names, analog readings, settings and calibration constants, and digital control and reading characteristics. All of this information is organized in tables accessed through a standard mechanism. Because of the table driven nature of the software, device calibrations can be changed and new channels of known types added "on the fly". Readings and settings are handled by device drivers and each channel has a code assigned so the software knows which device driver to use to read or set that channel. This modularity makes addition of new types of devices extremely easy for the software developer.

A local station or the main console can examine the data of any other station by requesting this information via a "list". This list specifies what channels of data (or entries

in a table) the requester wants, what frequency the answers should be delivered at (once only or 1/15 second to 17 seconds) and where the answers should be put. The list format allows one to request many different types of information for a whole set of channels at the same time. Once the request has been made, the requester waits one cycle to allow the stations which will deliver the data to see the request and get set up to send answers. From then on, the requester simply calls a routine which updates all of the data (which arrives at different times from any number of stations) in the requester's data structures. All of the details of the data structures necessary to support this request and collection scheme are hidden from the program making the request. Any station can have a number of requested data lists and a number of lists it is returning data for outstanding at the same time. Cancellation of any one list does not effect any of the other lists. Again the modularity that comes from the table driven nature of the software makes a difficult job look easy.

The software in a local station falls into two categories - "system" software and "application" programs. The system software contains the interrupt service routines and tasks and is written exclusively in assembly language. The application programs interface to the user via the local console and are written almost entirely in Pascal. The following paragraphs will look at the interrupt routines, tasks and application programs.

The time base in our system is 60 Hz to allow us to collect data at this rate. After any 60 Hz data collection is done, we count which 60 Hz interrupt this is and trigger the 15 Hz cycle code every fourth time. The 15 Hz cycle code acquires all of the non-60 Hz analog and binary data in this station, scans it for alarms and triggers the application program, all by scheduling tasks which perform these functions. The cycle code also sets a timer which will interrupt 40ms into the cycle and trigger communication with the local console.

There is an ARCnet receive interrupt service routine (ISR). This ISR simply alternates between the two receive buffers and saves some diagnostic information. The transmit side could be run off of interrupts also, but this has not been needed yet.

There are also transmit and receive interrupt service routines for the serial port on the CPU board.

The eight tasks in the system software are listed below:

1. The Update task is triggered each cycle to read all local data, update active data requests from other stations and return answers. A Data Access Table in ram contains the parameters that specify how dta is collected. This table can be changed as devices are added or deleted. Since the data acquisition is table driven, all local stations have the same software.

2. The Alarms task scans all active analog channels and binary status bits each cycle for changes in alarm conditions.

3. The Console task handles all the functions necessary for talking to the local console - keyboard input, cursor activity, knob, light and switch changes.

4. The Pcom task processes commands received from outside of this atation - requests for data lists or device control and answers to active data requests.

5. The Small Memory Dump task displays eight bytes of local memory on the bottom line of the local console display as a diagnostic tool.

6. The Date and Time task keeps track of the time by counting 15 Hz triggers. It also updates the date and time shown on the top line of the local console display each minute.

7. The Qmonitor task monitors the queues used by the system software.

8. The Application Program task provides a task environment for the application program which is currently active.

There are four application programs in the basic package. The Parameter page is the main workhorse - displaying and controlling up to 14 analog channels from anywhere in the system. Readings, settings, nominal or tolerance values can be displayed in engineering, volts or hex units. The knob, keyboard and raise/lower switches provide analog control. Digital status and control of bits associated with analog channels is also supported. Displayed values are updated slightly more often than once a second. This rate was chosen so that one can see that the values are being updated without the data being blurred. This page provides a very nice one-knob control console.

The Analog and Binary Descriptor pages allow one to display, list or change any local station's database. The Memory Dump page displays eight lines of eight bytes each from anywhere in the network, updated at 15 Hz.

An appropriate amount of data for one local station to support is on the order of one hundred analog channels and one hundred bits. This will vary depending on how much work is necessary to acquire the data each cycle. The amount of time the alarm scan takes depends on the number of channels and bits active in the scan, more than the number of channels defined.

6. MAIN CONSOLE HARDWARE AND SOFTWARE

The core of the main console is a DEC microVax. This computer will in turn give commands to one or more local stations. The local stations each drive a graphic display screen with touch screen and/or trackball coupled with a set of four knobs and four meters. A seperate screen and keyboard will be used by the operator to communicate with the microVax. The local stations sit on ARCnet and acquire readings and make settings of devices directly, without going through the microVax. The microVax is also on ARCnet and acquires data and makes settings to support the display and control interfaces not tied to the local stations. The microVax also resides on DECnet with the present Vax's.

By using graphics displays, "soft" controls and readings will be available. This will allow for different and new configurations to be generated without physically restructuring the main console. In addition, the operators could set up the screens in any fashion convenient to them. Provisions have been made to allow the plotting of data on the screens. The actual control and reading of devices will be done by the local stations, as previously described. The selection of displays will be controlled via the microVax through its control screen and/or keyboard. The microVax will also do logging of data, storing it on its own disk or passing it to any other Vax on the network, and will display safety interlock status from the Modicon.

The main console (figure 3) will contain four units consisting of a graphics monitor, touch screen/trackball, four knobs, four meters and the controlling local station, giving a total of 16 knobs and 16 meters at one time. Single units will also reside in the data "U"'s allowing the experimenter access to any device in the system. This modular structure allows for expansion if necessary at any time without any change to the system, as it is just another node on the system. In addition, if a module breaks down, the system as a whole will continue to operate and that module's functions can be transferred to another unit via the microVax.

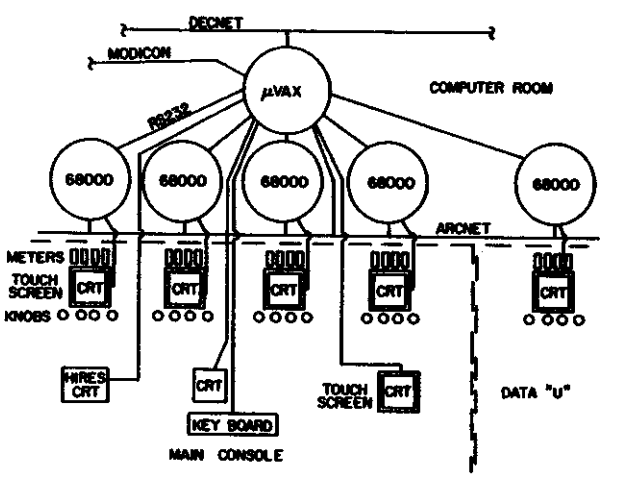

FIG. 3

Because of this modularity, maintenence will consist of replacing the unit as a whole with a backup and then the unit will be repaired offline when convenient. As designed, the operator can do this if a technician is not available.

7. PROGRESS TO DATE

Once the decision was made to use the Fermilab Linac local station as the heart of the control system, we needed to acquire hardware and software. Hardware that is commercially available was ordered. For the Fermilab designed hardware, printed circuit boards and parts were ordered and assembled here. We have built four local stations so far and are ordering and assembling the hardware for another eight or more stations. Our original plans called for 10 to 12 stations, but now that we intend to use the local stations as part of the main console also, we will need 18 to 20. The hardware has required very few modifications.

Of the four stations built so far, two are controlling equipment, one is being used as part of the main console and one is a development station. Both of the stations which are controlling devices (one is servicing the K- 500 beam line magnets and the second controls the 40/20 power supply for the K-800 main magnet) use the I/O channel as the device interface. The 40/20 station also uses a GPIB interface to a Hewlett-Packard Digital Voltmeter. One unique feature of the 40/20 station is its use of a second CPU board to do the power supply regulation.

The local station software was developed on a Motorola Exormacs development system, so we needed to find a way to port it to our Vax. A software package consisting of a Motorola 68000 assembler, linker and Pascal compiler that run on the Vax and accept the exact same source code format and conventions as the Exormacs software was found and purchased. This package has been found to work extremely well for program development and modification. Software developed is either burned into proms or downloaded to ram in the form of Motorola S-records. The local station software includes a monitor program which accepts S-records. T h e software will see many additions (device drivers and application programs) as we develop it to suit our particular control system needs. Some of these additions have been made already, and have been relatively easy to do. As our control devices are more clearly defined, more device drivers and application programs will be written. It has taken a portion of this past year to understand the details of the hardware and software to the point where modifications could be made.

Main console development has begun and a prototype unit has been developed. This unit, which includes a local station, knobs, meters and graphics monitor, is being used to control the K-500 beam line. The main console local station, using ARCnet, sends messages to the K-500 beam line local station which in turn controls the beam line devices.

8. CONCLUSIONS

This system of distributed local control stations and main console networked together will provide the speed, flexibility and processing power needed to handle all of the devices we plan to have under computer control. Control and monitoring will be available from many sites around the lab - control room, data "U"'s and experimental vaults.

9. ACKNOWLEDGEMENTS

We have received outstanding assistance from M. F. Shea and R. W. Goodwin of Fermi National Accelerator Laboratory.

PHASE II CONTROL SYSTEM: LOW LEVEL NETWORK

J. H. Jenkins

The interfacing of the 68K VME computers of the control system to the equipment of the Cyclotrons is accomplished by of a mix of methods. Some VME crate mounted ADCs and DACs are employed. We have also developed a interface that is specially suited for a class of instruments found in cyclotrons. This interface, called The Low Level Network (LLN), is the subject of this paper.

An example of a instrument on the LLN interface is a very sensitive beam current digitizer. It has a multi-range preamp, an offset adjustment DAC, saturation detectors, an integrating ADC for noise filtering, band width switching, and some built in diagnostic functions. All these must be controllable by the cyclotron operator. The circuit must be isolated from the control system ground to permit the use of a true guard shielding system.

The LLN interface is built around a single chip microcomputer with on-chip networking facilities. The microcomputer chosen for the interface was the Motorola MC68701. It was chosen because it has an on-chip FM modulator and demodulator which permits the serial data from its on-chip serial transmitter and receiver to be sent bi-directionaly through a single, small, signal transformer. Thus achieving isolation from the VME ground.

Our MC68701 subcircuit can be placed in the printed circuit for the beam current preamp, mentioned above, to provide all the necessary outputs and inputs to the control system. The subcircuit has 6 active chips and covers about 4 by 6 inches of printed circuit board. The MC68701 has on-chip EPROM, on-chip RAM and has several modes of interfacing to the instrument. The two modes most often used here are Mode 7 - where the pins of the MC68701 chip are all configured as I/O ports, and Mode 5 -where 8 pins are a data bus, 8 pins are a small address bus and the rest of the pins are configured as

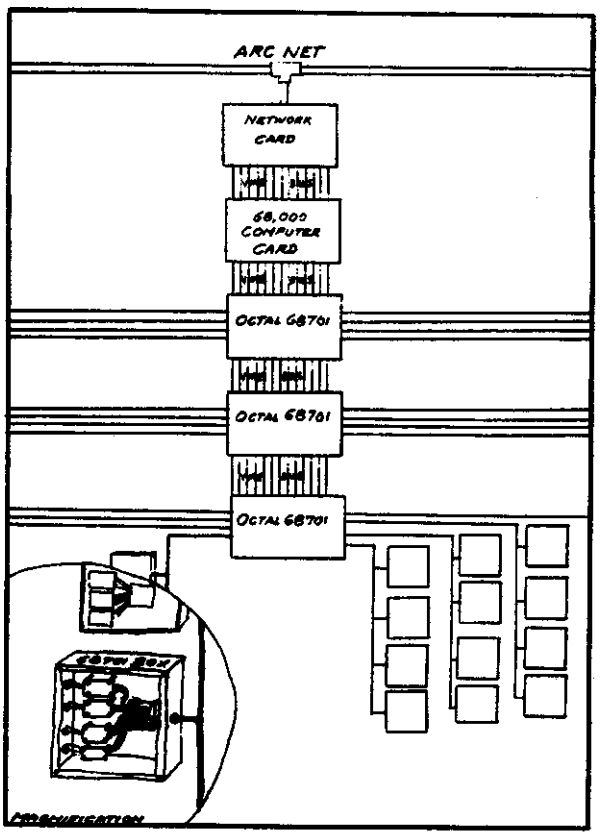

Fig. 1 The Low Level Network

I/O ports. The subcircuit also provides a driver for a LED that is software driven. It is used to flash short, coded messages that serve as diagnostics.

The program in the MC68701 that drives the flashing LED is part of the program module for the serial communications activities of the instrument. This program module is provided to the instrument designer in a ready to use form. The cross assembler automatically joins this program module with the program module provided by the instrument designer to make the compleat program that is loaded into the on-chip EPROM of the MC68701.

The instrument designers program module is the main program of the MC68701. LLN seial communication activities are interrupt driven

and unseen by this main program. The two programs interact through a pair of buffers, called the In Basket and the Out Basket, in the on-chip RAM of the MC68701. The serial activity updates the Inbasket Buffer and transmits the Outbasket Buffer. The instrument designer does not need to deal with how the serial communication program works except to know how to interact with these two buffers.

UTILITIES SUPPLIED BY THE MC68701 SUBCIRCUIT

The subcircuit also provides the designer with a local, isolated, D.C., power supply. It contains a line transformer, rectifier, filter, and regulators to provide:

- plus and minus 24 volts (the rectifier output)
- plus and minus 15 volts (regulated down from the 24)
- plus 5 volts (using a single chip switching regulator)

ADVANTAGES AND DISADVANTAGES

The main advantage gained by the designer using the new Low Level Network Interface is that it makes posible smaller, less costly, and more accurate computer controlled instruments. For us, the advantage was gained at some cost in development time because there was little equipment available commercialy for developing programs for networked single chip computers and for interfacing the networks (using FM signaling) to the labs 68K VME computers. Our MC68701 software development system uses a Kaypro computer, an Avoset cross assembler and a lab developed Emulator Board running a decendant of the Motorola Lilbug program. The Emulator Board also contains firmware to control a serial line and produce a live screen display on a CRT terminal. This feature can be used as an independent repair tool for the front end instruments.

VME INTERFACE

The interface for the 68K VME Computer uses

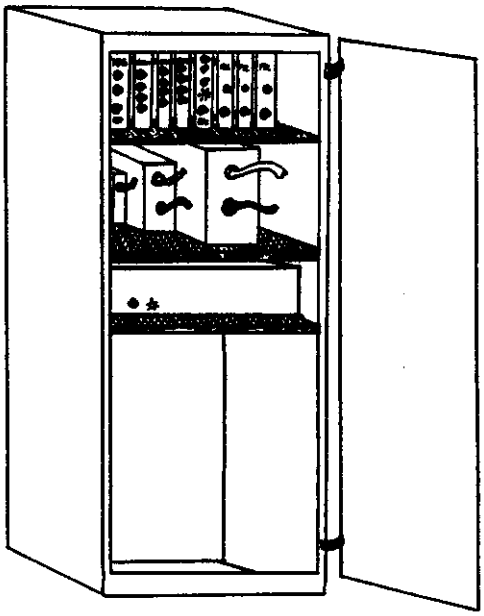

Fig. 2. Box dimensions for Instruments on the LLN are unconstrained.

eight MC68701 single chip computers on a single VME board and sharing an 8K by 16 dual port RAM with the VME computer. Each MC68701 controls one of the eight serial lines connected to the board. A high speed logic sequencer stands between the MC68701s and the dual port RAM to make up for their inability to operate a dual port RAM themselves. The seqencer also provides a second index register for the MC68701 to help it do large data moves more efficiently. Arbitration between the eight MC68701s, for control of the sequencer and hence of the dual ported RAM is achieved using signals from port 1 of each MC68701. Port 3 and Port 4 of the

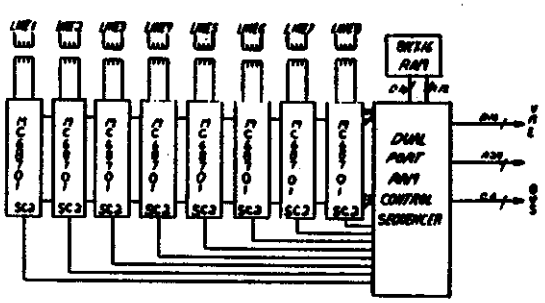

Fig. 3. Octal-68701; 8 line serial interface for the VME computers.

MC68701s are concatenated to move 16 bit data words to and from the sequencer. The seqencer receives a trigger signal when a MC68701 reads or writes its 16 bit port from the CS2 pin of the MC68701. The sequencer then executes the kind of memory access dictated by the value the MC68701 places on its port 1 pins.

SEQUENCER COMANDS

The comands the sequencer can execute are: Load the sequencer index. Fetch a word from the DPR at index. Fetch a word from the DPR at index and increment index. Write a word to the DPR at index. Write a word to the DPR at index and increment index. A set of comands to do test-and-set (semifore) manipulations at the memory pointed to by the index are being considered for the next production of the interface board in April, 1985. The current equipment in service on the system uses a simple asynchronous buffer protocol with the 68K VME computers for lack of the the semifore comand set.

SERVICE EXPERIENCE

We have not had much operational experience so far. One instrument has been in service intermittantly for a few weeks with no breakdowns but most experience will be gained over the next few months. More tests will be provided by running the following: A magnet power suppy controller board, a beam current digitizer board, and an A.C. induction motor positioner board. In addition the new interface is being retrofit into many of our existing magnet power supply controllers.

An encouraging thing so far is the lack of noise induced errors picked up by the serial lines even during very noisy events like the RF system sparking. The transformer coupled, ballenced serial lines seem to be good at rejecting the type of noise we experience here.

TECHNICAL DETAILS OF MC68701 SUBCIRCUIT

This small circuit is transformer isolated from true ground and from the control system network ground. Although it contains a MC68701 microcomputer, it is considered reliable for interlock protection service in its local domain. It has a watch dog timer which times out in 250 ms if it crashes and starts it again. It has 27 pins available to control the local device. They are TTL levels which may be used as input bits or output bits in any combination or they may be used as address and data lines for expansion up to 64K of memory and I/O in the local device. Three additional pins are available as interrupt inputs. The subcircuit has an on-board A.C. line power supply that can provides 5 volts at 500 ma, +24 volts at 300 ma, and -24 volts at 300 ma. Plus and minus 15 volts is regulated down from the 24 volt supplies.

USE OF MC68701 FACILITIES

The MC68701 has two simultaneous program activities in operation. The instrument program runs as the main program of the MC68701. The serial communication program runs as a background program interrupting the main program. The average load on the microcomputer due to the interrupts is 1/8 to 1/16 of the processor time. The peak load is 50% of the time. This peak occurs during the sending or receiving of messages and can peak at one 65 microsecond interrupt every 130 microseconds.

The MC68701 on-chip timer is largely used by the serial activity. The MC68701-U4 chip could be substituted for the MC68701 chip in the subcircuit thus gaining 64 more bytes of RAM and 2 extra on-chip timers.

The maximum sized load that can be handled by the local function can be optimized by trading maximum message length for local variable space. A typical allocation would be:

Stack		9(minimum)
Serial Process Variables	13	
Serial Inbasket	24	12 words in
Serial Outbasket	24	12 words out

Serial Packet Check Buffer	24	12 words in message
Local Instrument Variables	32	bytes for instrument process
	128	Total RAM on MC68701

The MC68701 has 2K of EPROM. About 500 bytes of this are used for the serial communication and LED drive, leaving about 1.5K available to the local instrument control program.

The single chip switching regulator used is a ua78s40. The 15 volt regulators are 78M15 and 79M15 type. In addition to the regulators and the MC68701 chip, the subcircuit contains 4 other active chips; A 74HC14, a HC4053, a 74LS05, and a 75118 line tranceiver. The HC4053 is used for multiplexing the mode switch, serial address switches, flashing LED, and line driver enable signal onto only 3 pins of the MC68701.

Fig
ful

gr

PROTOTYPE BEAMLINE QUADRUPOLE PROGRESS REPORT

A.F. Zeller, R.T. Swanson, J.A. Nolen, D. Landry, M.J. Dubois, and J.C. DeKamp

The prototype beamline quad has been constructed and is presently being attached to a test section of the cryogenic distribution system. It will be used to test our magnetic and cryogenic designs. Additionally, a "dummy" quad (actually a surplus quad from Argonne National Lab) will also be installed to further test the cryogenic aspects of the line. The quad is described more fully elsewhere[1], and this report will describe briefly only the important features of the quad.

Fig. 1 shows a schematic of the cryogenic and magnetic features of the design, minus the coils which are omitted for clarity. The actual quad is shown in Fig. 2, prior to its final blanket of superinsulation and installation in the outside vacuum box. The magnet itself is sealed in the helium vessel and the insides of the bore tubes are likewise invisble.

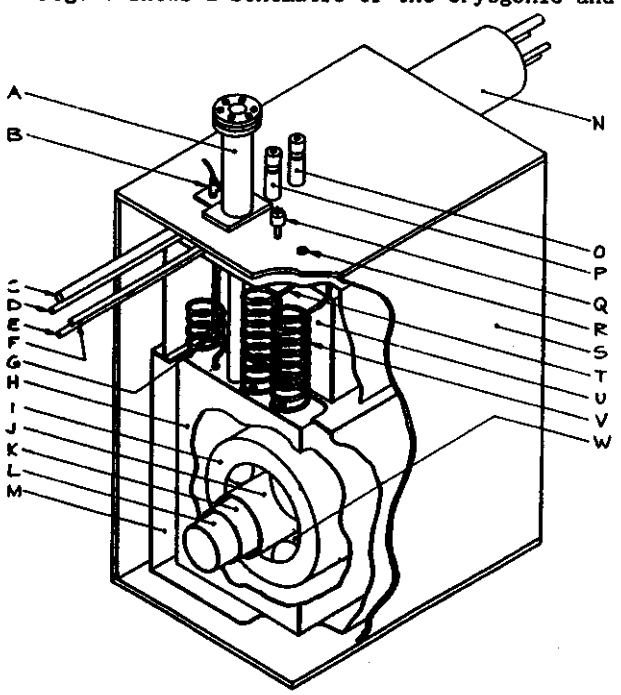

Fig. 1. Schematic drawing of the superconducting quadrupole showing parts indicated by the following letters:

A) Rupture disk port B) Instrumentation and coil lead feed-thru C) 300 K He return line D) LHe supply line E) LN supply and return F) Cold He gas return G) Vapor cooled coil and instrument leads H) LHe reservoir I) Magnet iron J) Inner Cryostat Wall K) 77 K inner shield L) Warm bore beam tube M) 77 K radiation shield N) Transfer line vacuum jacket O) LHe supply valve P) Cold He gas return valve Q) Vacuum transducer R) Thermocouple feed-thrus S) Vacuum box T) Cold He gas return U) LN reservoir V) LHe supply W) Coil space (coil not shown). The room temperature vacuum box (S) is 48 cm wide, 66 cm long, and 88 cm tall.

The iron yoke and pole tips are shown in Fig. 3 prior to installation of the coils. One of the four superconducting coils, consisting of 3600 turns of 0.3 mm diameter wire is shown in Fig. 4. These coils require about 5 hours each to wind. All four coils have been tested in the cryogenic test stand. They exhibited little training before reaching current limits of 21-26

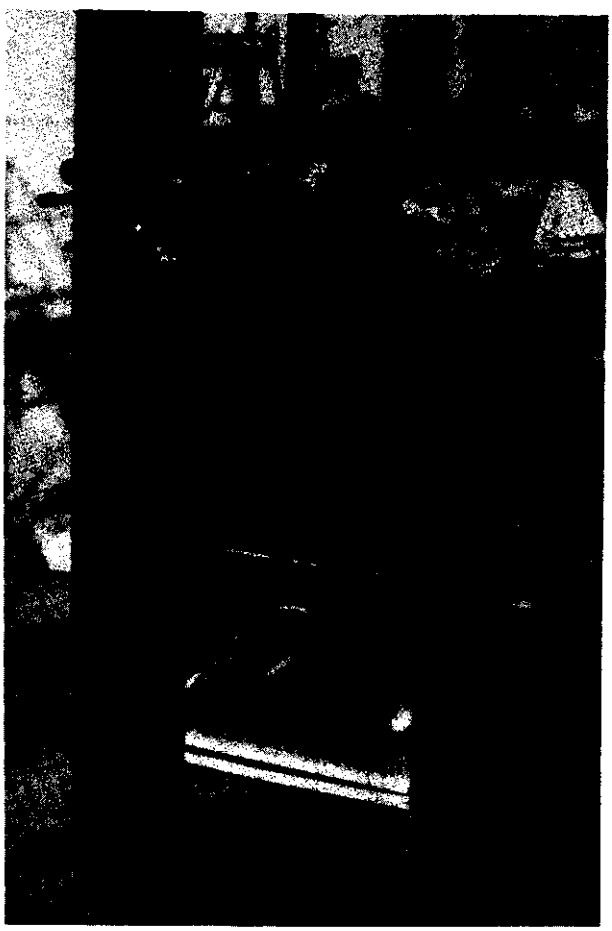

Fig. 2. Photograph of the quad.

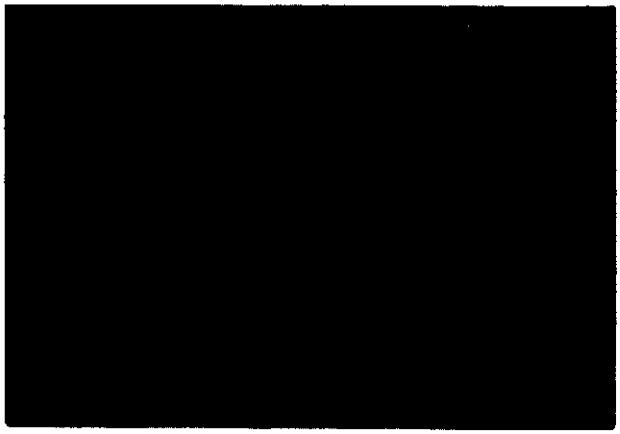

Fig. 3. Photograph of the steel yoke and pole tips.

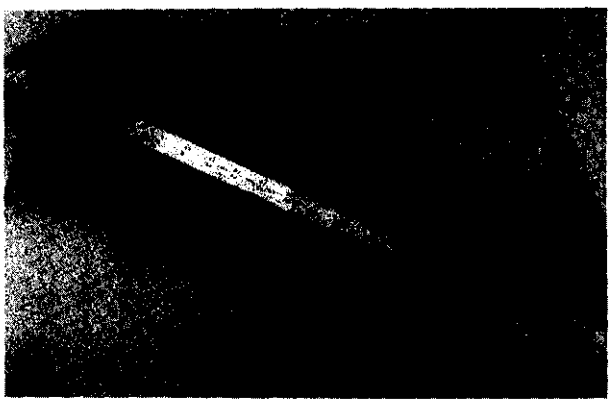

Fig. 4. Photograph of the superconducting coil. The scale is in inches.

A in their own self fields. The maximum gradient, 7.3 kG/in, requires only 13.0 A. Figure 5 shows the coils installed around the pole tips, with the leads connected to the superconducting bus bar (K800 conductor) assembly.

The current leads, shown in figure 6, are a modified version of a design originally devloped by John Purcell. The leads each consist of 9 superconducting wires of 0.010" diameter and 11 instrumentation leads wound together in a single stainless steel tube. The wires are formvar insulated and exit the warm end through a G10 plug epoxied to the stainless steel end form. The whole assembly is vapor cooled and requires only 40 ml/hr of liquid helium boil-off at peak current.

Fig. 5. Photograph of the coils assembled around the pole tips.

Fig. 6. Photograph of the current leads.

The rupture tube assembly was originally designed with a fiberglass composite tube to keep the heat loads small, but still strong enough to withstand 60 psi internal pressure.

However, making reproducible epoxy/stainless steel joints that don't leak at 4°K proved very difficult. Therefore, a thin walled stainless steel bellows with fiberglass structural support was substituted. Because of its long effective length (~ 3X actual length) and thin wall thickness (0.006"), this bellows tube has a heat leak comparable to the original fiberglass tube.

Testing will be completed by this summer.

References

1. A.F. Zeller et al, Proc. of the Tenth Int. Conf. on Cyclotrons and Their Applications, 1984, 79.

HELIUM GAS DIELECTRIC STRENGTH TESTS

A.F. Zeller

The proposed superconducting ECR source requires floating the system, including the cryogenic fluids and gases, up to 20 kV. This necessitates knowing the dielectric strengths of the various components. Since materials[1] like G10 have dielectric strengths of 40 kV/mm, the only concerns are liquid nitrogen, helium and these gases at temperatures from their respective boiling points to room temperature(300K). Nitrogen gas has a dielectric strength of 1.8 kV/mm at room temperature[2], and since the dielectric strength increases with increasing density (with decreasing temperature), cold nitrogen should present little insulating problems. Liquid helium has a dielectric strength[2] in excess of 20 kV/mm and hence is no problem. Likewise cold helium gas is also a good insulator, with 10K gas having a strength of 6 kV/mm. It is known, however, that warm helium gas has poor insulating properties.[2-7] In addition, it has also been observed that flowing helium gas has poor electron transfer properties, ie., the flowing room temperature helium gas from the source has very poor insulating properties.

In order to understand these effects and to determine a minimum length of insulator which will isolate 20 kV with a safety factor of 50%, a series of tests were undertaken. An apparatus was constructed to flow He gas from a high potential to ground thru a composite cylinder. Samples of RANDOLITE, G10 and G7 were used, with no apparent dependence on the tube compostion. This was expected since the dielectric strength of G10 is about 40 kV/mm. Samples from 6 to 126 cm were used.

All samples $\geq 10^{-4}$ cm did not break down at the maximum available 30 kV when only air or nitrogen was used. Static He gas broke down at 15 kV in the 10 cm sample, but supported more than 30 kV for lengths > 20 cm.

Gas flow tests of 0.2 to 52 mg/sec confirmed that warm He gas does indeed have poor electron transfer properties. The results are shown in Fig. 1, where the voltages represent

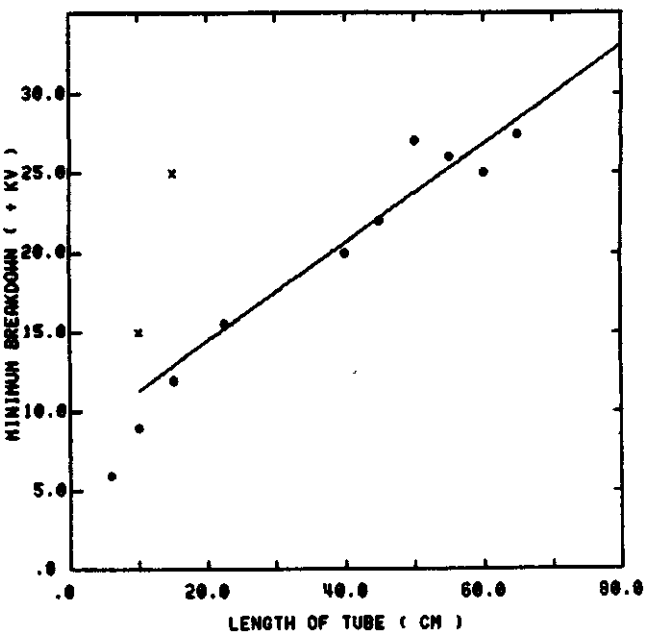

1. Circles are flowing helium, crosses are static helium and the line is the best fit for lengths >13 cm. The power supply limit is 30 kV. Air did not break down at less than 30 kV for a 7.5 cm length.

the minimum observed for each length. Above 13 cm the effective dielectric strength is a linear function of the length. It was observed that the break down voltage depended on flow rate, with a threshold value of 0.6 mg/sec (0.25 SCFH air or corresponding to a boil off of 18 ml/hr). The minimum break down voltages showed a variation of about ± 20% with flow rate, although the data in Fig.1 are the worst case points. There was also a slight dependence on the polarity, with negative potentials worse than positive ones, for the shorter lengths only. The resulting points for lengths less than

20 cm are about 2 kV lower than the corresponding positive voltages. All lengths exibited a conditioning phenomenon. From the detection of the first sparks, the tubes could be readily conditioned up another 25-30%, before complete break down and/or high leakage currents occurs. As an example, the 40 cm tube readily went to 27.5 kV after a single spark at 20 kV. The best fit line for the break down voltage for lengths >13 cm is given by:

$$V(kV) = 0.3 * L\ (cm) + 8.5$$

Thus to return warm He gas at 20 kV with a 50% saftey margin requires a 70 cm length.

---

1. H. Brechna, "Superconducting Magnet Systems" (Springer-Verlag, NY, 1973),p.398
2. J. Gerhold, Cryogenics 24,73(1984)
3. B. Fallou, J. Gerhold and B. Bouvier, ibid. 10,142(1970)
4. J. Gerhold, ibid 12,370(1970)
5. J. Thoris, et al, ibid 10,147(1970)
6. J. Gerhold, ibid 19,571(1979)
7. G. Bogner, ibid 15,79(1975)

BEAMLINE DIPOLE PROGRESS REPORT

J.C. DeKamp, M.J. Dubois, D. Landry, J.A. Nolen, R.T. Swanson, A.F. Zeller

The component parts for the prototype ± 16° superconducting switching magnet, described in earlier annual reports[1-3], are presently being assembled. The complete description of the final design and initial testing of components is given elsewhere[4], and will not be repeated here. This design is shown schematically in figure 1. Note that this drawing shows large dewars for liquid helium and nitrogen not present in an earlier design[1], which is consistent with our philosophy of batch filling each device on a weekly basis.

The superconducting coils, consisting of 600 turns of 0.6 mm diameter wire, have been wound and are awaiting installation in the bobbin. The coils were very easy to wind, requiring only 1 hour each. The coils are 0.5" X 1.0" in cross section and will carry 50,000 A-turns each at the nominal peak field of 17.5 kG in the magnet. Small test coils, described previously[3], as prototypes for the dipole coils were tested in the cryogenic test stand. The coils exhibited no training effects and went readily up to the calculated short sample limits. Current densities greater than 50 kA/cm² were achieved, well in excess of the 17 kA/cm² required for peak field operation. The disconnectable current leads and persistance switch, necessary to achieve the design goals of less than 50 l/week consumption of liquid helium and nitrogen, were also tested in the test stand.

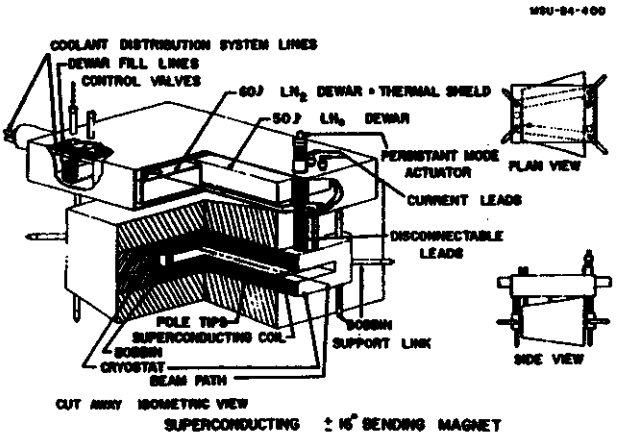

Schematic drawing of the complete magnet.

The approximately 6000 pounds of machined, low carbon (1003) iron yokes and pole pieces are in house and ready for final assembly. This assembly awaits the bobbin which is currently being repaired since it developed leaks during cold shocking. Testing of the complete magnet will start this summer.

---

1. A.F. Zeller et al, MSU Annual Report 1981-1982, 101.
2. M.J. Dubois, A.F. Zeller, & J.A. Nolen, MSU Annual Report 1982-1983, 155.
3. A.F. Zeller et al, ibid, 151.
4. J.C. DeKamp et al, IEEE Trans. on Mag. Mag 21,990(1985)

ECR ION SOURCE STATUS

T. A. Antaya, J. Moskalik, and D. Lawton

Introduction

We are in the first phase of a project to add external ECR ion sources to the NSCL superconducting cyclotron facility. The immediate goal is to produce and transport heavy-ion beams from an ECR to the K500 cyclotron. The construction of a vertical, room temperature ECR for this purpose is now well under way, with first operation projected for July 1985. This source, the subject of the first part of this report, has several new features not common with existing room temperature sources, including having the largest bore of any room temperature ECR fabricated to date, a complete iron return yoke, and MHD stability in both stages.

The long term goals of this project are directed towards the development of an advanced ECR ion source for coupled-mode and stand-alone operation of the K800 cyclotron. For this purpose an engineering study was made of an advanced large ECR ion source with superconducting coils and an iron return yoke. The superconducting coils give the source a wide magnetic range - capable of operating at frequencies from 6 to 15 GHz. In addition, the hexapole coils would be independently adjustable, a element of ECR ion sources that has not had adequate study in the past. The characteristics of this advanced ECR ion source will be presented in the second part of this report. Experience with the room temperature source, which shares many features, as well as further developments in the ECR field in 1985, will simply aid the design of the advanced source.

Finally, in the last part of this report, the performance of the NSCL superconducting cyclotrons with an ECR source will be considered.

I. The Room Temperature ECR Project

In October 1984, design studies for the superconducting ECR project were expanded to include a second, room temperature source, reduced 40% in linear dimensions. In a review meeting in East Lansing in November 1984, a consensus recommendation was made to proceed with the room temperature source coupled to the K500 cyclotron as the first step towards a facility involving two ECR's and the capability to transport beams directly to either cyclotron.

Design work commenced immediately on the small source. In conjunction with this effort, a joint NSCL/LBL study probed the relative importance of the number of magnetic poles in the transverse part of the minimum-B structure in the LBL source. One result of that study was that a large diameter hexapole was chosen for the NSCL room temperature source.

The Room Temperature ECR Ion Source Design

This ECR shares several design features with the superconducting source - the inclusion of a complete return yoke, the vertical orientation, stabilization of the entire axial magnetic field with a large bore hexapole structure (in fact the largest rare earth hexapole magnetic built to date), an adjustable first stage plasma position, the same source extraction geometry, and the operation of both stages at 6.4 GHz. Features of this ECR are shown in Figures 1-4.

The axial magnetic field will be produced by a set of nine circular coils, each composed of three double pancakes of .25 in^2 hollow, water cooled copper conductor. The pancakes are wound from an in house supply of conductor. The nominal power consumption for operation of both

stages at 6.4 GHz will be approximately 20 kWatts, with an average coil excitation of 200 A. The iron return yoke contributes approximately 25-30 % of the field.

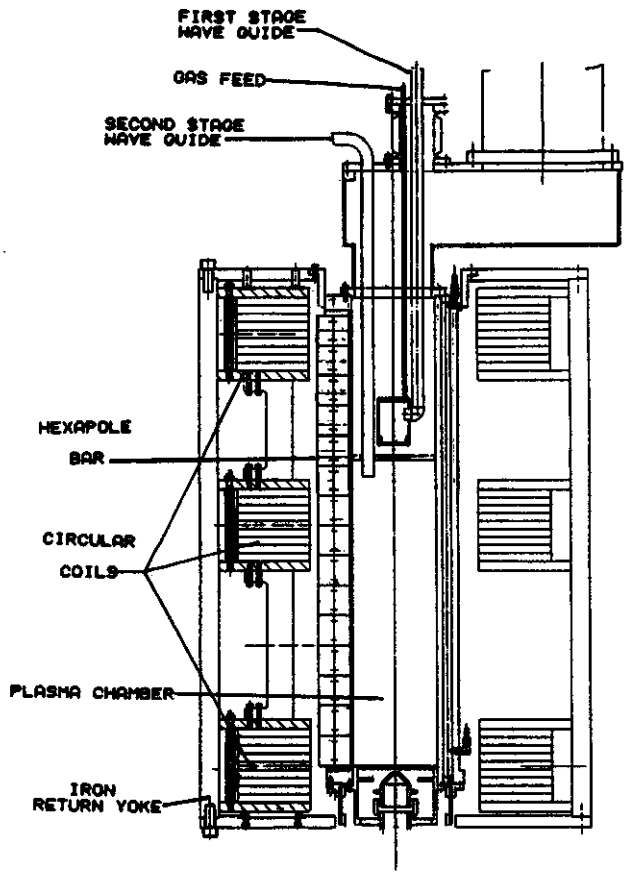

Fig. 1 The vertical room temperature ECR with copper solenoid coils and a permanent magnet hexapole is shown. The first stage is at the top, with beam extraction out the bottom end.

The plasma/vacuum chamber will also serve as the holder for the hexapole magnet. The hexapole consists of 360 pieces of 8.7 kG magnetized samarium cobalt. The pieces are held in place with a combination of gluing and mechanical clamping forces. Radial ports have been included in the plasma chamber, and the chamber will be water cooled.

Initially at least the microwave feeds for both stages will come in axially from the top, but radial feed is also possible. Two Varian

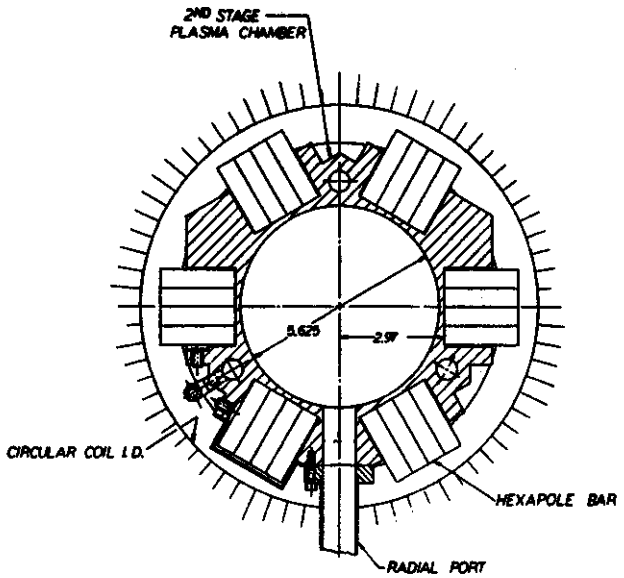

Fig. 2 A sectional view through the room temperature source, showing the position of the hexapole magnet relative to the plasma chamber and the solenoid coils.

6.4 GHz supplies at 3.3 kW each will be used to heat electrons at a resonance field of 2.29 kG.

Room Temperature ECR Ion Source Status

Work is progressing rapidly towards test operation on the room temperature source in early July 1985. Substantial progress has been made on all major sub-assemblies of the ECR source and the first beam line segment, as will be detailed below.

A total of 30 copper coil pancakes were wound for the ECR circular coils - a set of 27 required pancakes plus 3 spares. The three coil groups (1-first stage, 2-second stage), consisting of 9 pancakes each have been assembled and tested. The tests showed the coils going to twice the nominal operating current of 200 amperes and all coil design parameters were verified.

The fabrication of the plasma chamber from a solid 36 inch long by 9 inch diameter piece of oxygen free copper is complete. The hexapole magnet has also been assembled in slots in the plasma chamber. Individual samarium cobalt bar

magnets were arranged on six poles according to individual magnet strength, in order to minimize the variation in hexapole strength, both radially and axially. In order to obtain this ordered assembly, the total magnetic flux of 400 individual magnets was measured and this information was used to devise an assembly scheme using a 360 magnet subset of the original group. A theoretical variation in the magnetic field of less that 0.2 % from an homogeneous hexapole is expected over most of its axial length, and whether this was indeed achieved will be determined in an upcoming mapping of the actual field.

Three microwave transmitters operating at 6.4 GHz with a maximum power rating of 3.3 kW each were received from Varian Microwave Division in early March 1985. (We expect that only one supply is need to meet the power requirements of the room temperature ECR. We will however use two supplies initially to separate the tuning of the first and second stages of the source.) All three supplies have been assembled and tested to the maximum output power levels, and are now ready for ECR operation.

The overall design of the vacuum system is complete and most of the required vacuum hardware has been received.

The control system is of the same type that is being developed for the K800 cyclotron. The remote microprocessor station has already been used to control power supplies for the circular coil testing. The color monitor display screens and control software are under development.

For test operation of the room temperature ECR in July 1985, the first segment of the ECR to K500 beam line must be fabricated. The 90° magnet in this segment will do the analysis of the extracted ECR beam. Major components of this segment include one 90° magnet, one focussing solenoid, and three slit boxes: 90° object, 90° image, and divergence slits. Two of the slit boxes also have faraday cups and vacuum pumps.

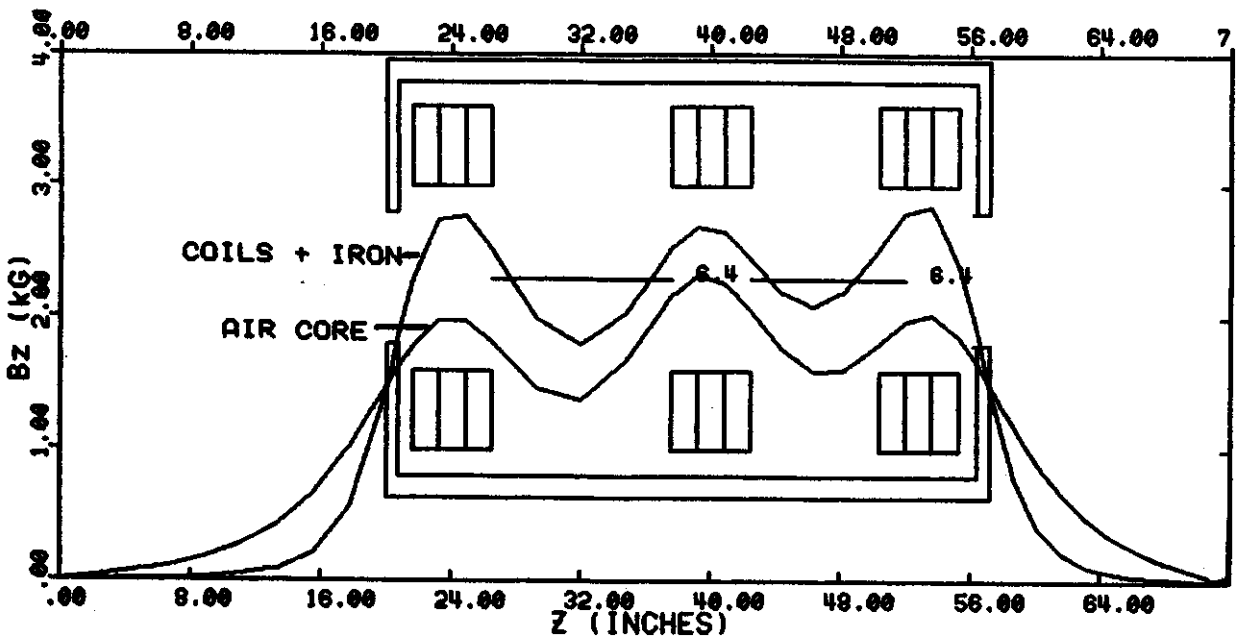

Fig. 3 The axial field profile of the room temperature ECR ion source is shown. The air core coil contribution to the field is indicated. The position of the coils and return yoke relative to the magnetic field is also shown.

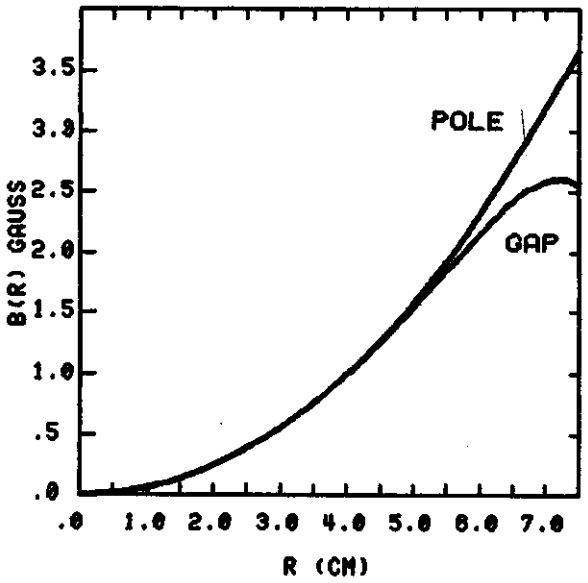

Fig. 4 The magnitude of the radial magnetic field of the permanent magnetic hexapole in the room temperature ECR shown along a radial line from the source axis and through a gap along a line from the source axis between magnet poles, and through the center of a magnet pole. (In an ideal hexapole these two fields would be identical.)

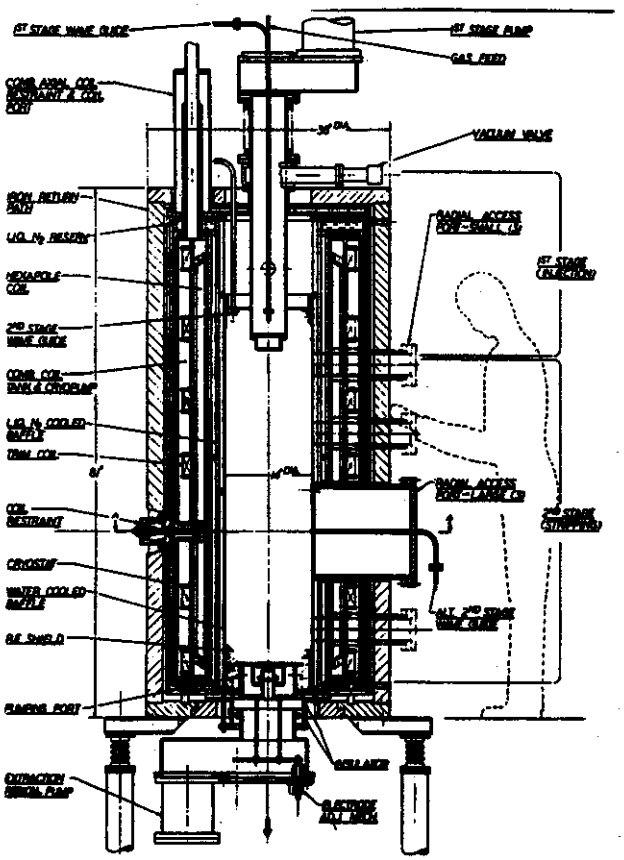

Fig. 5 A drawing showing the updated design of a vertical superconducting ECR ion source with a return yoke and second stage cryopumping off the coil vessel surface. To ease modification, the entire first stage can be retracted through a vacuum lock. Both radial and axial access to the second stage will be possible.

II. The Superconducting ECR Design Study

A large superconducting source ($\ell \approx 1$ m, $\phi \approx .35$ m) based on Ecrevis and Hiska, with improved pumping in the second stage coming from a large cryopanel, represents the current status of the NSCL advanced source design. Some features of this ECR ion source are shown in Figures 5-8. There is a clear shift in the charge state distribution of Ecrevis towards higher charge states, not shared by the smaller room temperature sources, that would be exploited in this new source design. The large plasma volume under consideration here necessarily implies the use of superconducting coils. A major decision to use the 4° surface of the the coil vessel, suitably baffled, as the second stage pumping surface, has resulted in substantial simplifications, as well as a large reduction in the volume of the device.

The essential features of the source design are as follows. The source orientation is vertical, with the injector stage at the top and the extraction geometry at the bottom. The axial magnetic field is produced by a set of six circular coils. Two of these coils span the first stage and the remaining four the second stage. To these coils are added a full length superconducting hexapole. All coils are of the epoxy impregnated superconducting type, mounted in a common helium vessel. The mirror coils will be wound in place on a stainless steel bobbin while the hexapole coils will be wound separately on forms and installed. The plasma chamber and the coil tank share a common vacuum, coming from the cryopumping action of the helium vessel outer surfaces. The separation between

the plasma chamber and the coil tank is a sequence of screens and baffles. An rf screen is mounted on the inside of a cylindrical water cooled baffle at a radius of 17.5 cm., forming the plasma chamber. A nitrogen cooled baffle backs the water baffle to provide radiation shielding for the helium cooled surfaces.

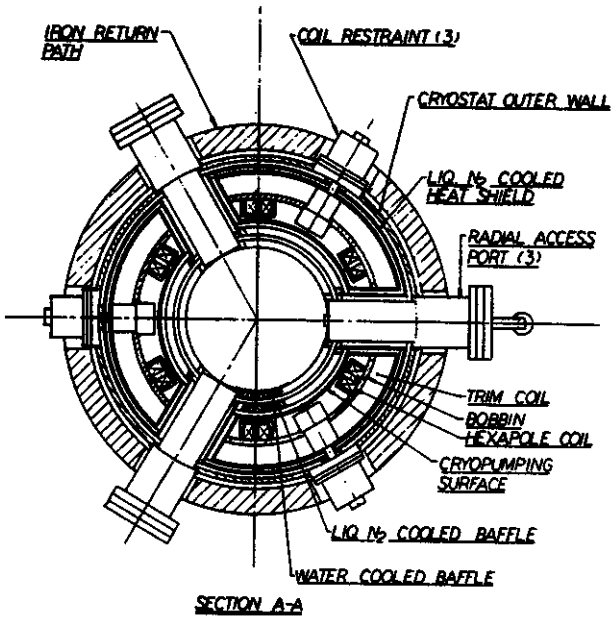

Fig. 6 A sectional view through the median plane of the second stage, shows the main elements of the coil vessel, including radial support links, radial penetrations through the cryostat to the plasma region, baffling for the coil vessel surfaces that provide the cryopumping, and the locations of hexapole and solenoid coils.

The addition of a complete iron yoke to the design has several advantages. The base of the yoke serves as the primary mechanical support for the source. The flux return path provided by the iron significantly reduces the fringe field of the source, as well as increasing the efficiency of the coils. At the same time the iron will serve both to shield the source from external magnetic fields and to shield the outside from the X-ray flux from the source. Three axial support tube structures, each consisting of concentric axial stainless steel tubes, take the net downward force of the coil tank, while three glass link members provide the radial support. The present plan calls for source operation at 6.4 GHz in both stages, but the coils and coil support system have actually been designed for operation at 14 GHz in both stages, corresponding to approximately twice the peak fields at 6.4 GHz. The build up of coil forces is the chief limiting factor on operating at high magnetic fields. The coils have a wide dynamic range, allowing operation at frequencies

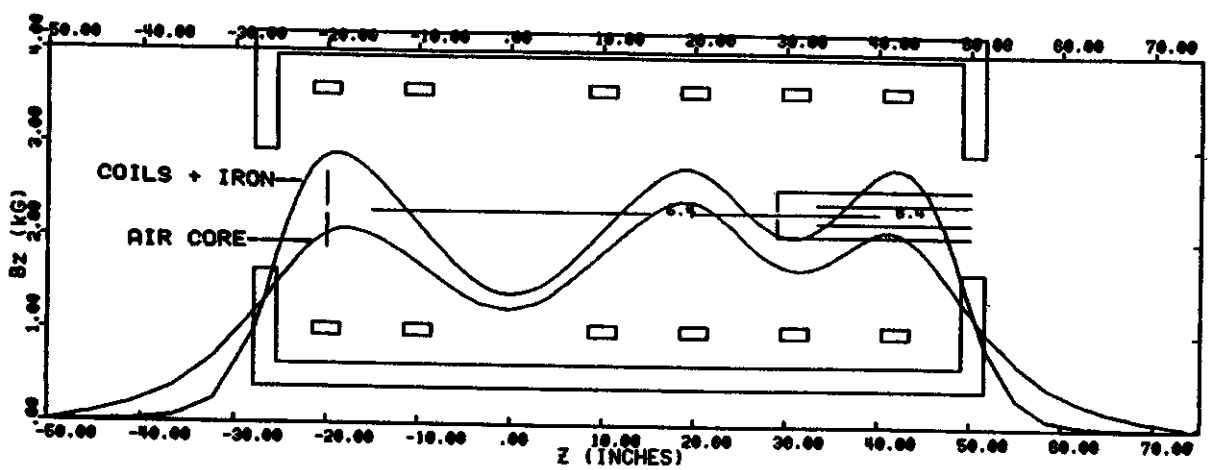

Fig. 7 The axial field profile of the superconducting source is shown for operation of both stages at 6.4 GHz. The positions of the coils, yoke, injector stage and extraction electrode are shown, as well as the positions of the resonances in both stages.

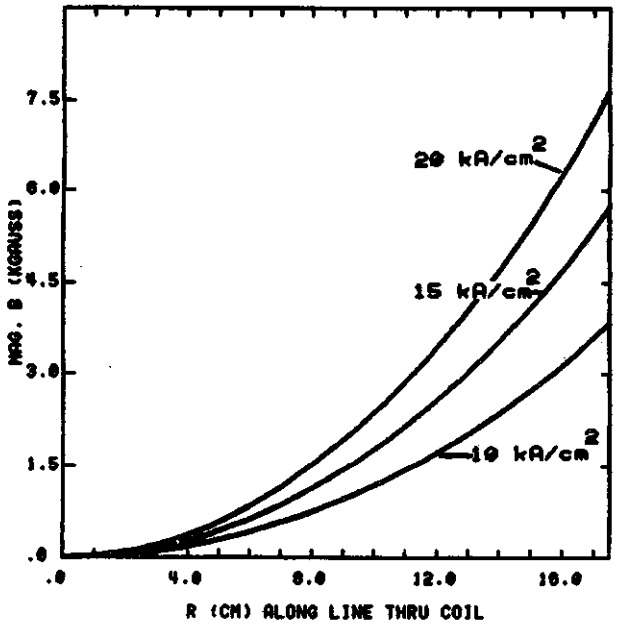

Fig. 8 The radial field profile of the superconducting hexapole coils is shown for different coil excitations.

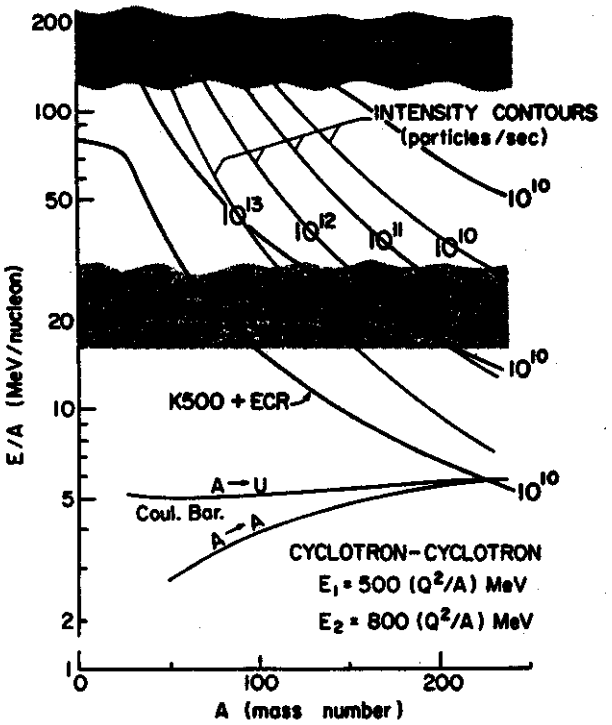

Fig. 9 Final beam energies versus mass from the 1978 NSCL Proposal for coupled cyclotron operation with an internal ion source, and those anticipated with an ECR injecting the K500, K800 and K500 + K800.

as high as 15 GHz.

A spherical pierce extraction geometry with built in space charge compensation will be employed. The puller electrode is biased negative to operate the extraction in an accel-decel mode, and has external position adjustment. The extraction region turbopump will provide the main chamber high vacuum during source cool down. As a consequence of the common vacuum for the plasma and coils chambers, the entire source assembly, including the power supplies and controls, will reside inside a high voltage platform. For axial injection into the cyclotrons, source bias voltages as high as 20 kV will be required.

The first stage resonance is defined in a 13 cm diam. chamber that inserts axially through a vacuum lock into the top of the source. This chamber is removable without breaking the main chamber vacuum, and the retraction motion will potentially allow us to use the position of the first stage as a tuning parameter. A circular wave guide located along the axis of this chamber provides the first stage microwave feed, and serves as the gas feed as well. A removable waveguide end section is shown. After the waveguide end, there is a differential pumping section, terminated in a removable end flange that separates the first stage from the second. Pumping there will be provided by a 1000 ℓ/s turbomolecular pump mounted off the external end of the first stage chamber above the iron yoke, giving a 330 ℓ/s pumping speed in the differential pumping region. Adding slots in the chamber wall to get additional pumping will also be possible.

The second stage has dimensions similar to Supermafios and Ecrevis. The overall length of the stage is 115 cm. with a plasma chamber diameter of 35 cm. Three large radial ports through the median plane of the second stage will provide access for microwave feed, solid feed and diagnostic purposes. Additional ports at other vertical positions, shown as ghosted lines in drawings, are under consideration as well. Two Varian supplies at 6.4 GHz and 3.3 kW

each will provided the second stage microwave power through separate waveguide feeds.

In making the 6.4 GHz choice, we have considered the rf power requirements of this large ECR to be more important initially than the rf frequency. Given the experience with Ecrevis, as much as 10 kW could be required to reach the limits of ultra high charge state performance. However the source itself can be operated at much higher frequencies.

III. Projection of NSCL Cyclotrons' Performance with an External ECR ion Source

We have made estimates of the performance of the two NSCL superconducting cyclotrons for stand-alone and coupled mode operation with an ECR. These are shown in Figure 9. In making the estimates, dc extracted currents of multiply-charged ions for several sources were averaged and a 10 % transmission from source to cyclotron extraction were assumed. (These data were current in mid-1984, so that the increases reported in late 1984 and early 1985 would of course favorably raise the curves somewhat.) In particular, the K800 cyclotron operated stand-alone would offer something like 50% of the anticipated performance of the coupled-mode operation with an internal source, at large A. Coupled with the high reliability, low maintenance and relatively uncritical tuning already demonstrated by ECR sources, this performance would add an important new option, but it should be noted that the K500 stand-alone and the coupled-modes would also benefit. There is a significant gain in final energy for coupled-mode operation at large A. Clearly, ECR sources will be an important addition to the NSCL facility.

Acknowledgments

An ECR project like this would not be possible without the full support of the laboratory, and the efforts of this large and diverse group are gratefully acknowledged. We would also like to acknowledge the continuing support and guidance lent to this project by our director Henry Blosser. In addition, many discussions of ECR concepts with R. Geller, Y. Jongen and C. Lyneis, during the development of this project, have proved very valuable—it has been a pleasure to work with all of these individuals.

ECR SUPERCONDUCTING COILS DESIGN STUDY

A.F. Zeller, J.A. Nolen, K. Subotic

Design studies of the main solenoid coils for the MSU superconducting ECR source (see contribution by Antaya and Lawton) have been carried out for the most demanding RF frequency. The design philosophy is one of using very conservative values for current densities and operating currents at the highest fields that may be required, even though a lower frequency RF system (lower required fields) may be chosen. Because of the necessarily higher currents, hence higher liquid helium usage, and expensive protection resistor requirements that go with a cryostable coil, a potted coil design was chosen. Additionally, we are familiar with these types of coils since most of the beam transport magnets will use potted coils.

The six solenoid coils described below are numbered consecutively from top to bottom, i.e., coil number 1 in the first coil in stage 1 and number 6 is at the exit of the second stage. The physical parameters of the wire and the coils are listed in table 1. The packing factor is

Table 1

Wire parameter for ECR main coils

Wire	NbTi
Diameter	0.9 mm
Cu: Sc ratio	7:1
Coils	59% packing
Turns per coil	2225
Coil cross sectional area	3 x 8 cm^2

consistant with those obtained in other coils wound in this lab. This example is for the 14/14 GHz case which requires the maximum field levels. Table 2 presents the appropriate magnetic and superconducting parameters. The peak fields are calculated with POISSON and include the contribution due to the iron yoke,

Table 2

ECR main coils for 14/14 GHz case without sextupole coils

Coil #	Current Density (A/cm^2)	$I_{operating}$ (A)	B_{max} (kG)	$I_{critical}$
1	8267	89.9	8.3	520
2	1000	10.8	2.1	640
3	7936	86.3	8.0	520
4	3307	36.0	3.7	620
5	3307	36.0	4.5	600
6	7275	78.1	8.0	520

but do not include any contributions from the sextupole coils. The critical currents are based on the current densities measured for the S800 conductor. As can be seen, this conductor is very conservative, but the cost decrease in going to a smaller wire with more turns is offset by the increased time needed to wind these extra turns. A copper-to-superconductor ratio of greater than 7-to-1 is not readily available.

The most pessimistic case for a presumed quench is when coil number 1 quenches first (as is most likely since it has the highest current density), followed a short time later by the other coils. The case shown here is for a delay of 0.8 seconds after coil 1 quenches, although the delay time is not especially critical since a longer delay results in more of the stored energy going into coil 1 as opposed to being more uniformly distributed. Coil 1 can, in fact, absorb all the stored energy without damage. The likely scenario for this 0.8 second delay is coil 1 flashing all the liquid helium, which quenches the other coils. The calculations[1] for the changes in current as a function of time are shown in figure 1. The hot spot evolutions are shown in figure 2. These calculations show that the coils will readily survive a quench. The case where all coils quench at the same time, e.g., a sudden loss of helium, results in even

lower peak temperatures.

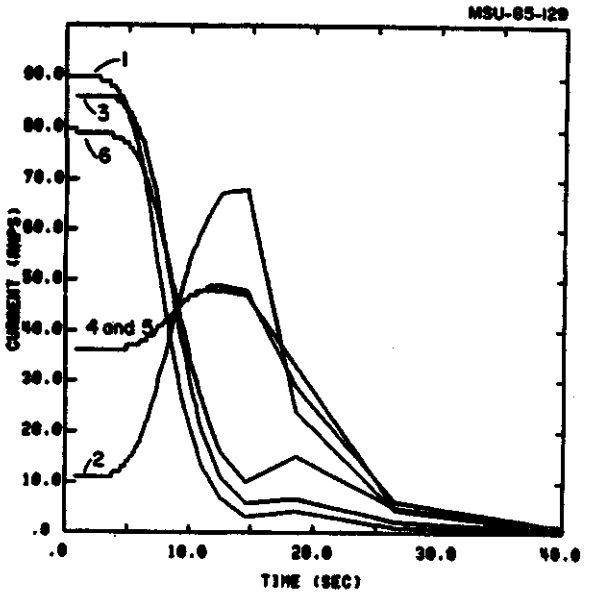

Fig. 1. Current changes in main coils after an assumed quench in coil number 1. After 0.8 sec all the others then quench.

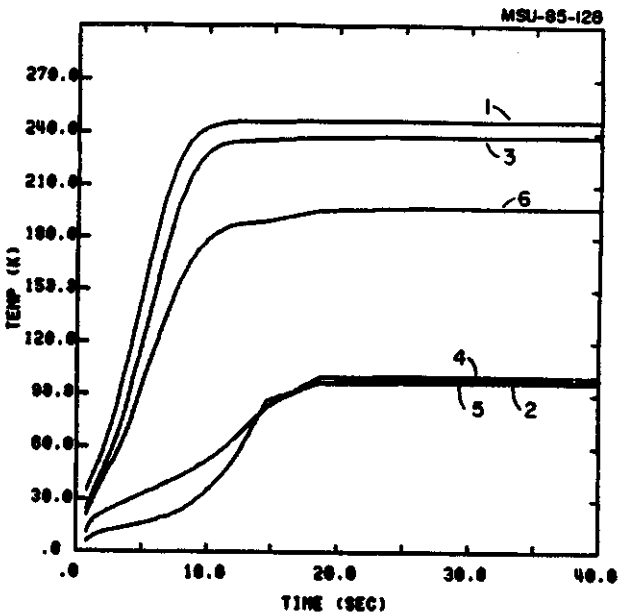

Fig. 2. Hot spot temperatures for the case described in figure 1.

When the effects of sextupole coils are included, the magnetic field at the conductor increase, as shown in table 3. This, however,

Table 3
Peak fields at the ECR main coils due to the sextupole coils

Coil #	B_{max}(kG)	$I_{critical}$
1	14	350
2	10	450
3	30	240
4	20	320
5	21	300
6	21	300

only decreases the hot spot temperature since the increased magnetic field propagates the quench faster. The sextupole coils are considered to only contribute a background field, but do not participate in the quench process directly, since they are only weakly coupled inductively to the solenoid coils. Reducing the field at the solenoid coils raises the peak temperature only marginally.

When the final decision on the RF system is made, based partially on experience gained in using the room temperature, small ECR source, the coils will be optimized to their final configuration.

1. M.N. Wilson, Program "Quench", Rutherford Lab Report, RHEL/MI5I,(1968).

ANALYSIS AND TRANSPORT OF BEAMS FROM THE ECR ION SOURCE TO THE K500 AND K800 CYCLOTRONS

L.H.Harwood

As part of the feasibility study for the ECR ion source, beam transport lines had to be designed. The first step in the design procedure was to determine the layout and optical criteria. The layout criteria were straightforward: 1) take the extracted beam from the vertical ECR and put it into the horizontal plane, 2) transport the beam through the trenches to the axis of the cyclotron, and 3) turn the beam onto the vertical, central axis of the cyclotron. The three optical requirements on the beamlines are: 1)separate the desired ion species from the rest; 2) transport the beam to the cyclotrons, and 3) match the emittance of the beam to the acceptance of the injection system. The latter two requirements are functionally very similar and will be discussed below. Analysis of the beam can be accomplished by forming a small waist in the beam and simultaneously having as large a dispersion as possible. Dispersion is produced by bending and a waist by focussing; thus, analysis of the beam could be done with the dipole that bends the beam into the horizontal plane.

Before doing any design calculations for the beamlines the emittance to be transmitted must be determined. The emittance used in the study was 3 mm x 30 mrad (300 mm-mrad) in both planes. A calculation using this emittance and the LBL magnet system accurately reproduced the LBL calculated beam envelopes; thus, it should be useful for calculating the NSCL beam lines as the extraction geometry in the NSCL design is the same as that in the LBL source. Calculations to determine any changes in the emittance ellipse due to the different magnetic field geometry of the NSCL source vs. the LBL source were not complete at the time of the transfer line design study; so a match to the LBL emittance was considered the most reasonable. Likewise, the effects of the emittance mixing by the fringe field awaits the results from this study.

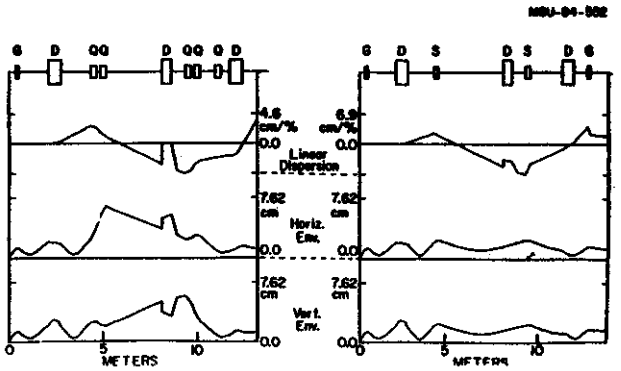

Fig. 1 Plots of the element arrangements, horizontal and vertical envelopes, and the linear dispersion for the quadrupole (on the left) and solenoid (on the right) based transfer lines from ECR extraction to insertion on the K500 cyclotron axis. Dipoles are denoted with a "D", quads with a "Q", solenoids with an "S", and the Glaser lenses with a "G". Note: the large discontinuity in the plots at the second (small) dipole is an artifact of the TRANSPORT calculation which required a axis rotation (x-y interchange) to make that dipole bend in the horizontal plane while the first and last dipoles bend in the vertical plane.

After the beam exits the ECR it must transported to the cyclotrons and be emittance matched to the injection system. The ECR beam will be injected into both cyclotrons, thus separate transfer lines are needed. The beam as

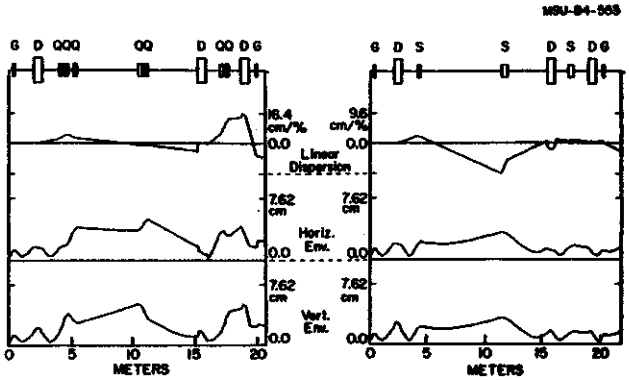

Fig. 2 Same as Fig. 1 except for ECR to K800 axis.

extracted from the source will be symmetric in the plane transverse to the beam direction; likewise it injects into the cyclotron center where the field is dominantly cylindrical (with some third-harmonic component) which would tend to maintain any symmetry in the beam. It would be most efficient if the transfer lines also maintain the symmetry of the beam from beginning to end. Possible choices for focussing elements are: 1) quadrupoles and 2) solenoids; electric options also exist but have been discarded to date based on the fact that electric elements would tend to destroy the beneficial effects of space-charge-neutralization needed for the more intense (> 50 μA) beams. Other laboratories have used both quads and solenoids so it was decided to study configurations using alternately quads and solenoids.

Some details were common to all designs. The first focussing element outside the ECR was a short solenoid ; this is optically similar to the Glaser lens used in this location for the ECR's at LBL and Louvain-la-Neuve. All dipoles used are double-focussing with approximately equal focal lengths; this choice will maintain the beam shape as much as possible; another choice might minimize the gaps of the magnets, but large gaps do not pose an amp-turn problem with such non-rigid beams so gap-size was not considered an important parameter but was to be kept small during the design process if possible. The solenoid forms a waist at the object of the dipole that bends the beam into the horizontal plane; there is dispersion at the image waist of the dipole so the analyzing slits would be placed at the object and image positions of the dipole.

The results of the design study are shown in Figs. 1 and 2. The solenoid-based designs proved optically superior to the quad-based designs with easily achieved, smaller, less tuning-sensitive envelopes. Practically speaking, the solenoid-based designs involve fewer and simpler-to-build elements. The solenoid strength required for the transfer lines is similar to that needed for the final injection into the cyclotron; so similar solenoids could possibly be used. Specifically, for a 10+ Ar^{40} beam the highest field required in a solenoid is 1.9 kG and would require use about 4.6 kW of power assuming four layers of the conductor used for the K800 trim coils operating at 250 amps (its limit is 400 amps) on the 0.5 m long solenoid. It should be pointed out that these are preliminary estimates and that the construction details could change.

ECR on the cyclotron axis:

As a design option, mounting a small ECR ion source on the same axis as the cyclotron was considered. Such a mounting would greatly reduce the length of the beam transport, but would not simplify it's functions, ie. to analyze the beam into different M/Q species and to match the emittance of the source to the acceptance of the cyclotron. Before a major investment in design of an ECR appropriate for this task, the viability of the transport was considered an important question. Thus, the purpose of the design study reported here was to determine the minimum space needed for an analysis/transport system which would give acceptable M/Q resolving power (resolving power of 50 with the full beam and/or 100 with half the beam).

The first function of the transport system, analysis, requires a dispersive device; options include electric septa, magnetic dipoles, wien filters, and any combinations thereof. For the present, basically co-axial geometry, the wien filter appears most appropriate as it could be fit between the RF dee-stems most easily ("Dipoles" would require a deflection off the axis of the cyclotron and out between the dee-stems); the dispersion produced by the wien filter is the same as for a magnetic dipole of the same length and field. The wien filter should thus give sufficient resolving power.

Three systems were tried. In all

calculations, an emittance of π x 5 mm x 40 mrad was used in both planes. The three differed more philosophically than they differed in number or arrangement of elements. The first was the most flexible, most similar to the earlier designs, and longest. It used a short solenoid to make a waist at the object of the analysis system which consisted of a drift, y-focussing quadrupole, a wien filter (effective radius of curvature = .4 m and length = .5 m), another y-focussing quad, and a drift to the image location. The wien filter provides the "x" focussing and the quads provide the "y" focussing. After the momentum dispersed image, the beam is matched to the nominal acceptance of the cyclotron by a pair of solenoids; a pair of solenoids is not strictly necessary (as described below) but provide a measure of flexibility, especially when combined with the asymetric focussing of the quads. The second system discarded the intermediate waist and one of the the last two solenoids. This system provides acceptable dispersion with reasonable envelopes and is 1 m shorter than the first system; it would not be as flexible, however. Interestingly, the resolving power of the present system is more than that of the earlier study using a 90 degree bending magnet; this is due to the earlier y-focussing (in the quads rather than on the magnet edges) which increases the "Karl Brown" integral. The shortest system discarded the initial Glaser lens altogether, but the lack of flexibility was considered an over-riding negative aspect.

The injection study reported by Bellomo, et al. (1) had a solenoid as its final element before entering the yoke of the magnet. This is similar in beam size and shape to the beam at the last solenoid in the present transport systems. Thus, if we put the last solenoid of the systems at the edge of the yoke, we will have an estimate of how far the ECR exit must be from the yoke. For the longer system, this distance is about 4.5 m and it is about 3.5 m for the latter. In either case, the ECR would be at the bottom of the sub-basement or, even worse, in the sump. Either case would require major engineering changes in the source and great inconvenience in modifying and/or servicing the source.

Conclusions:

After examining alternatives for the NSCL transfer lines, we conclude that the best purely magnetic design uses solenoids rather than quadrupoles for focussing and uses symmetrically focussing dipoles for bends. This "best" design is consistent with all design criteria.
Additionally, we find it is possible to do acceptable beam analysis and matching with a distance of as little as 3.5 m from the exit of an ECR to the outside of the yoke. The system would require two solenoids, two quads, and a wien filter. The flexibility of the system would be be minimal, however.

ECR 90° ANALYSIS MAGNET

A.F. Zeller, J.A. Nolen, & R.T. Swanson

A compact bending magnet for the ECR source has been designed and is under construction. This magnet will be used as the beam analysis magnet for the room temperature source and as a prototype for the other 90° magnets which must fit between the "D" stems to inject beam into the cyclotron.

First order optical calculations using TRANSPORT were done to get the edge angles necessary to obtain a double focus. Calculations were done using the finite gap, sharp-edge, non-saturating correction[1] to the fringe field. This has the effect of reducing the amount of transverse focusing produced by the zero-gap solution, which requires only 26.5° edge angles, requiring an increased edge angle of 30.5° to obtain the necessary focusing power. Second order calculations show that the spot size will more than double due to the large coefficient for x/θ^2 and x/ϕ^2, coupled with the 40 mr divergence expected for the source. Karl Brown[1] has shown for an n = 1/2 magnet that the sum of these two terms is a constant, so while one of the terms can be reduced, the other increases by the same amount. Therefore, no second order corrections were applied. (Actually, since this is not an n = 1/2 magnet the x and y envelopes are not symmetric so the above theorem is not strictly applicable. A second order correction inside the magnet could be used to improve it.) If the resolution turns out to be unacceptable, then the magnet will be replaced with one having the necessary second and/or higher order corrections, while this first magnet will be relegated to the injection line. Optical parameters are listed in table 1.

In order to accept as large a phase space as possible, a large gap and pole width were desirable. To minimize cost, a simple window frame geometry was chosen. However, at a field level of 2.5 kG, and especially later when the same type magnets are in the strong cyclotron fringe fields, large amounts of iron must be used to maintain field uniformity (≤ 0.1 % for a width of 5") as saturation occurs. Although high permeability iron can be used, it is hard to obtain in small quantities. The brute force method of adding iron cannot be used since spacing of the "D" stems limits the size. To compensate for the reduced permeability of the more readily available 1020 iron, a small (0.06" width) slot was introduced above the coil, at the start of the "pole tip". The purpose of the slot is to cause the field lines to straighten out near the coils. This has the effect of keeping the field flatter over a larger width than would normally occur. This is shown in figures 1 and 2. In addition to buying permeability, the slot allows an easy method of adding the beam vacuum box. The 1/2" thick slabs will be welded to stainless steel spacers, keeping the entire gap available for beam. The

Table 1

Optical Parameters for ECR 90° Magnet

Radius	40 cm
Max. Rigidity	30.5 MeV/c
Max. Field	2.5 kG
Edge Angles	30.5 °
Phase Space (x and y)	±5 mm ± 40 mr
1st Order Spot Size (x)	±5 mm
2nd Order Spot Size (x)	±11.6 mm
Object and Image Drift Distances	100 cm
Dispersion	1.98 cm/%

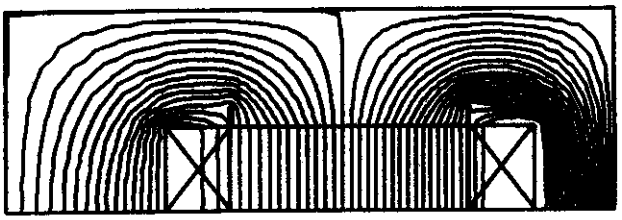

1. POISSON calculation in cylindrical coordinates for a cross section through the upper half of the magnet.

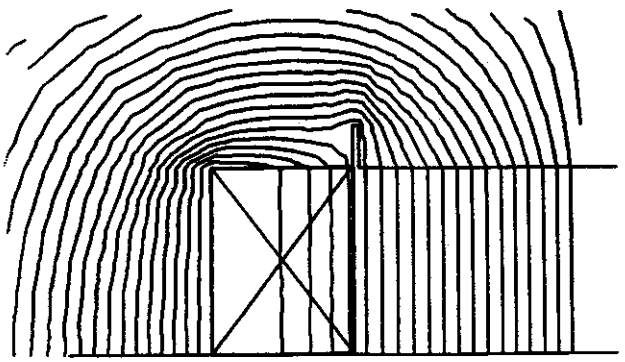

2. Enlarged portion of Fig. 1 showing the coil package and the 0.060" slot. The slot is 0.5" tall.

complete magnet parameters, including power supply requirements, are listed in Table 2.

Construction will be complete at the same time as the room temperature ECR source.

Table 2
Magnet Parameters

Type	Window Frame
Gap	4.17"
Field Uniformity (Δ B/B)	0.1 % over a 5" width
Pole Width	6"
Yoke Thickness: top	3"
inner side	4"
outer side	2"
Iron weight	625 lbs.
Conductor	1/4" square (hollow)
Total turns	96(6 dbl. pancakes)
Peak current	230 A
Peak Power	5.4 kW
Peak Voltage	23.6 V
Max. Temp. Rise	10° C (each pancake)
Total Cooling Req.	2.05 gal/min (@ 80 Psi)

---

1. K.L. Brown, SLAC 75, 1982.
2. This idea was suggested to us by Klaus Halbach.

ECR BEAMLINE SOLENOIDS

A.F. Zeller and J.A. Nolen

The first optical element after the ECR source is a solenoid lens[1] to provide focusing for the diverging beam, in both planes. Once the choice to use a solenoid instead of quadrupoles is made, the lens can be constructed in one of two basic shapes: 1) a normal solenoid, with or without an iron return yoke or 2) a Glaser lens, which is a truncated iron core solenoid[2].

A Glaser lens has an optimum ratio of magnetic length (where the field decreases to half its central value) to its inner bore diameter of 1.5. Thus a 4" diameter lens has a magnetic length of 6". Because the focal power of a solenoid/Glaser is proportional to the square of the field (B) times the length (L), reducing the length by a factor of two, while increasing the field by the same amount gives an overall increase in B^2L of a factor of two. Thus a properly designed Glaser which can produce fields over 15 kG, without saturating the iron, yields strong focusing within a short length. To keep the device from saturating, and changing the field shape, the inner iron core must be approximately three times the bore diameter. These lenses were originally developed for electron beams, with their small sizes, where the inner bore is only a small perturbation in the iron core. To scale up a Glaser to a 4"-6" diameter requires large amounts of iron, and makes the lens power hungry, simply because the average diameter of the coil is so large that the electric length becomes very big, very fast. Large bore Glaser lenses do not use this traditional proportion. A large (4") bore Glaser lens capable of a central field value of 7kG without saturating, is shown in figure 1.

Solenoids have long been recognized[3] to have some optimum geometry for their length, diameter and coil thickness, but the addition of an iron return yoke changes the optimum ratio. However, the use of POISSON solves the problem with real iron (finite permeability). The Glaser has empirical formulas which allow the field profile to be calculated analytically[2], which is probably one reason these devices were used for large bore applications. Taking a fixed bore diameter and current density, solenoids have an optimum thickness in terms of B^2L and power consumption P.

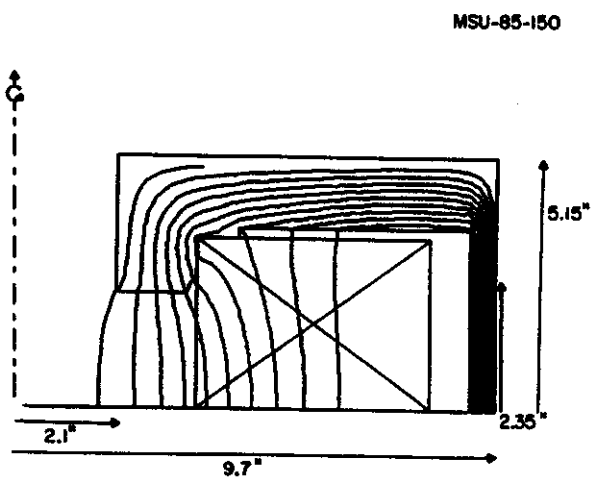

Fig. 1 A Glaser lens based on the Berkeley design showing the field lines calculated by POISSON. The scale is in inches. Note that this is only a section thru the top half.

A 6" bore solenoid with an iron yoke which is optimized in the ratio of B^2L/P is shown in Fig. 2 . This optimization process is shown in Fig. 3, which plots B^2L versus power.

Depending on the distance the lens is placed from the source, the required B^2L for a 30.5 MeV/c, maximum rigidity beam is between 10 and 15. The 15 figure represents a drift length of 1.6', the mimimum possible and the 10 figure is a more conservative 2.5'. The Berkeley Glaser[4] has a field of 7.2 kG and a 4" diameter bore with a calculated 13.5 cm magnetic length giving a B^2L of 7. POISSON calculations reproduce the exact magnitude of the measured

central field when the appropriate number of amp-turns are used, together with the permeability table for low carbon iron. This length is in agreement with the standard Glaser calculations[2]. The Berkeley Glaser's characteristics are shown in Fig. 1. The comparison of a 14.86" long solenoid (the optimum from Fig. 3) with a scaled up version of the Berkeley Glaser is shown in Fig. 4 and in Table 1. The optimum solenoids are extended to larger values of B^2L using the premeability curve for 1020 iron. A 3/4" yoke gives essentially the same results as the infinite permeability solution. The Berkeley Glaser lens, beyond a B^2L of 7, is scaled up using the somewhat unrealistic assumption of no increase

MSU-85-151

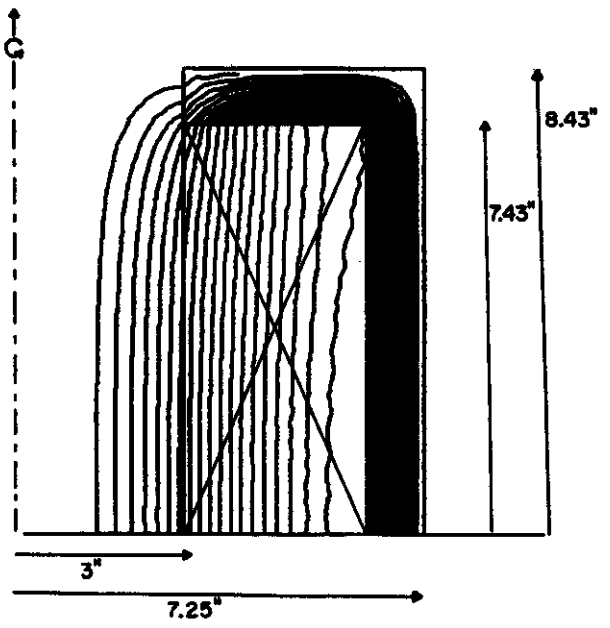

Fig. 2 An iron-yoked solenoid for comparison with Fig. 1.

MSU-85-137

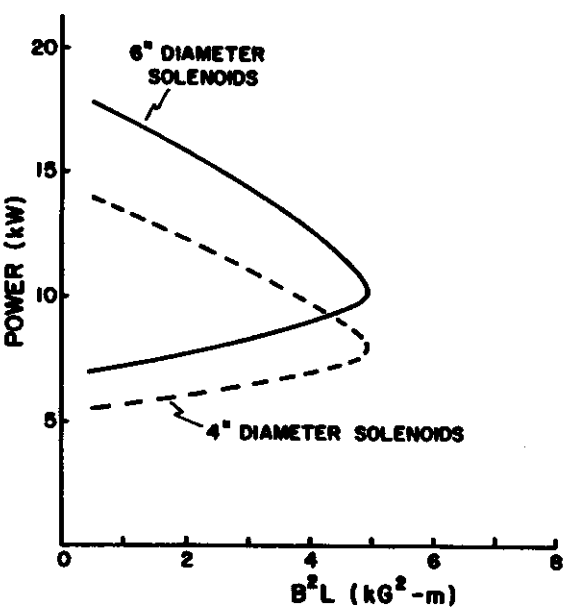

Fig. 3. Power consumption versus focal power for solenoids without an iron yoke and with fixed current density.

MSU-85-149

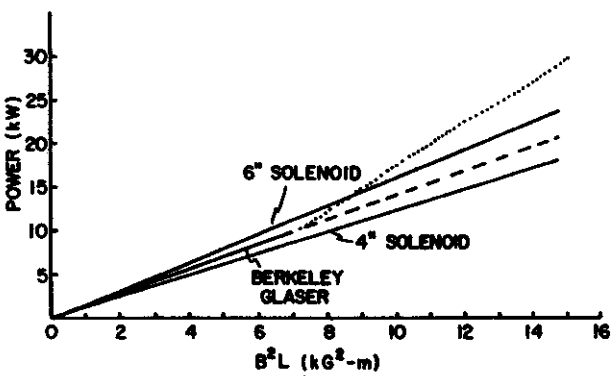

Fig. 4. Optimized solenoids with iron yokes compared with Glaser lenses based on the Berkeley design. The line up to 7 kG^2-m for the Berkeley Glaser is measured. The dashed line is an extrapolation assuming infinite permeability and the dotted line assumes the permeability of 1006 iron. Both extrapolations assume no increase in the coil resistance.

Table 1

Comparison of 14.86" long solenoids with Berkeley Glaser lens.

	$B^2L(kG^2-m)$	B(kG)	Power (kW)
6" Solenoid	10.0-15.0	5.2- 6.3	16.2 -24.6
4" Solenoid	10.0-15.0	5.2- 6.3	12.6 -19.0
4" Glaser	10.0-15.0	8.6-10.5	14.1*-21.1* (18 - 30)

* μ_∞ assumption. Numbers in parenthesis are for 1006 iron.

in resistance in the coil. The dashed line assumes no saturation in the iron, while the dotted line uses a finite permeability curve for 1006 iron. It must be mentioned that the 2.5' solution (B^2L = 10) is not avialable for the 4" devices because of the beam divergence. Also note that the Berkeley scale-up is very optimistic, since infinite permeable iron is not readily available. The complete details of the 14.86" solenoid are listed in Table 2.

Table 2.

ECR solenoid parameters.

Length		14.86"
Inside diameter of coil		6.0"
Number of turns of 1/4" wire per layer		55
Number of layers		12
Water flow @ 80 psi.		3.6 gal/min
current:	3.36kG	157A
	5.2 kG	240A
	6.3 kG	293A
Power:	3.6kG	6.7 kW
	5.2kG	16.2 kW
	6.3kG	24.6 kW
Max. Temp. rise:	3.36 kG	12^0C
	5.2 kG	27^0C
	6.3 kG	42^0C

In the regime of focusing power needed for the beam line after the 90^0magnet, about 3-4 kG^2-m, the 4" Berkeley Glaser is a little more energy efficient than a 6" diameter solenoid and comparable to a 4" solenoid. The smaller diameter is a drawback because of the reduced beam volume and the higher pumping impedance, as well as the 500 lbs. of iron needed for the Glaser. At larger values of B^2L, the 6" solenoid is probably more efficient, although it is possible that a more efficient design, eg, the infinite permeability extrapolation, may exist. This would undoubtedly involve an increase in initial costs in terms of more iron and conductor, as well as an extended design study not consistant with an early summer completion.

The solenoid that will be used just outside the ECR source will be completed when the source itself is finished.

1. L.H. Harwood, Contribution to this report.
2. A.B. El-Kareh and J.G.J. El-Kareh, "Electron Beams, Lenses and Optics, Vol 1',(N.Y.,N.Y.)1970.
3. D.B. Montgomery, "Solenoid Magnet Design", (Huntington, N.Y.)1980.
4. D.J. Clark, Y. Jongen & C.M. Lyneis, Tenth Int. Conf. on Cyclotrons and Their Applications 133(1984).

AXIAL INJECTION STUDIES FOR THE ECR BEAM

F. Marti and J. Griffin

Introduction

The original feasibility studies for an axial injection system in a superconducting cyclotron were performed by Bellomo et al. (Ref. 1) considering the K800 as the model cyclotron. With the goal of building an ECR source to inject in both of our machines (K500 and K800), we decided to update and extend those studies. The previous conclusions indicated the likelihood of using an electrostatic mirror to inject the beam in the median plane and, that if we did not use the magnetic bumps to center the orbits, we had to inject the beam off the axis. A solenoid was used to confine the beam just outside the yoke, and a buncher was suggested.

Mirror Studies

We use the Q/A=0.5, B_o=3.62 T and E=80 MeV/A ion as a test particle because it has the smallest radius of curvature injection orbit and will determine the space available for the central region.

The injection voltage and the tilt angle of the mirror determine the magnitude of the electric field needed to bend the particle 90 degrees into the median plane.Fig. 1 shows the electric field E (top), transit time τ_D (middle), and grid transparency T (bottom) as a function of the tilt angle α. The electric field decreases when α increases, but at the same time the transit time gets larger and the transparency through the grid gets smaller. Lowering the injection voltage lowers the required electric field, but makes the confinement of the beam more difficult during its transport.

We have studied several combinations of injection voltages and tilt angles. Assuming that the electric field in the mirror is 35 kV/cm and the injection voltage is 20 kV (10 keV/A), we obtain α=51.7°. The value of 35 kV/cm comes from the test stand that the Orsay group (Ref. 2) built to test electrostatic mirrors under actual beam conditions. The orbits were tracked inside the mirror with a uniform electric field. With this set of parameters, the

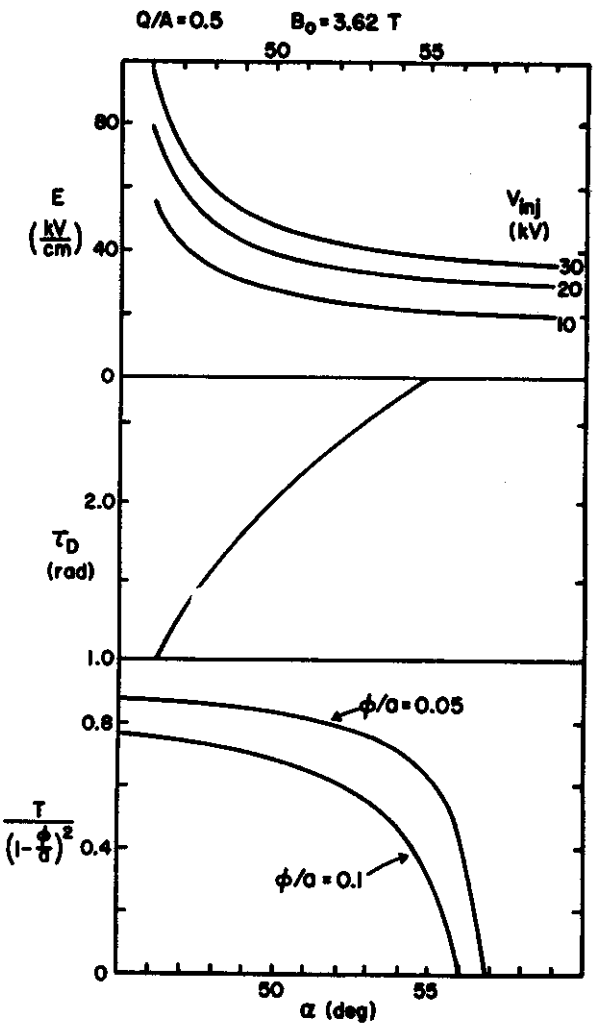

Fig. 1.- Electrostatic mirror parameters for an ion with Q/A=0.5 in a B_o=3.62 T magnetic field as a function of the mirror tilt angle α. At the top, we have the electric field in kV/cm for three different injection voltages. In the middle, we plot the transit time in radians, and at the bottom the (geometrical) grid transparency T for two different grid configurations. ϕ is the wire diameter and a is the distance between wires.

orbits exit the grid at a large angle with respect to the normal to the grid in the median plane (66°), making it difficult to clear the housing of the mirror.We can make the orbits exit at a smaller angle by making α smaller; but to keep the electric field below 35 keV/cm, we have to decrease the injection voltage to 10 kV. Fig. 2 shows the cross section of a mirror working under these conditions and the vertical projection of the ion trajectories. In this case we had to depend on the penetration of the RF field created by the puller to extract the ions from inside the mirror, but this field is not symmetric around the median plane due to the inclination of the grid. We tried different schemes to solve this problem but were not successful.

If we assume that the electric field can reach values close to 50 kV/cm (very close to the value used by SIN but in a larger mirror) we can use α=47.8° and V_{inj}=20 kV. The ions leave the mirror without any help from the RF field. A problem appears in the design of the central region with the post in the third dee that helps to define the electric field and also holds together the upper and lower dees. There is no room to put this post between the orbit first turn and the mirror, making it necessary to place the post between the first and second turn which raises some questions about centering versus RF phase. The position of the mirror (that interferes with the post) is determined by the requirements that the ion gains maximum energy between mirror and puller and has a positive phase in the first turn.

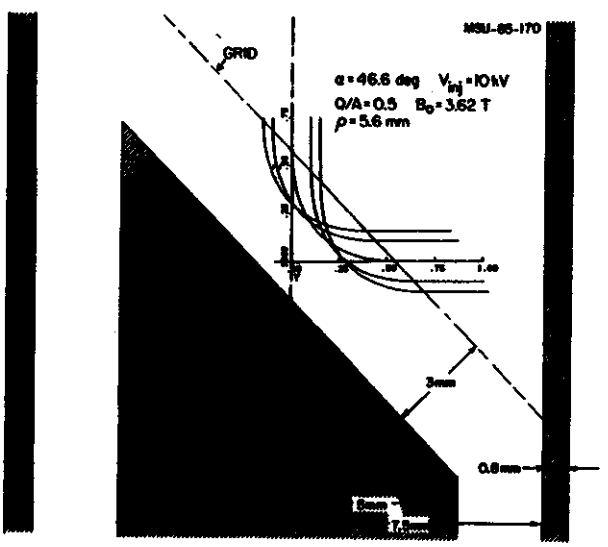

Fig. 2.- Cross section of the electrostatic mirror with the projection of the orbits in the vertical plane. The beam starts parallel outside the mirror.

Even though the orbits were tracked in a uniform electric field, we performed relaxation calculations of the electric field in the mirror to study its uniformity and help us in picking the sizes of the different components of the mirror. If we decide to go ahead with the design of the mirror, we will run the orbits in the calculated field.

Center Plug

The studies done by Bellomo et al. (Ref. 1) showed that the sharp edge termination of the present center plug in the K500 was not well suited to axial injection when the beam was off-centered because of the high gradients produced in that region. We explored the modifications needed to smooth out the field produced by the plug. Fig. 3 shows a comparison of the axial fields in the case of our previous test particle. The solid curve represents the field produced by a tapered plug while the dotted curve corresponds to the actual plug with a sharp edge. Both fields have been computed with Poisson. As we do not intend to measure the magnetic field again after modifying the plug, it is important to keep the median plane field as constant as possible. Fig. 4 shows the median plane B_z for both types of plugs and it will be very easy to adjust the shape of the modified plug to match the old field.

Buncher

We have studied the bunching effect of a double drift bunching system. It consists of two bunchers separated in space where the first one is excited at the same frequency as the cyclotron, while the second one is driven at twice the cyclotron frequency. These are

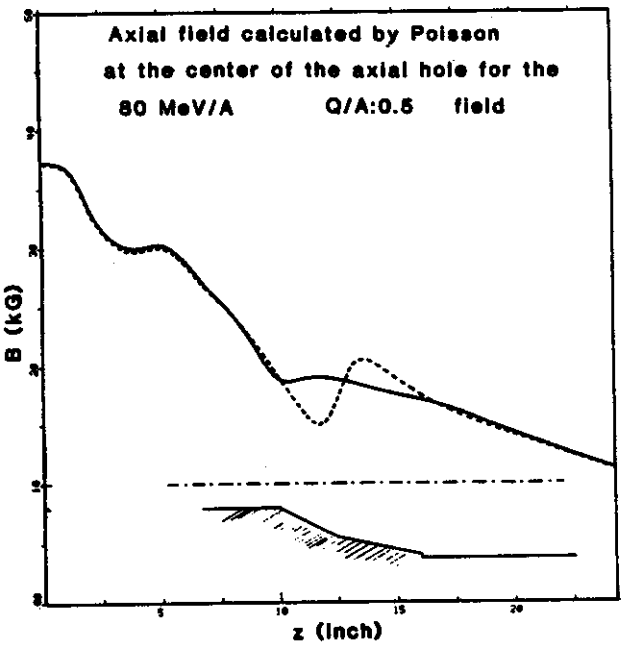

Fig. 3.- Axial field along the center hole as a function of z. The dotted curve corresponds to the plug used at the present time in the K500 cyclotron and has a sharp termination at z=12.5 inches. The solid curve corresponds to a tapered plug that has the profile shown at the bottom and extends up to 16 inches. The calculations were made with POISSON.

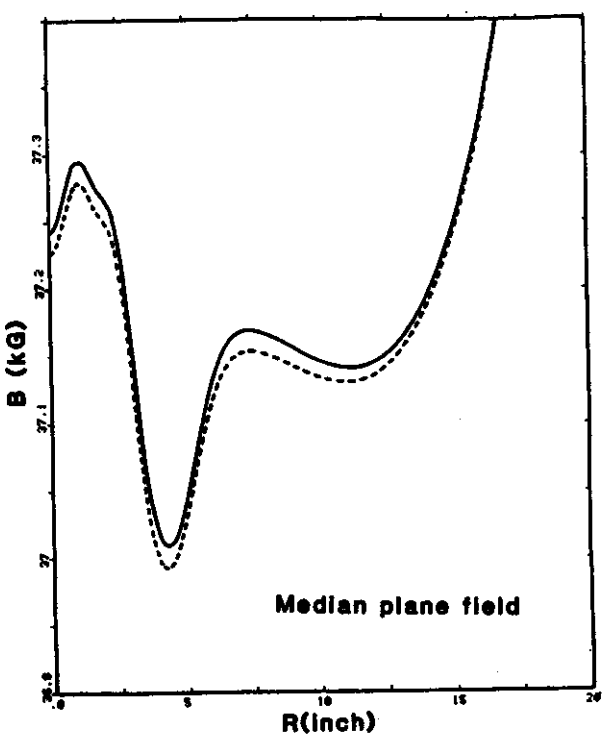

Fig. 4.- Similar to Fig. 3, but showing the field in the median plane.

preliminary studies in the sense that we have not included yet the energy spread of the ions leaving the ECR source nor the debunching effect produced by the space charge. We expect a voltage fluctuation of about 10 V for the ions extracted at 10 to 20 kV.

In the examples that we show here, the distance from the first harmonic buncher to the median plane is 40 inches, placing the buncher just inside the yoke (43 inches). If our beam envelope calculations show that the solenoid outside the yoke can be moved further away from the yoke, the buncher can be placed outside the axial hole making it easier to work on. We have performed calculations similar to those of Milner (Ref. 3) to determine the optimum distance between the two bunchers for a bunching range of ± 12 degrees. Fig. 5 shows a plot of the bunching efficiency as a function of the voltages in the two bunchers. We note that the

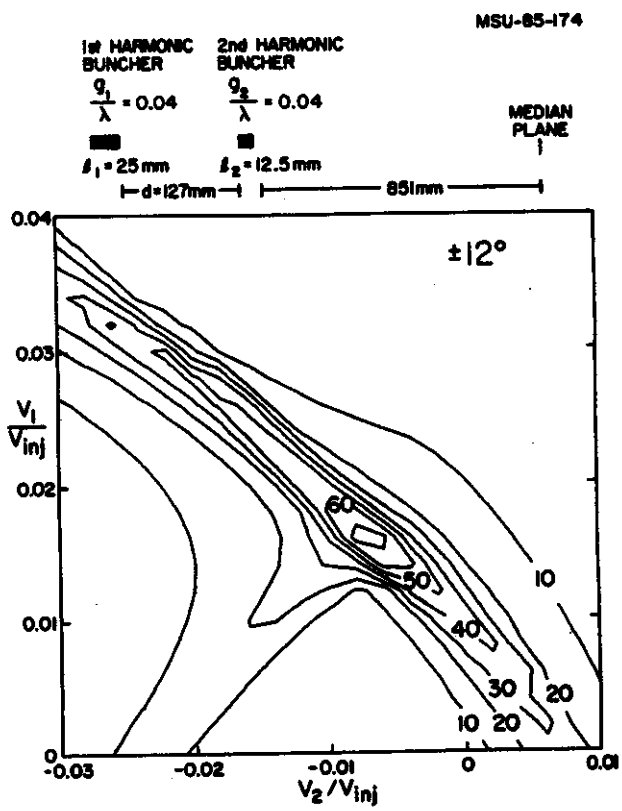

Fig. 5.- Bunching efficiency for the double drift buncher indicated at the top and a ±12° acceptance range. g/λ is the ratio of the buncher gap size to the distance traveled by the ions during one RF period.

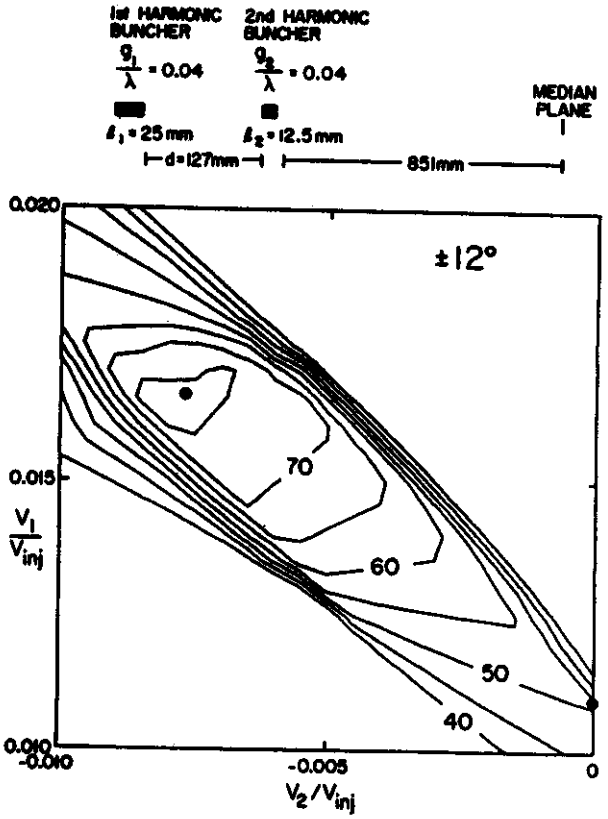

Fig. 6.- Enlargement of a section of Fig. 5 where we have indicated with black circles the running conditions for a two buncher system and for a single buncher (V_2=0).

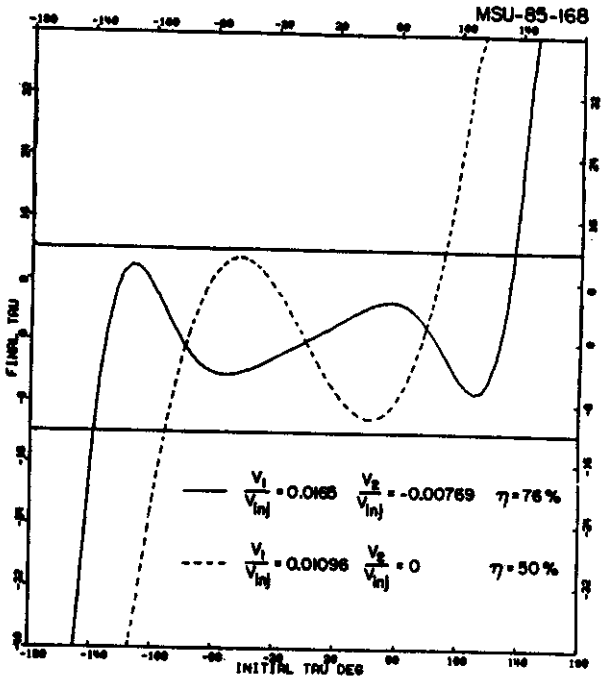

Fig. 7.- Arrival time at the median plane vs. starting time at the first harmonic buncher. The solid curve was obtained with the two bunchers operating at the point indicated in Fig. 6, and the dashed curve with only the first harmonic buncher similarly indicated in the previous figure.

efficiency changes slowly when $V_T=V_1+V_2$= constant. Fig. 6 shows an enlargement of a section of the previous figure where we have a peak efficiency of over 75 %, while working with one single first harmonic buncher (V_2=0) the efficiency is about 50 %. The two circles in this picture represent the running conditions for the double drift mode and the single buncher mode. The time distribution at the median plane is shown in Fig. 7 for the two cases indicated by the circles in Fig. 6. The beam intensity as a function of RF time is shown in Fig. 8.

The inflector in the median plane will have a debunching effect that we have to include along with the debunching produced by the different paths along the axial hole. These two effects depend strongly on the size of the phase space.

Spiral Inflector

Due to the difficulties associated with the electrostatic mirror, we decided to look into the design of a spiral inflector of the type built by Belmont and Pabot (Ref. 4) at Grenoble. The preliminary studies show very promising results. It seems possible to build an inflector in the small space left inside the first orbit. With a diameter of about 25 mm, this inflector has a gap of 4 mm. We are comparing two

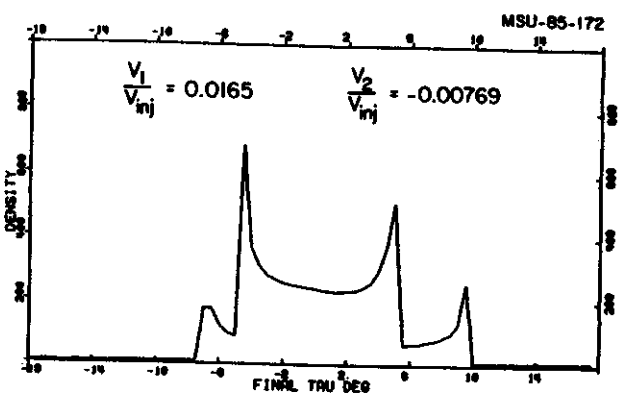

Fig. 8.- Current density (arbitrary units) as a function of RF time for the operating mode with the two bunchers, (plotted in the previous figure with the solid curve).

different designs: one with slanted electrodes and one with simple unslanted electrodes. The orbits are tracked in an electric field calculated with the RELAX3D4 relaxation code. So far, the advantages of the spiral inflector make it the most desirable choice over the electrostatic mirror.

1.- G. Bellomo, D. Johnson, F. Marti and F. G. Resmini, Nucl. Inst. and Meth. 206, 19 (1983).
2.- J. Depauw et al. Report IPNO GEPL 83-02 Injection axiale dans le cyclo supra conducteur du project a Orsay.
3.- W. T. Milner, IEEE Trans. Nucl. Sc. NS-26, 1445 (1979).
4.- J. L. Belmont and J. L. Pabot, IEEE Trans. Nucl. Sc. NS-13, 191 (1966).